Illuminating the Universe: new probes of Reionization and Cosmology

Oliver Zahn, Berkeley, Oct 17, 2006

Co-workers:

- Matias Zaldarriaga
- Adam Lidz
- Matt McQuinn
- Steve Furlanetto
- Lars Hernquist

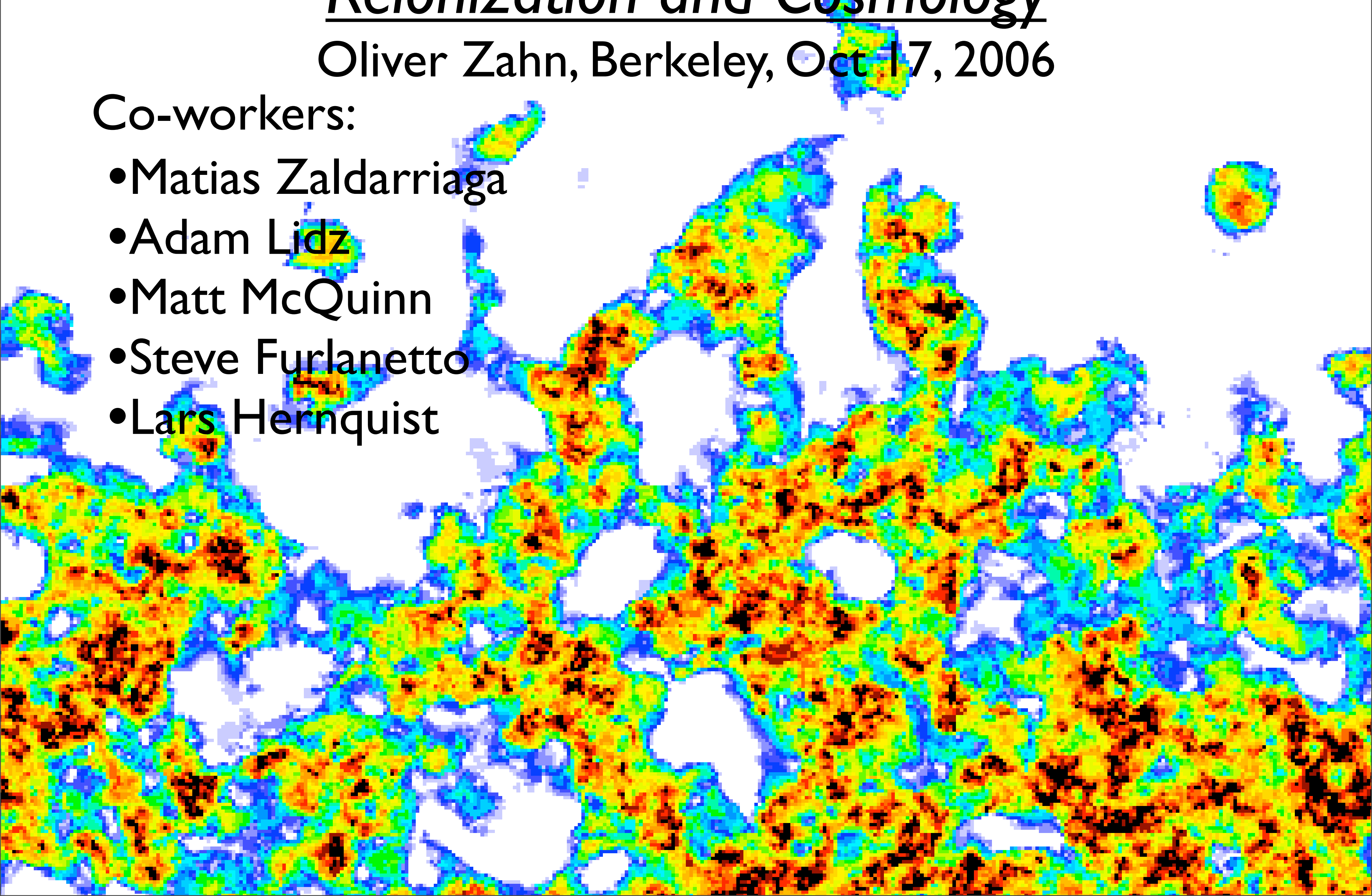

Outline

- Introduction: Motivation for reionization studies
- Simulations and analytic models: enhancing one another
- Applications
  - ★ kinetic Sunyaev-Zel'dovich effect (through power spectrum, etc)
  - ★ 21 cm line
  - ★ parameter space exploration
- Higher order contributions to the 21 cm power spectrum
- secondary anisotropy of 21 cm: lensing
- Other future probes, e.g. 21cm-galaxy correlation

The view from the CMB large scale polarization

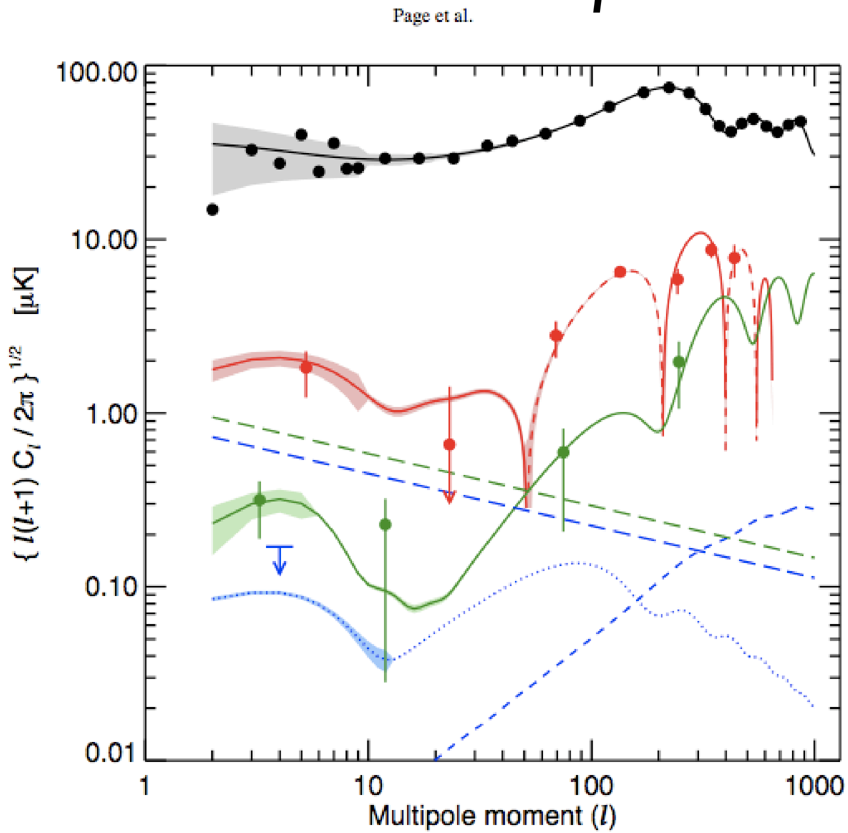

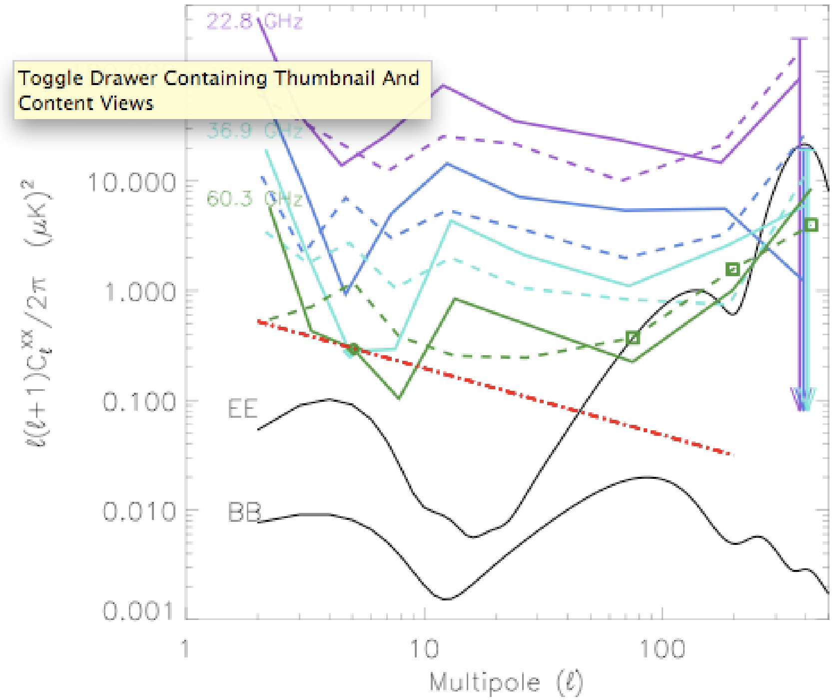

Page (2006), Spergel (2006)

•Large scale polarization, or cross correlation with temperature => size of a hubble volume during reionization => tau=0.09+/-0.03.

•large unknown foreground: galactic synchrotron, thermal dust. We're just beginning to understand the angular and frequency distribution of polarization inside our galaxy

•large scale CMB polarization only gives an integral constraint over Thomson scattering. Haiman&Holder (2003): we could learn a few additional numbers characterizing reionization, perhaps with Planck.

this result was at hand pre-WMAP3!

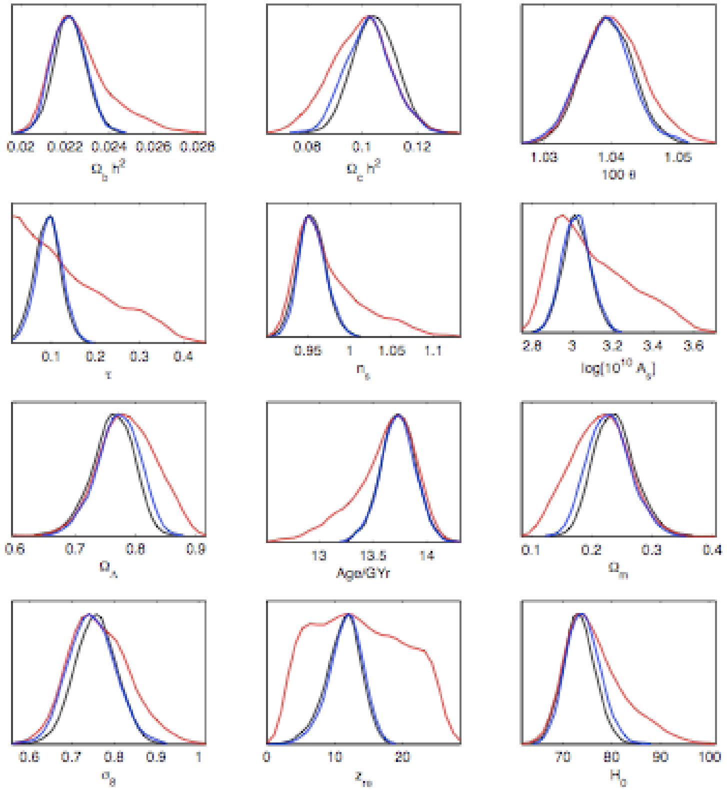

Lewis (2006)

FIG. 2: Constraints from WMAP 3-year temperature (red), temperature and polarization (black), and temperature with a Gaussian prior on the optical depth $\tau = 0.10 \pm 0.03$ (blue). The top six parameters have flat priors and are sampled using MCMC, the bottom six parameters are derived.

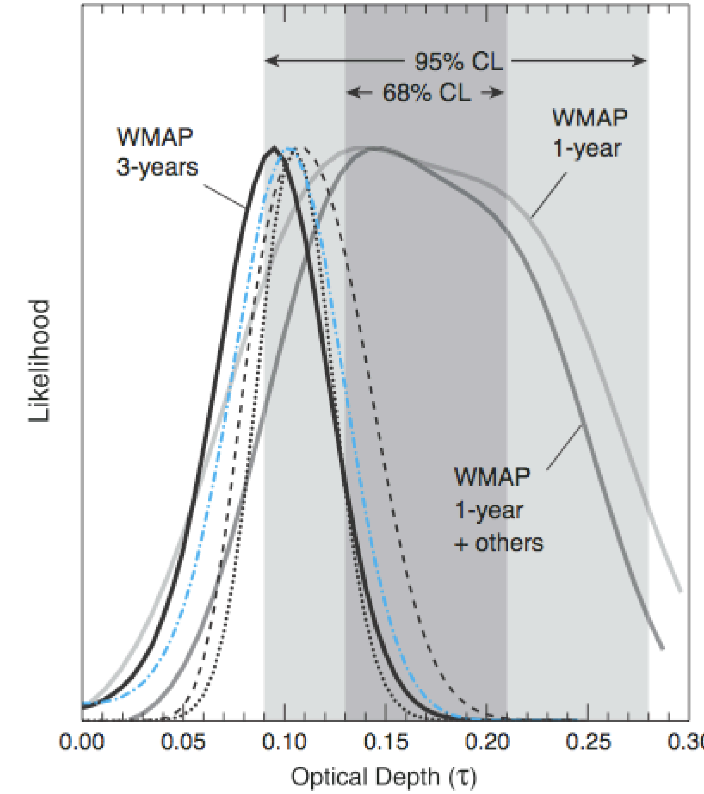

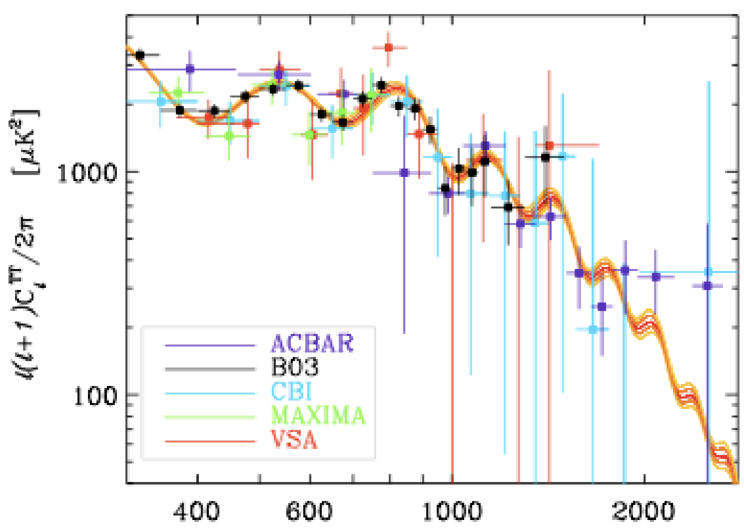

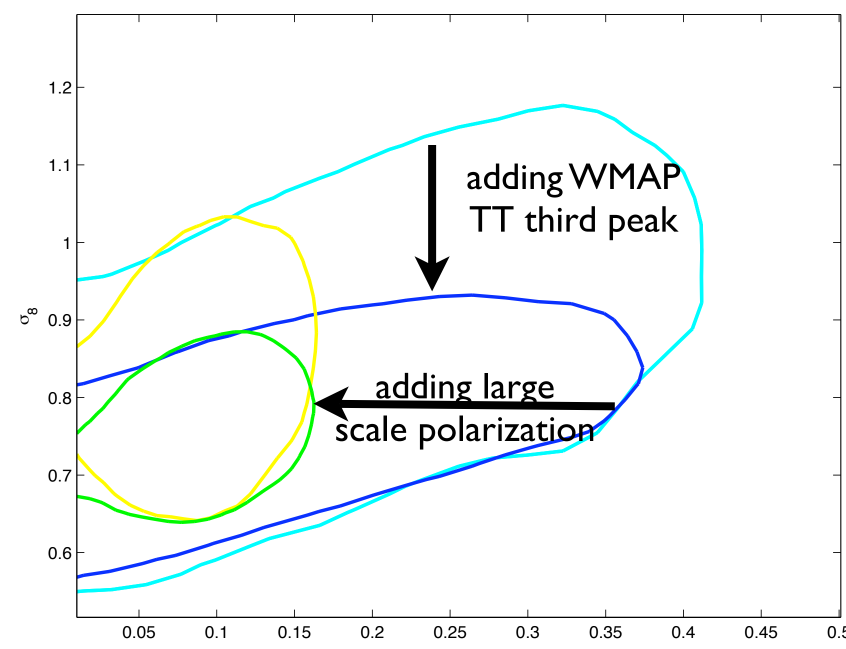

parameter values sensitive to third peak

Further probes

- Quasar absorption spectra:
  - in high z quasar spectra, significant transmission gaps occur (Becker et al. 2001, White et al. 2003/2005). These may reflect a strongly fluctuating radiation field/patchy reionization (Wyithe&Loeb 2005, Fan et al 2005).
  - Lidz et al. (2005) show that even for a uniform ionizing background, there will be a scatter in the mean transmissivity similar to the observed. Two reasons: z~6 transmission spectra are highly biased (4-5) tracers of underlying density fluctuations. Furthermore power from small-scale transverse modes is aliased to long wavelength line-of-sight modes => quasar spectra at present consistent with reionization at higher z (>7?)

- Constraints from the high-z galaxy luminosity function from narrowband Lyman-alpha searches (Malhotra&Rhoads 2005). Evolution seen there is mild, if at al. Because of the clustering of sources found in reionization models, narrowband searches may eventually extend deeper into reionization and probe ionization fractions x~0.5 (Furlanetto et al. 2005)

- Region of substantial transmission around some high redshift quasars. If they were able to ionize as much as they did, the surrounding medium should have been somewhat ionized (Mesinger et al. 2004; Wiythe et al. 2004).

21 cm from diffuse gas

Wouthuysen(1952)-Field(1958) mechanism

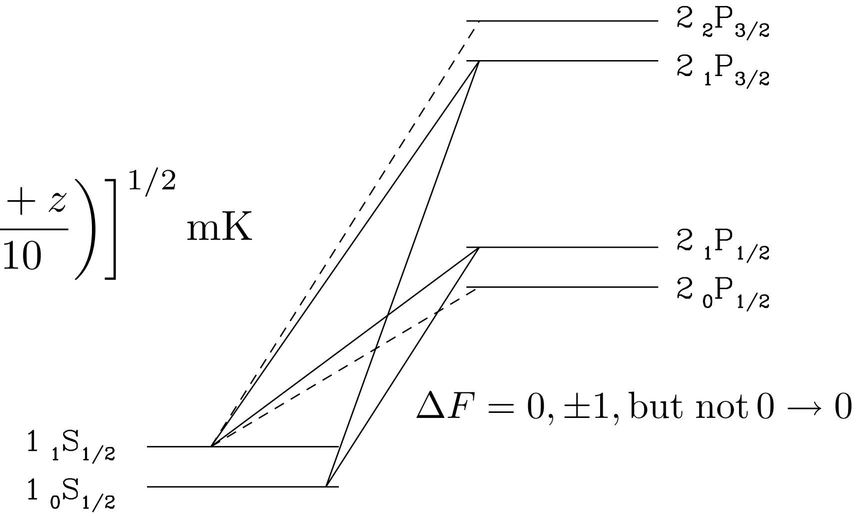

Lyman-alpha pumping couples T_s to T_k

Increment or decrement compared to CMB:

$$\delta T(\nu) \approx 26\, x_H (1+\delta_\rho) \left(\frac{T_S - T_{\rm CMB}}{T_S}\right) \left(\frac{\Omega_b h^2}{0.022}\right) \left[\left(\frac{0.15}{\Omega_m h^2}\right) \left(\frac{1+z}{10}\right)\right]^{1/2} \mathrm{mK}$$

(e.g. Zaldarriaga et al. 2004)

•initially Thomson scattering of CMB photons couples T_s to T_cmb, later adiabatic cooling away of the gas ~(1+z)^2, until first structures collapse (z~30)

•then kinetic temperature set by X-ray background from the first supernovae and accreting binary systems. Universe should have been transparent to these photons well before there are any extended HII regions.

•estimates suggest that Ly-alpha background will be strong enough to couple the spin and kinetic temperatures much before reionization occurs (e.g. Ciardi & Madau 2002, Furlanetto 2006)

•therefore expect that, during reionization, T_s >> T_cmb will be good approximation globally -- hence even regions outside HII bubbles will have T_s >> T_cmb. Good, because then we can infer the reionization morphology from the signal!

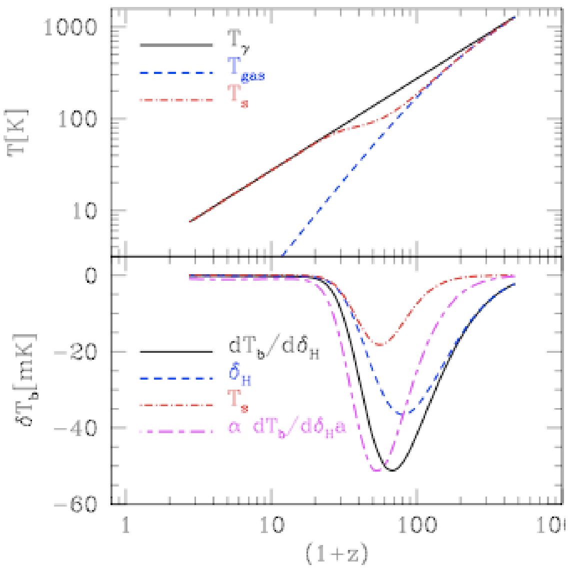

only Compton heating and collisional coupling

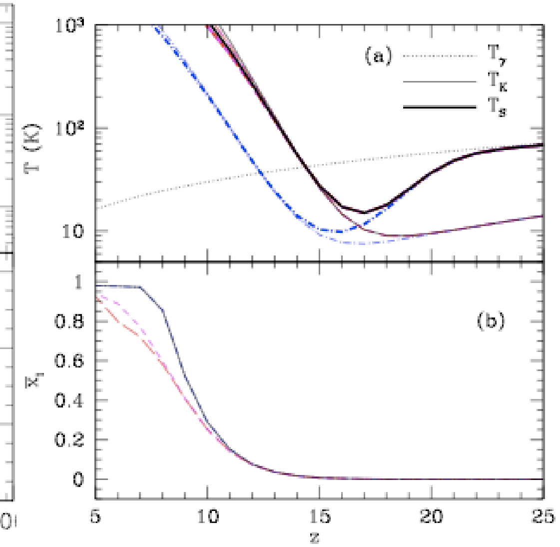

including the effect of first collapsed objects

21 cm, the future gold-mine of reionization and cosmology research?

Loeb & Zaldarriaga (2004)

•***in principle***, the number of available modes in this observable is enormous

$$N_{21\mathrm{cm}} \sim 3\times10^{16}(l_{\max}/10^6)^3(\Delta\nu/\nu)(z/100)^{-1/2}$$

•because of Silk damping in LSS, the number for the CMB is

$$N_{\mathrm{CMB}} = 2l_{\max}^2 \simeq 2\times10^7(l_{\max}/3000)^2$$

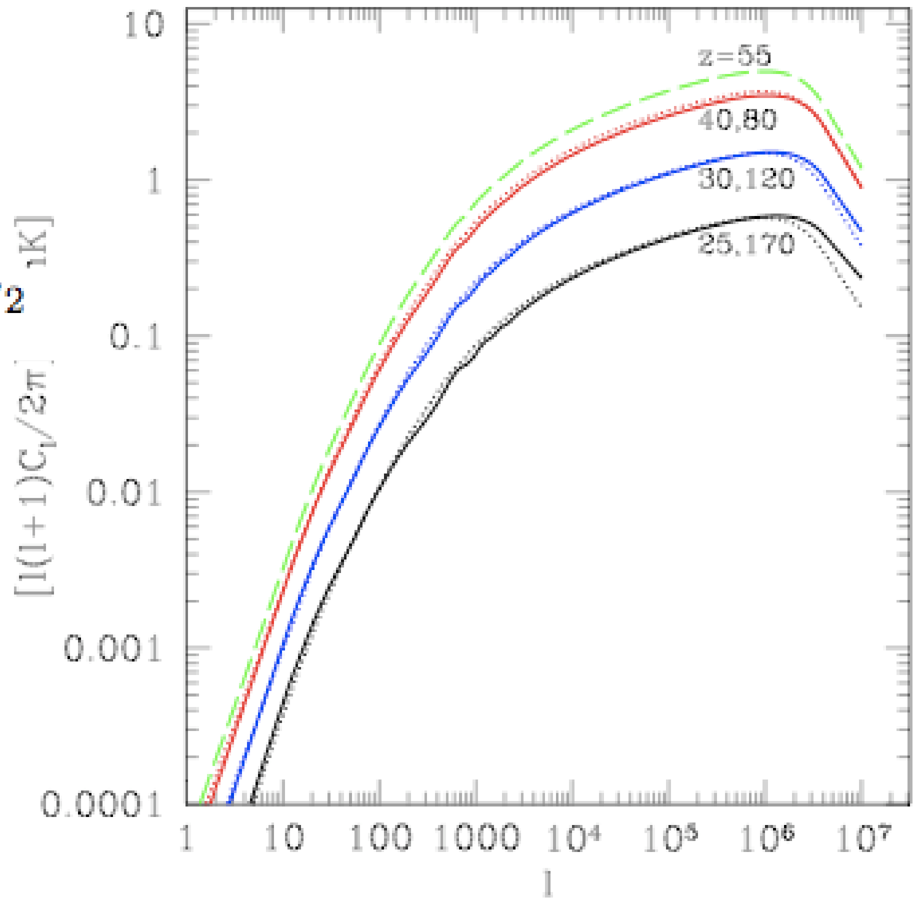

angular 21 cm power spectrum at various z

•21 cm offers full redshift information to probe reionization and cosmology (pre-reionization IGM as well as morphology (shape and clustering) of bubbles).

In practice: an experimental challenge

CMB:

- Background: 3K CMB
- Temperature Fluctuations: 30 μK (10^{-5})
- E mode polarization: 3 μK (10^{-6})
- B mode polarization: 0.1 μK (3×10^{-8})
- Wavelength: 0.3 cm
- Frequency: 100 GHz

21 cm Fluctuations:

- Foreground: 100-1000 K galactic synchrotron
- Temperature Fluctuations: 20 mK (10^{-4})
- Wavelength: 2 meters
- Frequency: 140 MHz

$$T_{sys} \propto \nu^{-2.55}$$

e.g.: 250 K at z=6
440 K at z=8
1000 K at z=12

$$\Delta T \propto \frac{\lambda^2 T_{sys}}{A\sqrt{\Delta\nu t_0}}$$

(Zaldarriaga et al 2004, Morales et al 2004)

=> to get to high redshift want to increase collecting area and survey speed

- several low frequency radio telescopes are gearing up to measure this: VLA, MWA, PAST, SKA, PAPER (small fast moving groups are important).


© ASTRON

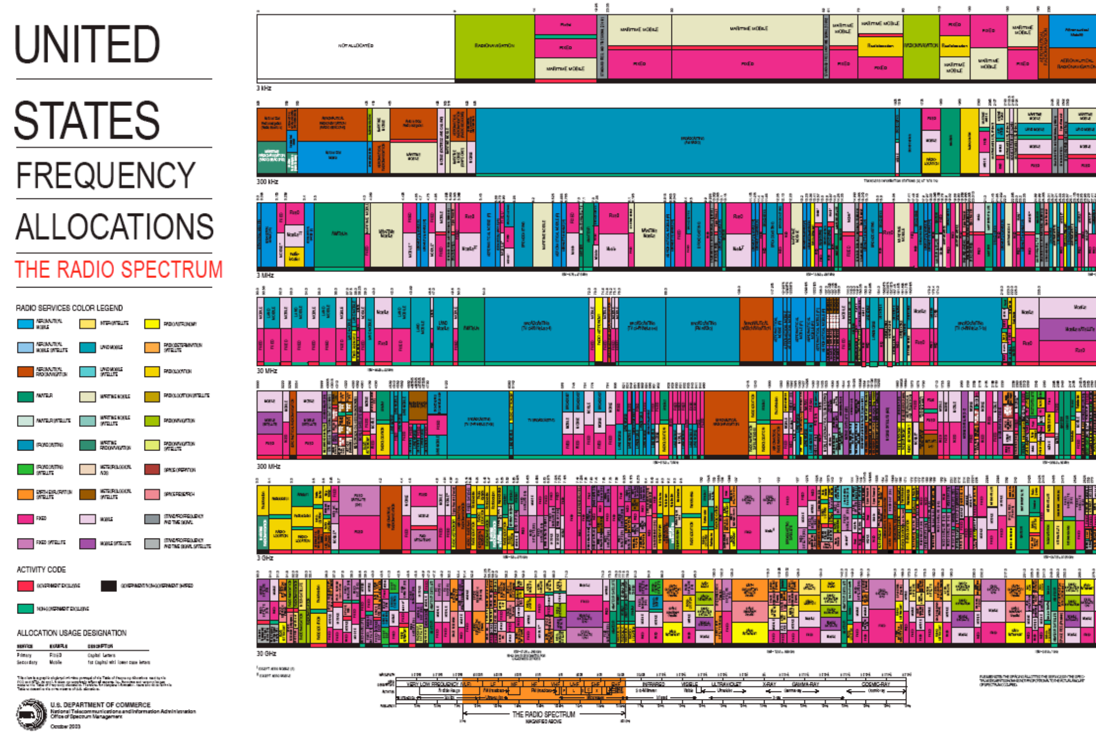
UNITED
STATES
FREQUENCY
ALLOCATIONS
THE RADIO SPECTRUM


Broome
Port Hedland
Dampier
Karratha
Yarrie
WESTERN
Newman
Paraburdoo
AUSTRALIA
Carnarvon
Meekatharra
Leonora
Geraldton
Kalgoorlie
Perth
Fremantle
Bunbury
Esperance
Albany
NORTHERN
Tennant
Creek
TERRITORY
Alice Springs
Yulara
SOUTH
AUSTRALIA
Coober Pedy
Ceduna
Port Augusta
Whyalla
Port Lincoln
Adelaide

Indication from simulation of extended HII due to source clustering

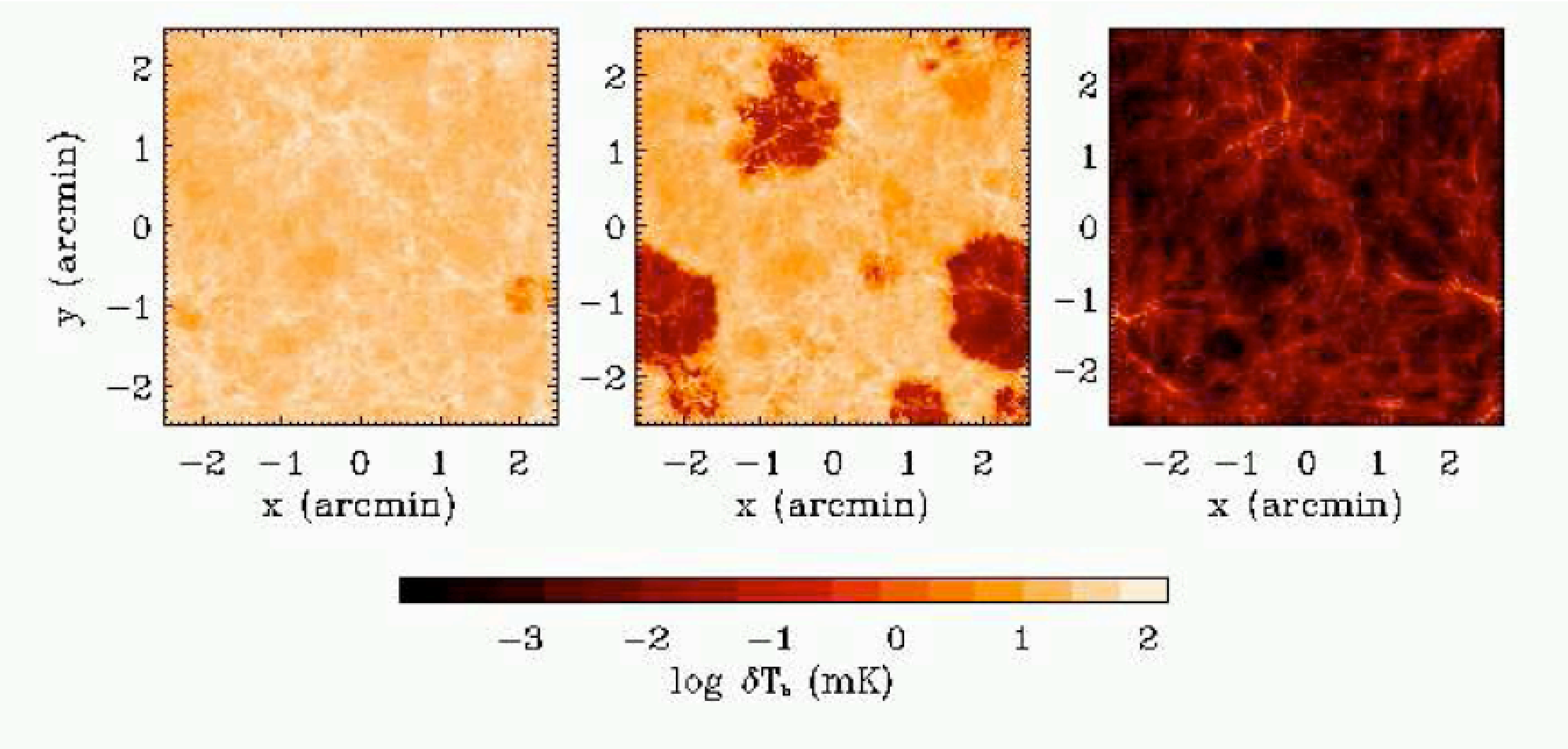

FIG. 1.— The brightness temperature of the 21 cm transition at several redshifts, as predicted by the "late reionization" simulation analyzed in Furlanetto et al. (2003). Each panel corresponds to the same slice of the simulation box (with width $10h^{-1}$ comoving Mpc and depth $\Delta\nu = 0.1$ MHz), at $z = 12.1$, 9.2, and 7.6, from left to right. The three epochs shown correspond to the early, middle, and late stages of reionization in this simulation. (For details about the simulations, see Sokasian et al. 2001; Springel & Hernquist 2003a,b.)

Sokasian et al. (2003)

What determines the sizes of the “bubbles”?

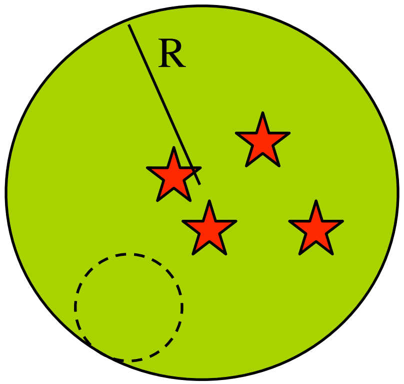

Region of size R containing mass M

\# of atoms

\# of ionizing photons

$$\bar{\rho}_m \frac{4\pi R^3}{3} = \zeta\, m_{\rm coll}$$

$$\zeta = f_{\rm esc} f_* N_{\gamma/b}\, n_{rec}^{-1}$$

Size of ionized region set by counting ionizing photons

$$f_{coll}(> M_{min}) = {\rm erfc}\left[\frac{\delta_c - \delta_M}{\sqrt{2(\sigma^2(M_{min}) - \sigma^2(M))}}\right]$$

Fraction of mass in collapsed objects that can cool.

$$f_{\rm coll} > \zeta^{-1}$$

Region produces enough photons to become ionized

Press-Schechter type/excursion set formalism

(Press&Schechter 1974, Bond 1991, Lacey&Cole 1993)

$$f_{\rm coll} > \zeta^{-1} \qquad f_{coll}(> M_{min}) = \mathrm{erfc}\left[\frac{\delta_c - \delta_M}{\sqrt{2(\sigma^2(M_{min}) - \sigma^2(M))}}\right]$$

Virialization at 11000 K, where atomic cooling becomes efficient

$$\delta_M > \delta_x(M, z) \equiv \delta_c(z) - \sqrt{2}K(\zeta)[\sigma^2_{\rm min} - \sigma^2(M)]^{1/2},$$

Furlanetto, Zaldarriaga, Hernquist (2004) (FZH04)

Approximate by: $B_0 + B_1\sigma^2(M)$

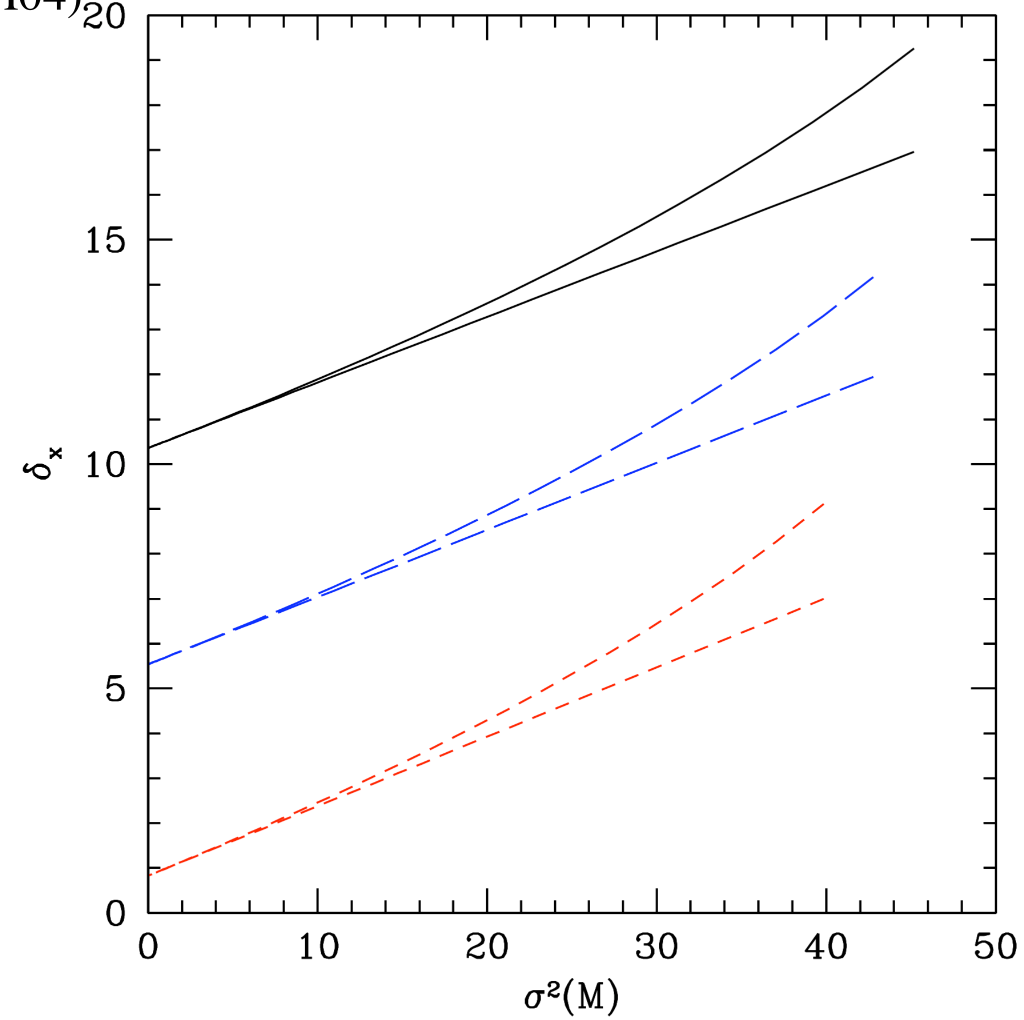

The barrier rises more rapidly than σ(M) so there is a small mass cut-off to the "mass functions"

Size distribution

$$m\frac{dn}{dm} = \sqrt{\frac{2}{\pi}}\ \frac{\bar{\rho}}{m}\ \left|\frac{d\ln\sigma}{d\ln m}\right|\ \frac{B_0}{\sigma(M)}\exp\left[-\frac{[\delta_x^{\rm fit}(M,z)]^2}{2\sigma^2(M)}\right]$$

(Bubble mass function)

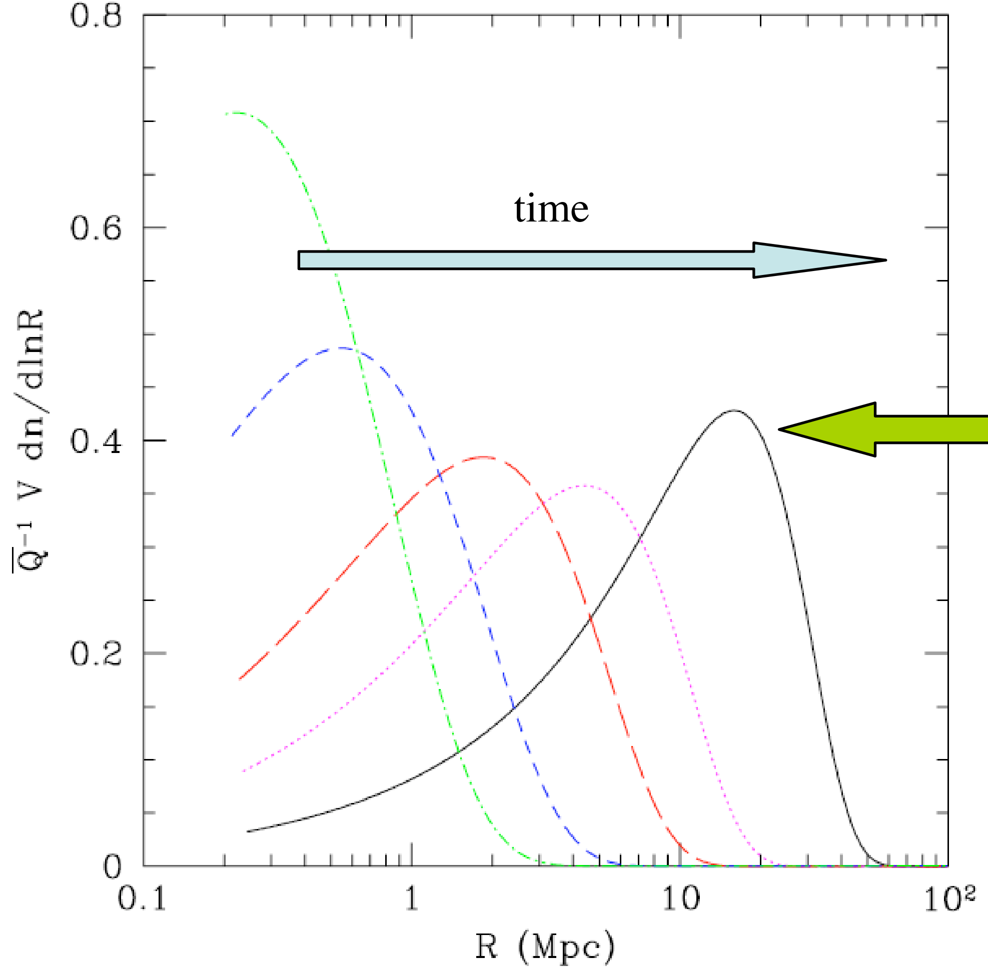

At any given redshift there is a characteristic size

$$R_{gal} \approx 0.7\ (\frac{M}{10^9 M_\odot})^{1/3}(\frac{\zeta}{40})^{1/3}\ \mathrm{Mpc}$$

$$R >> R_{gal}$$

FIG. 2.— The bubble size distribution $\bar{Q}^{-1}V dn/d\ln R$ at several different redshifts in our model, assuming $\zeta = 40$ (note that R is the comoving size). Dot-dashed, short-dashed, long-dashed, dotted, and solid lines are for $z =$ 18, 16, 14, 13, and 12, respectively. These have $\bar{Q} = 0.037, 0.11, 0.3, 0.5$, and 0.74.

Alternative barriers: gauging the importance of various physical effects

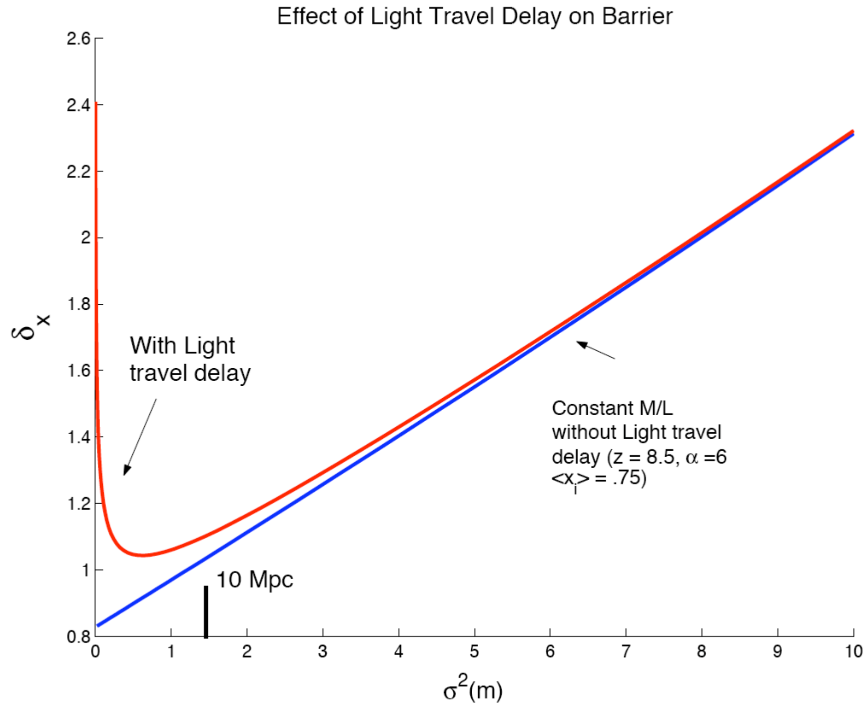

Luminosity vs Integrated flux

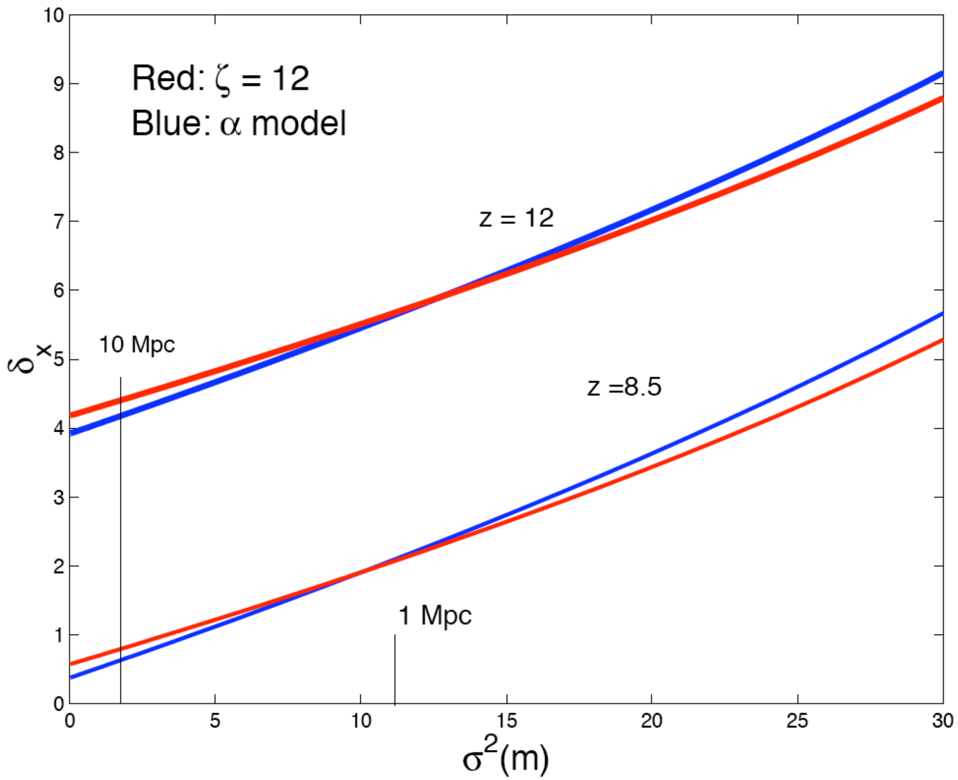

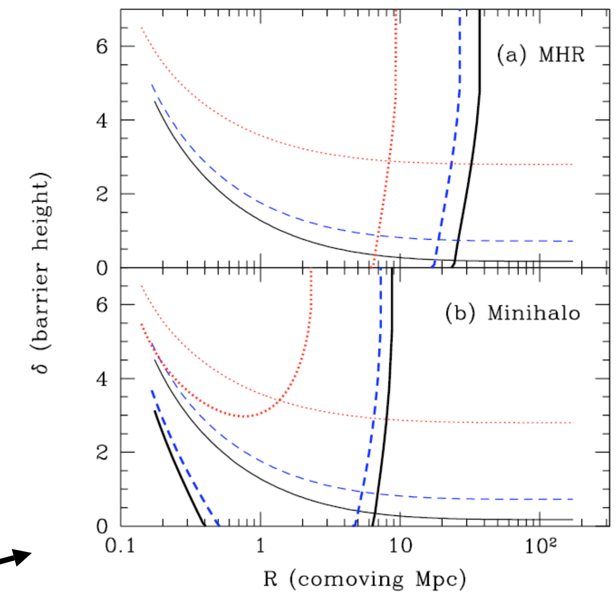

Figure 7. Barrier height as a function of comoving radius. The solid, dotted, and dashed curves have $\bar{x}_i = 0.95,\ 0.82$, and 0.49, respectively, at $z = 6$. Within each set, the thin curves show δ_x (from FZH04) and the thick curves show δ_r (from this paper). *(a)*: Uses MHR00 to compute δ_r. *(b)*: Uses the minihalo model described in the text to compute δ_r.

Recombinations
(Furlanetto & Oh 2005)

Cookbook for your homemade reionization simulation

=>With the threshold prescription, we can generate a `Monte-Carlo realization' of the analytic model. This has various advantages as we shall see.

1. establish a Gaussian random density and velocity field (based on linear theory for now)
2. smooth field on logarithmically smaller scales, starting from the box-size (to include ionizations resulting with the aid of neighboring sources).
3. if a point crosses the threshold, label it ionized.
4. in each step, record the number of crossings to generate a bubble pdf.
5. takes about 50 steps to achieve convergence in x_i.
6. then generate your favorite reionization observable in real or z-space.

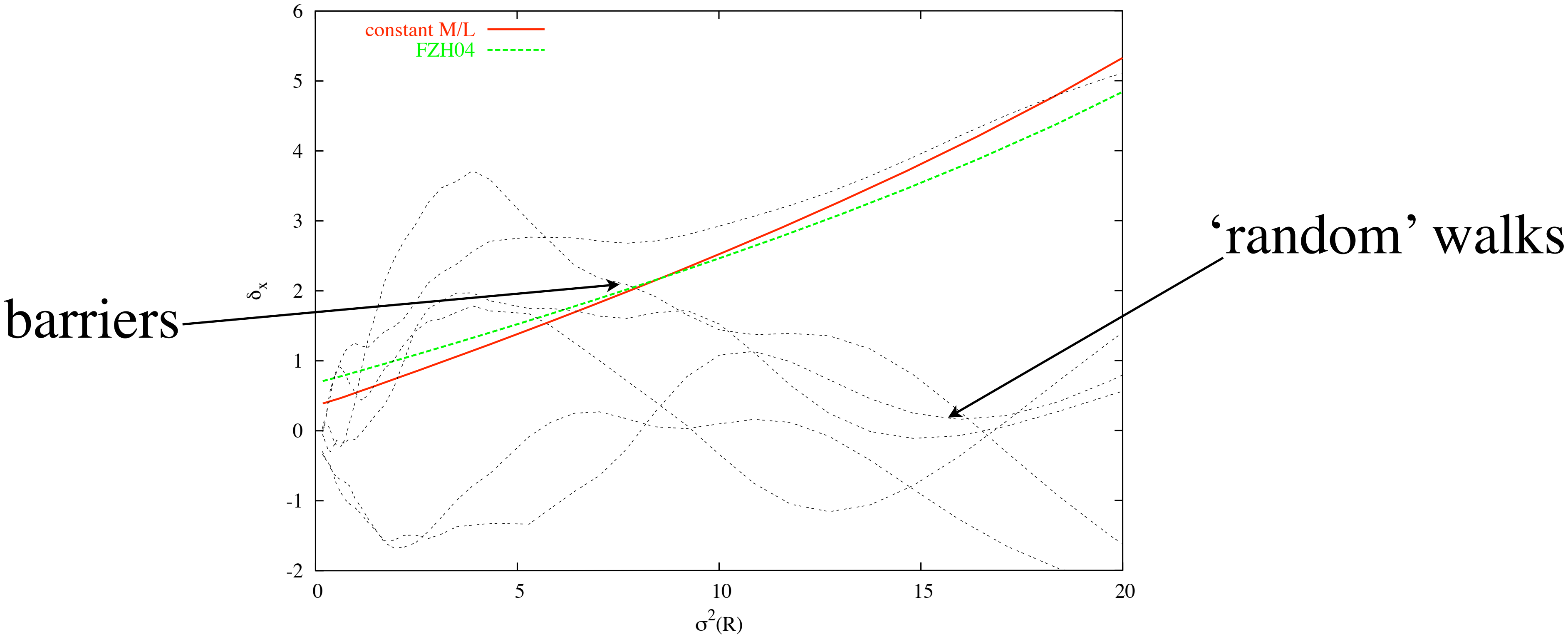

Radiative Transfer simulation

- post-processed from Gadget-2 N-body simulation, 65.6 Mpc/h simulation with 1024^3 particles
- find halos with friends of friends algorithm, linking length 0.2 times mean particle spacing
- resolve halos all the way down to 1e9 Msol, just one order of magnitude short of the cooling mass at z=6
- At high redshift, the mass function is still closer to Sheth-Thormen than Press-Schechter, except for highest

Zahn&Lidz et al (2006a)

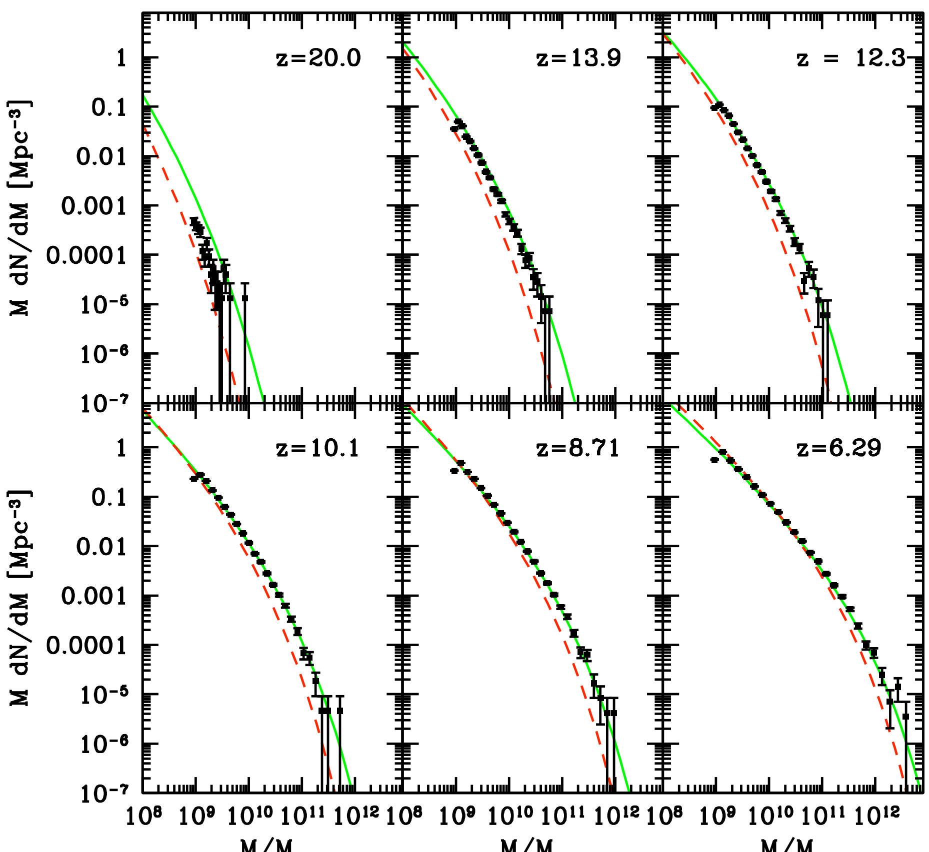

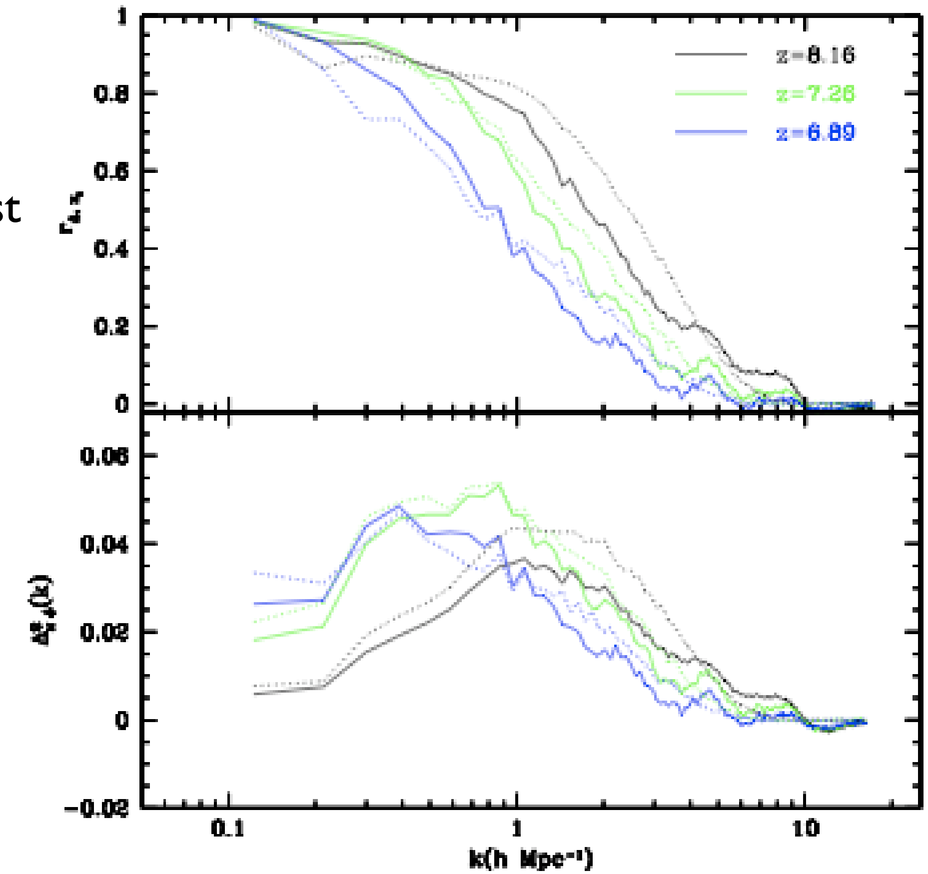

FIG. 7.— *Top panel:* Cross correlation coefficient between the ionization and density field. The solid (dotted) lines show the cross correlation coefficient between the ionization and density fields in the radiative transfer simulation (hybrid scheme) at several redshifts. *Bottom panel:* Cross-power spectrum between the ionization and density field. Solid lines are calculations from the radiative transfer simulation, while dotted lines are from the hybrid scheme.

A side-by-side comparison

- both analytic scheme and radiative transfer simulation track the density field very closely, with reionization happening `inside-out'
- bubbles grow and eventually merge at high x
- the analytic model seems to predict slightly more connected HII regions (we will see whether this is a bad thing)
- `collective clustering' morphology seems to win over individual source dominated clustering with our source prescription
- N-body simulation took 38 hours to run on 134 CPU's
- Radiative transfer simulation took about 3 days on large RAM machine
- analytic model: e.g. 10 minutes on my laptop

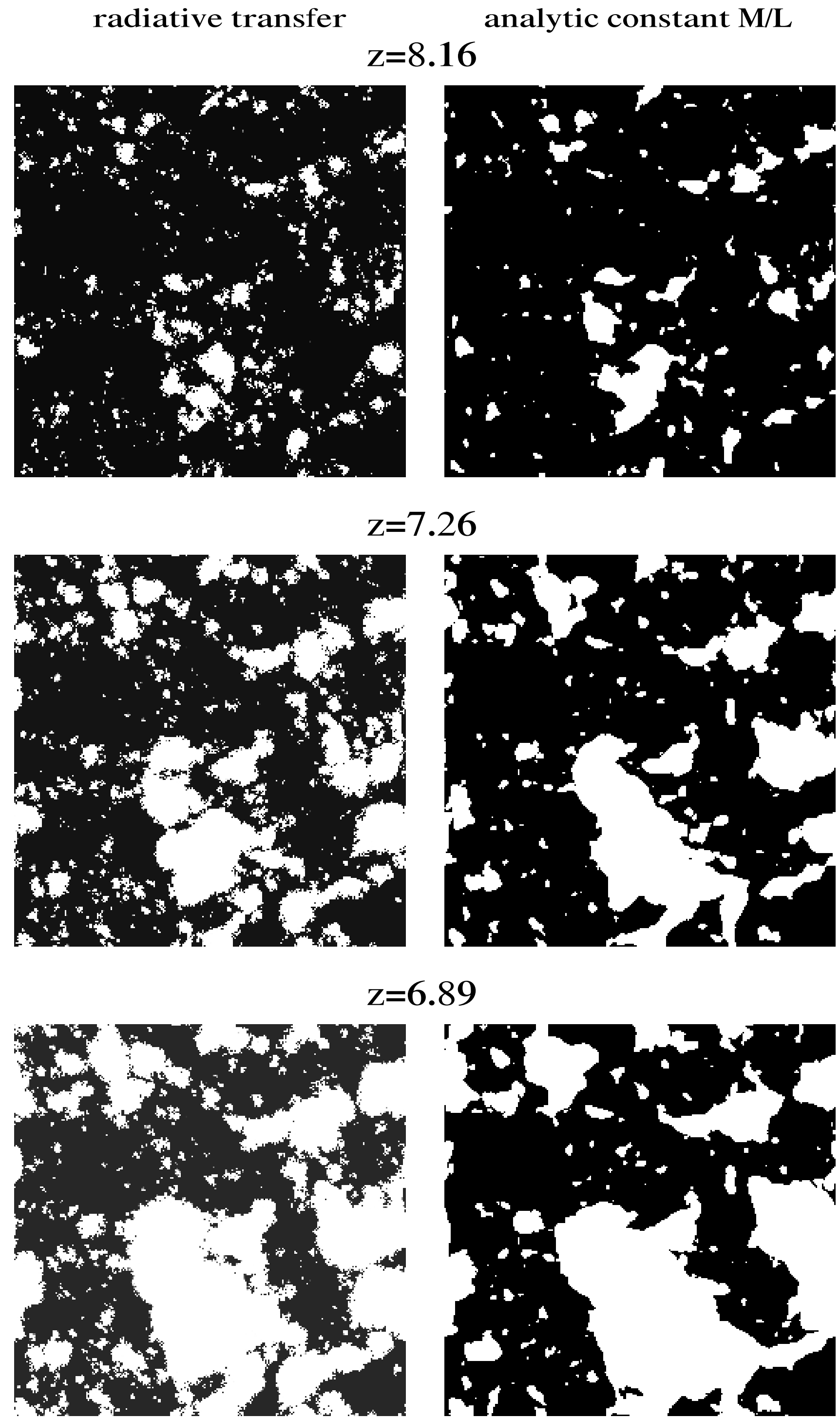

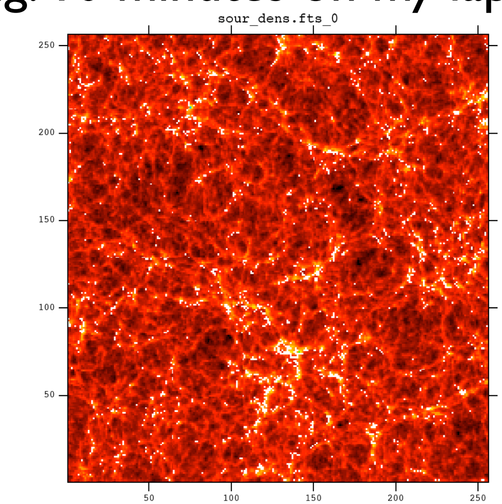

Zahn&Lidz et al (2006a)

A side-by-side comparison

- both analytic scheme and radiative transfer simulation track the density field very closely, with reionization happening `inside-out'
- bubbles grow and eventually merge
- the analytic model seems to predict slightly more connected HII regions (we will see whether this is a bad thing)
- `collective clustering' morphology seems to win over individual source dominated clustering with our source prescription
- N-body simulation took 38 hours to run on 134 CPU's
- Radiative transfer simulation took about 3 days on large RAM machine
- analytic model: e.g. 10 minutes on my laptop

radiative transfer analytic constant M/L

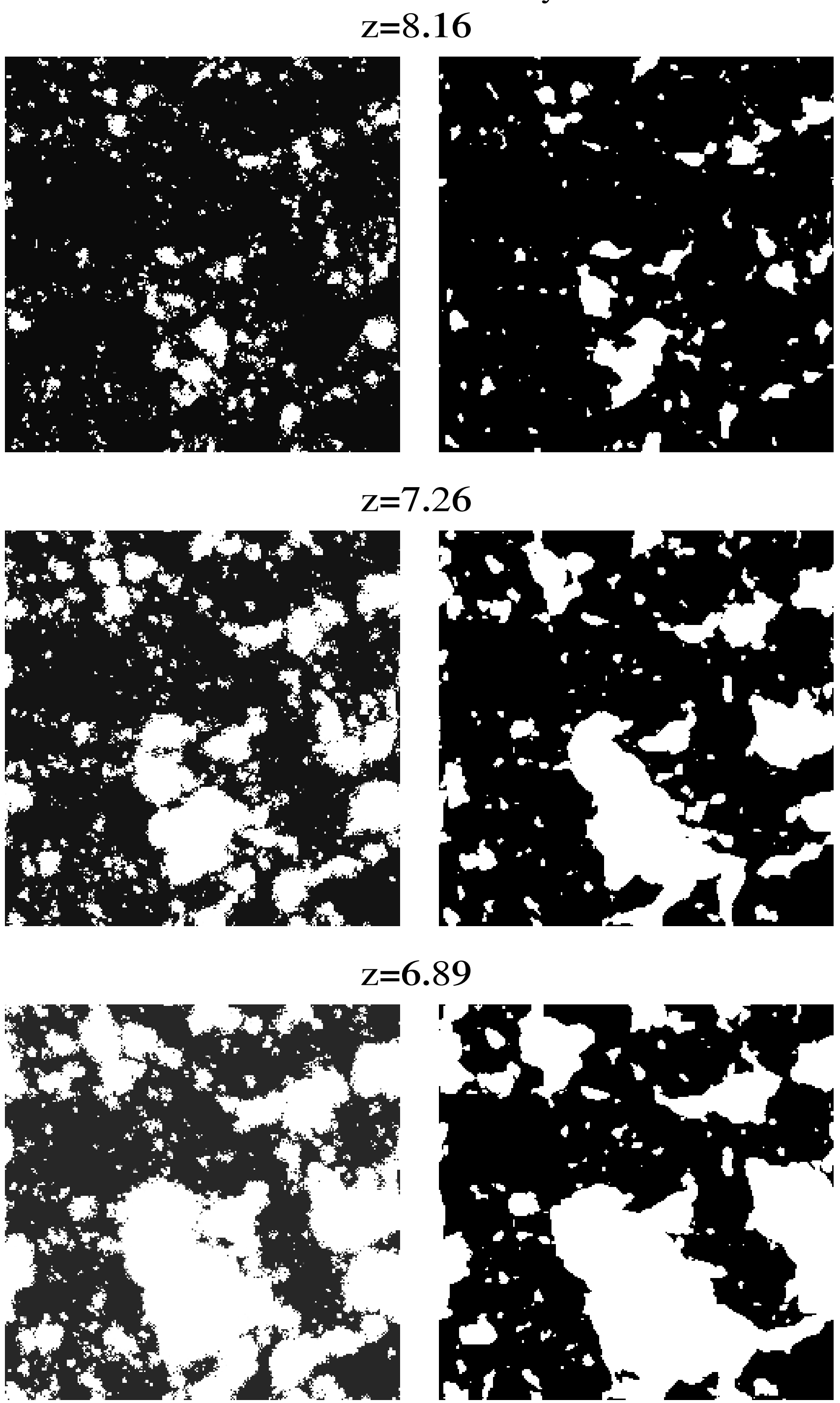

Zahn&Lidz et al (2006a)

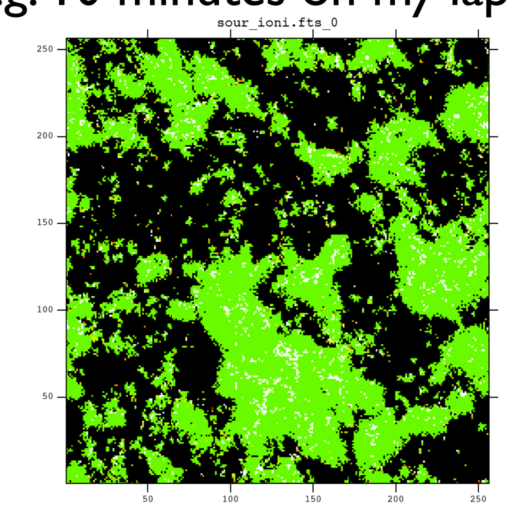

Comparison movie

65.6 Mpc/h box, 128 resolution, 1' smoothing

Radiative Transfer	improved MC, \`halo-smoothing'	Press-Schechter model (FZH04)

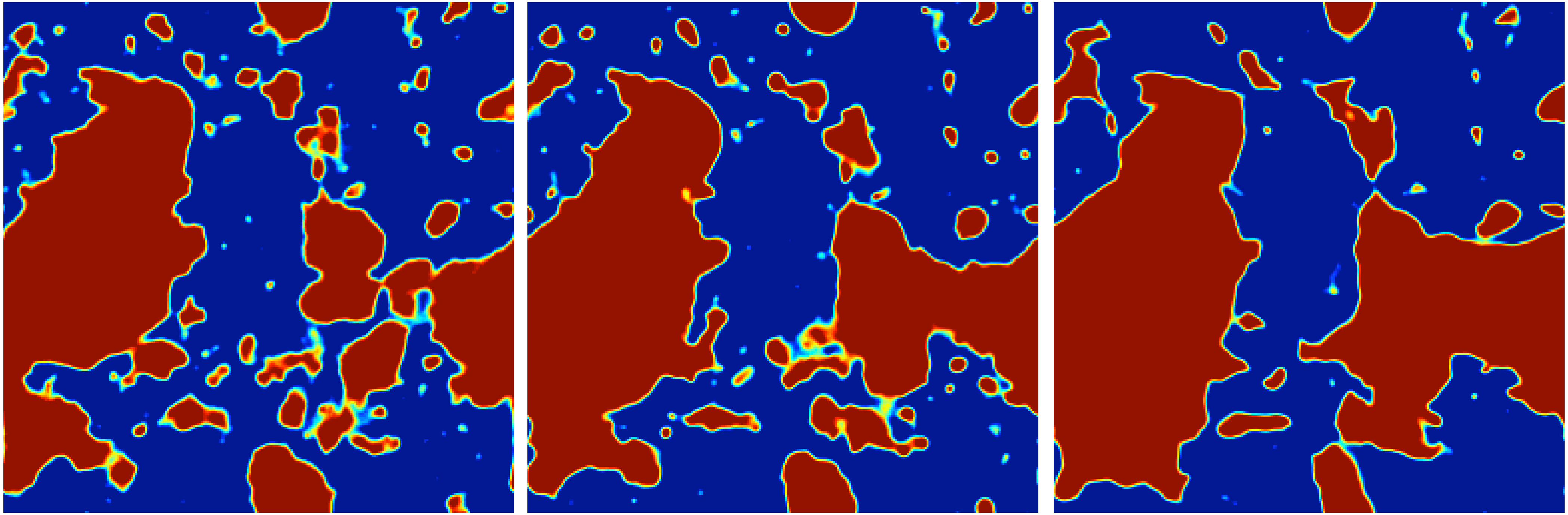

A more quantitative comparison...

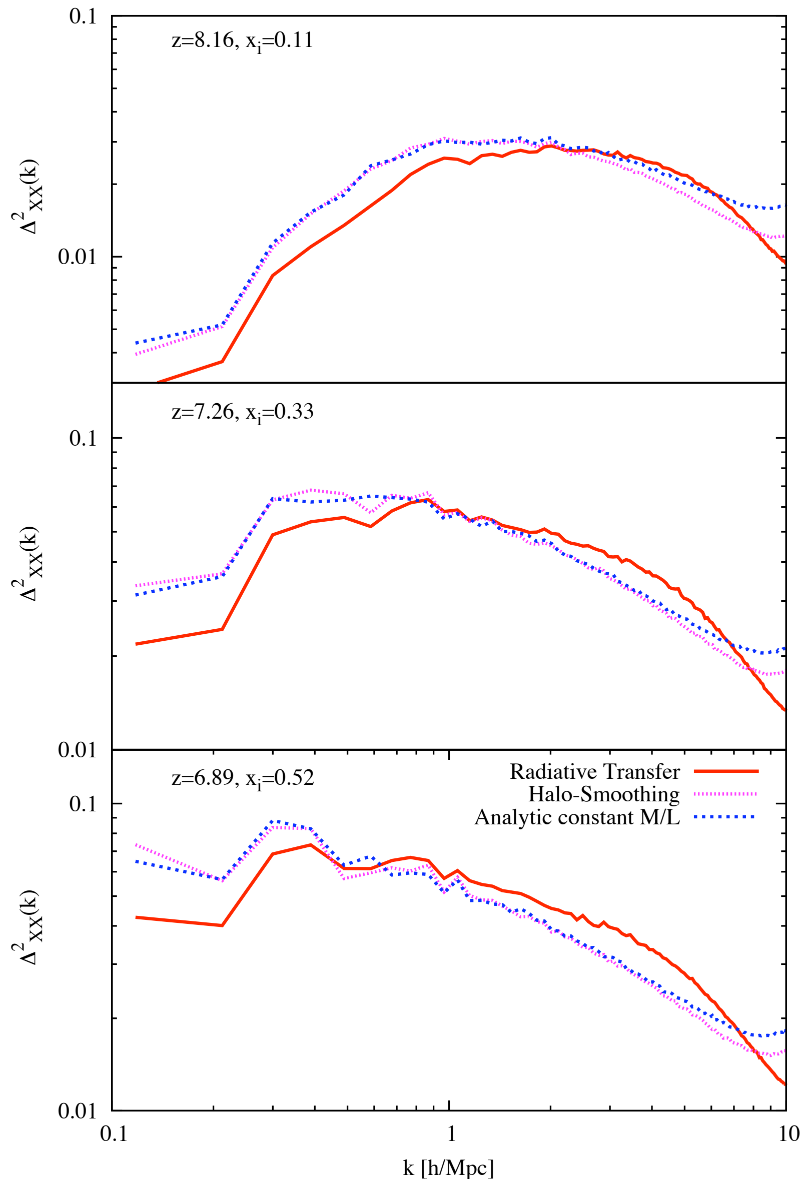

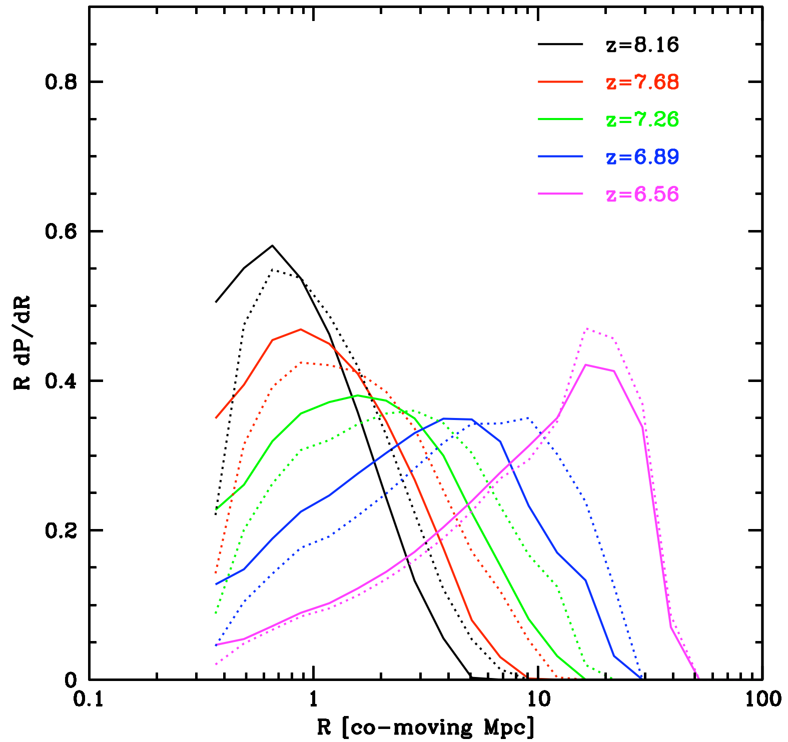

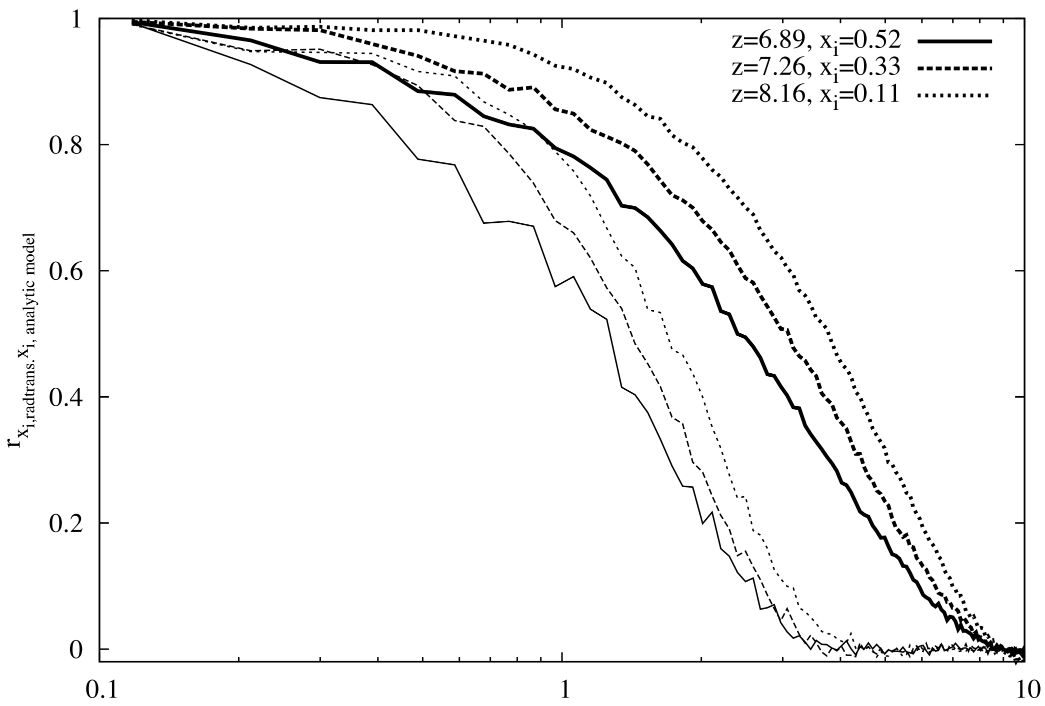

Zahn&Lidz et al (2006a)

To what extend does RT only amount to `photons counting'?

The fast numerical scheme is a kind of `Fourier space radiative transfer', at this point we're limiting ourselves to spheres, among all possible shapes

The spherical top-hat smoothing misses some structure in delta, but overall looks quite good

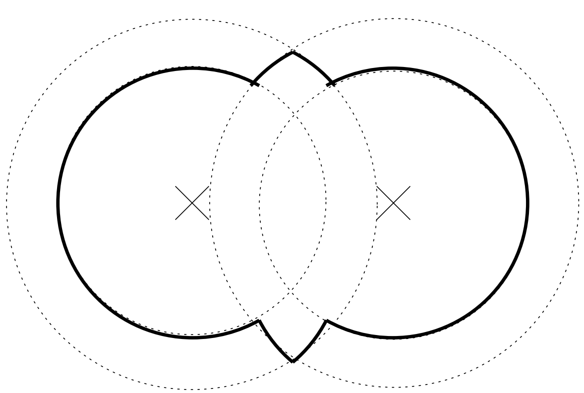

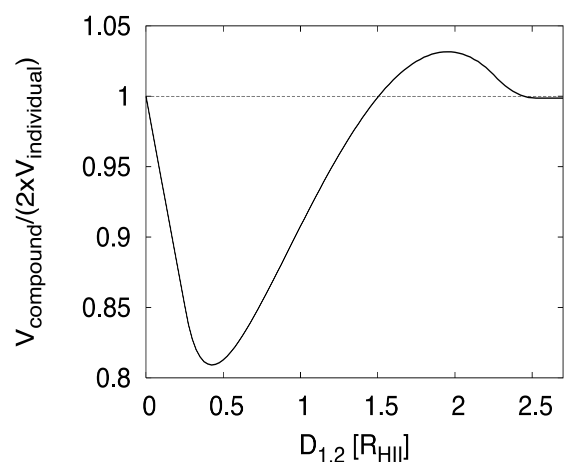

slight violation of photon conservation

RT-HA

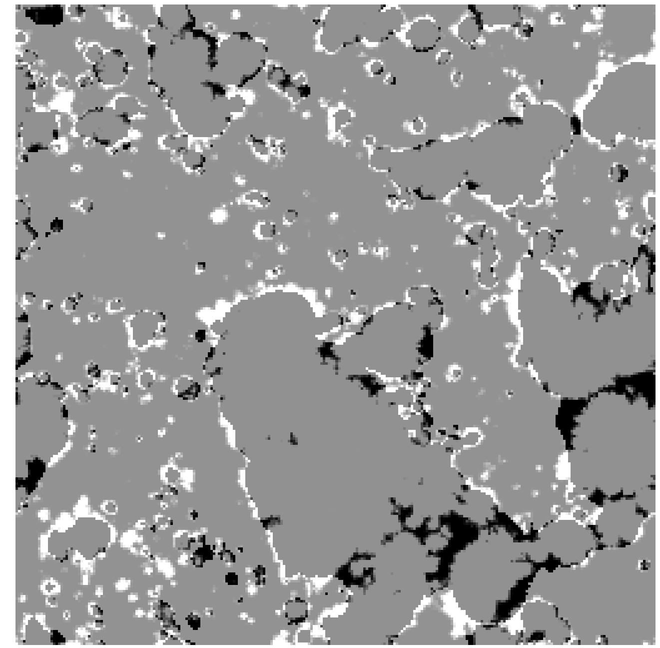

RT-AN

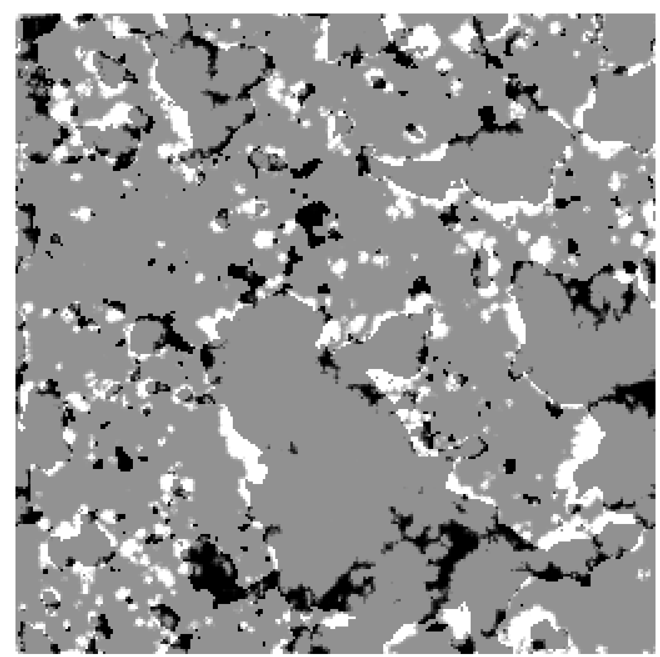

Comparing the predictions for 21 cm

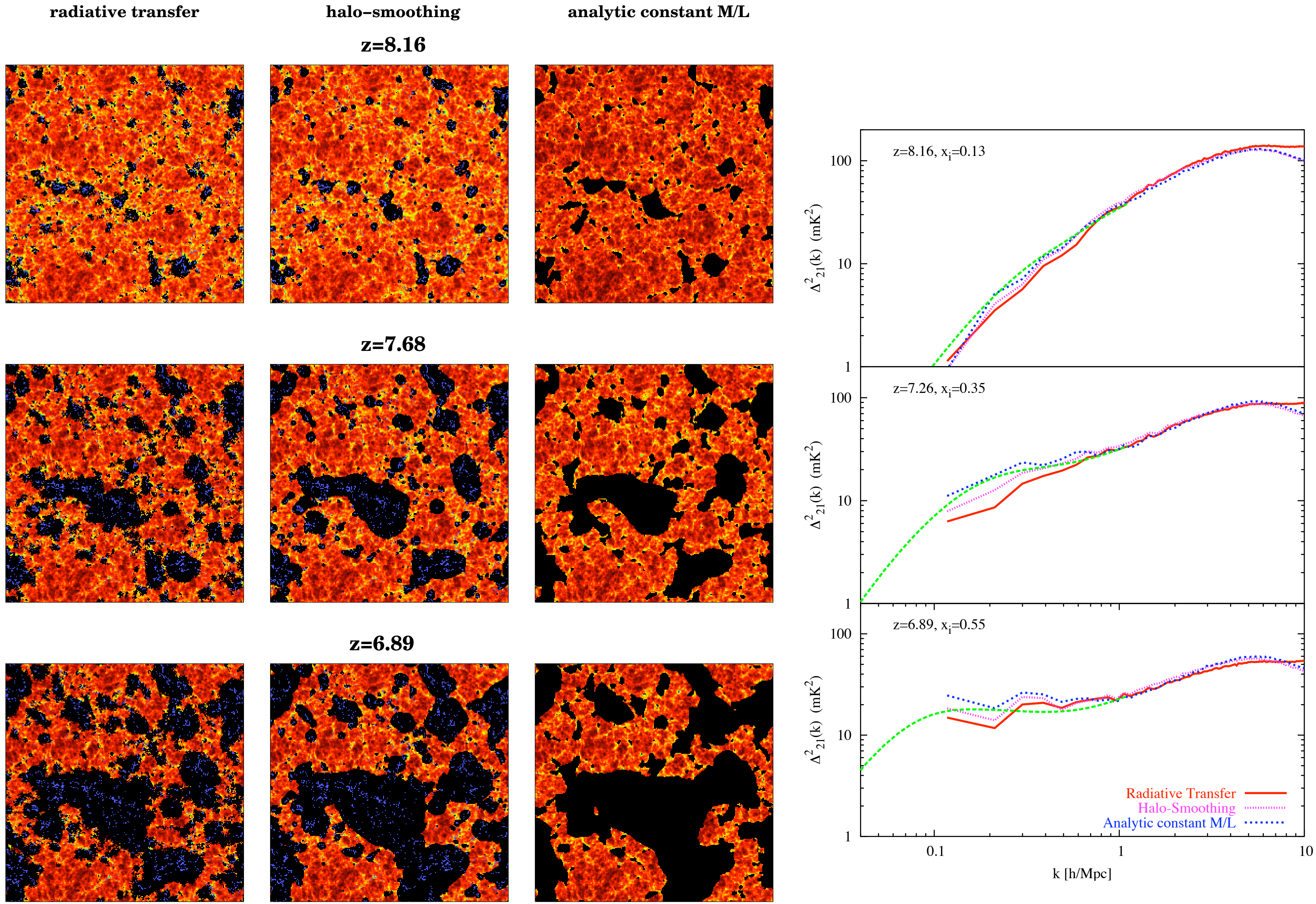

Recombinations, Mass Dependent efficiency

- Miralda-Escude et al. ('00) used numerical simulations of high z IGM and find for V weighted density distr. which they use to calculate the clumping factor in

$$\zeta \frac{df_{\rm coll}}{dt} > A_u C(\delta, R)$$

The mean free path of ionizing photons enters the derivation of C. The authors find from fitting to numerical simulations

$$\lambda_i = \lambda_0 [1 - F_V(\Delta_i)]^{-2/3}$$

Where

$$\lambda_0 H(z) = 30 - 60\, km/sec$$

Seems reasonable.

- To account for a higher luminosity of more massive sources, one can parametrize the ionization efficiency as

$$\zeta = m^{\alpha}$$

Original condition on the collapse fraction now becomes an integral

$$\int \mathrm{d}m\, \zeta(m)\, m\, n_h(m|\delta, M) = 1,$$

Which is solved numerically using

$$n_h(m|\delta, M) = \sqrt{\frac{2}{\pi}}\, \frac{\bar{\rho}}{m^2} \left| \frac{\mathrm{d}\ln\sigma}{\mathrm{d}\ln m} \right| \frac{\sigma^2[\delta_c(z) - \delta]}{[\sigma^2(m) - \sigma^2(M)]^{3/2}} \times \exp\left\{ -\frac{[\delta_c(z) - \delta]^2}{2[\sigma^2(m) - \sigma^2(M)]} \right\}. \qquad (12)$$

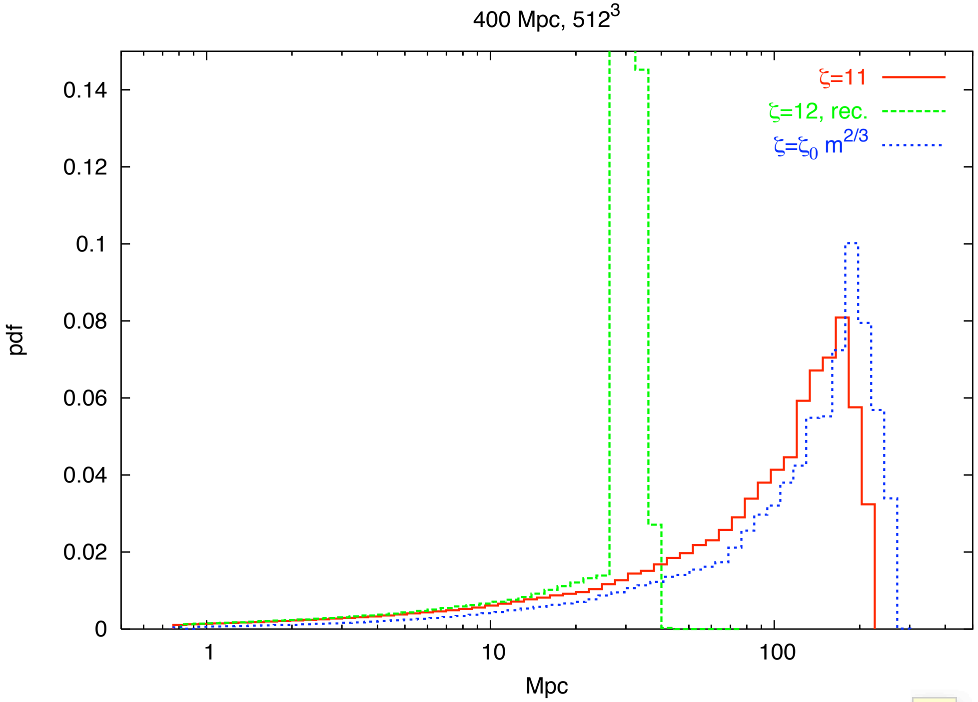

- peak in the bubble pdf: we assumed mean free path is homogeneous and isotropic

- while there will be a sharp limit in the bubble size, the power spectrum averages over this to some extend

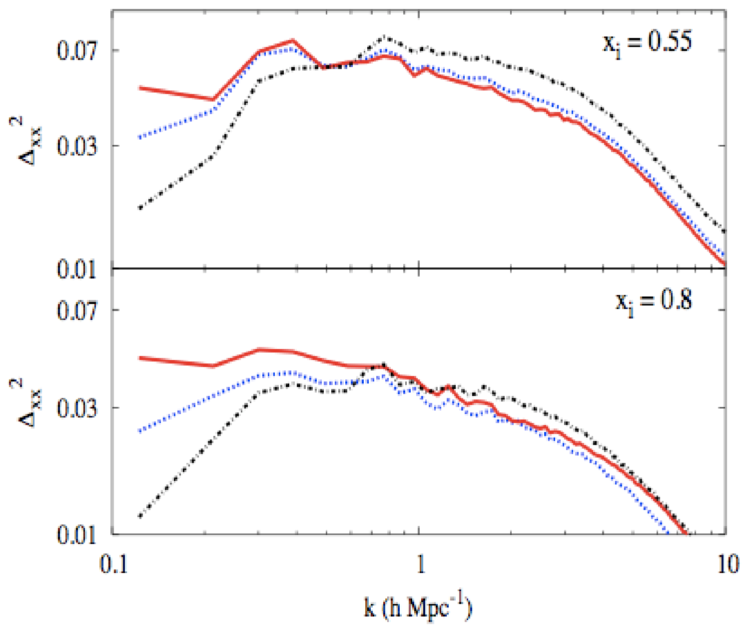

(McQuinn et al. 2006)

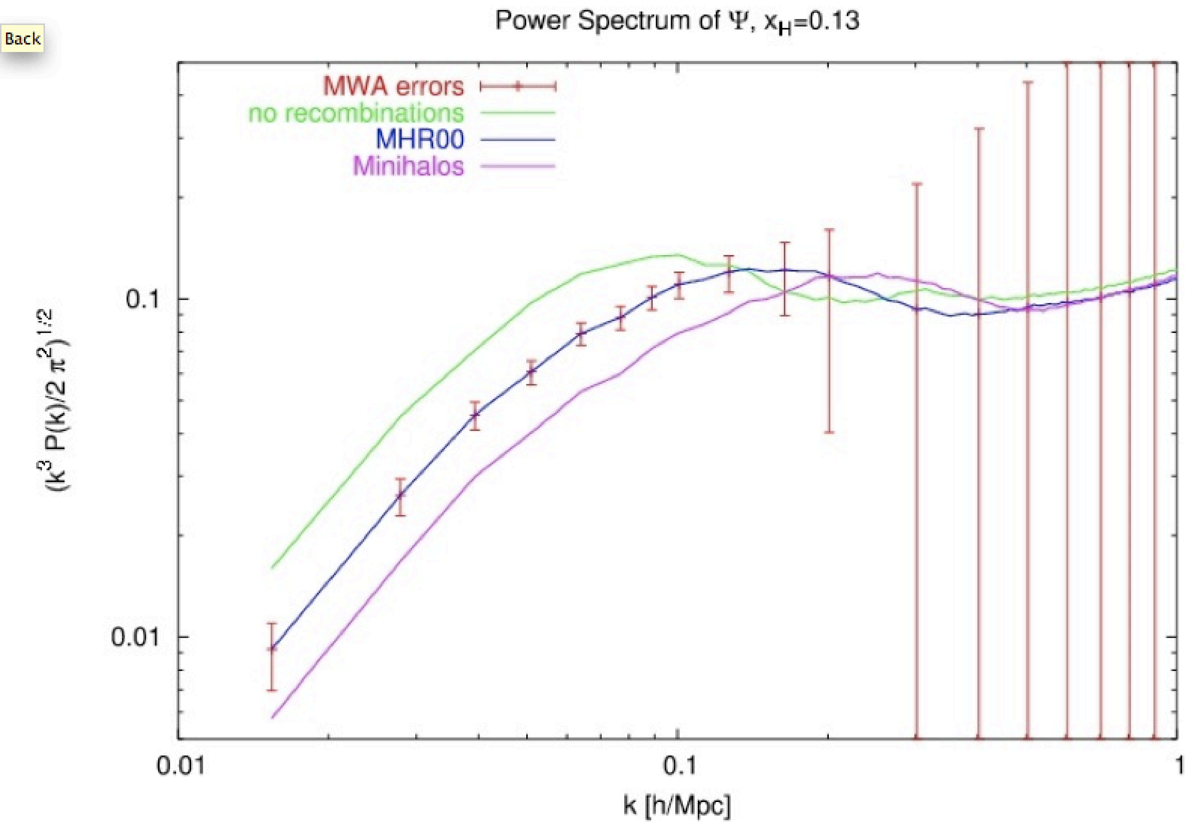

Back

Reionization on the light cone:

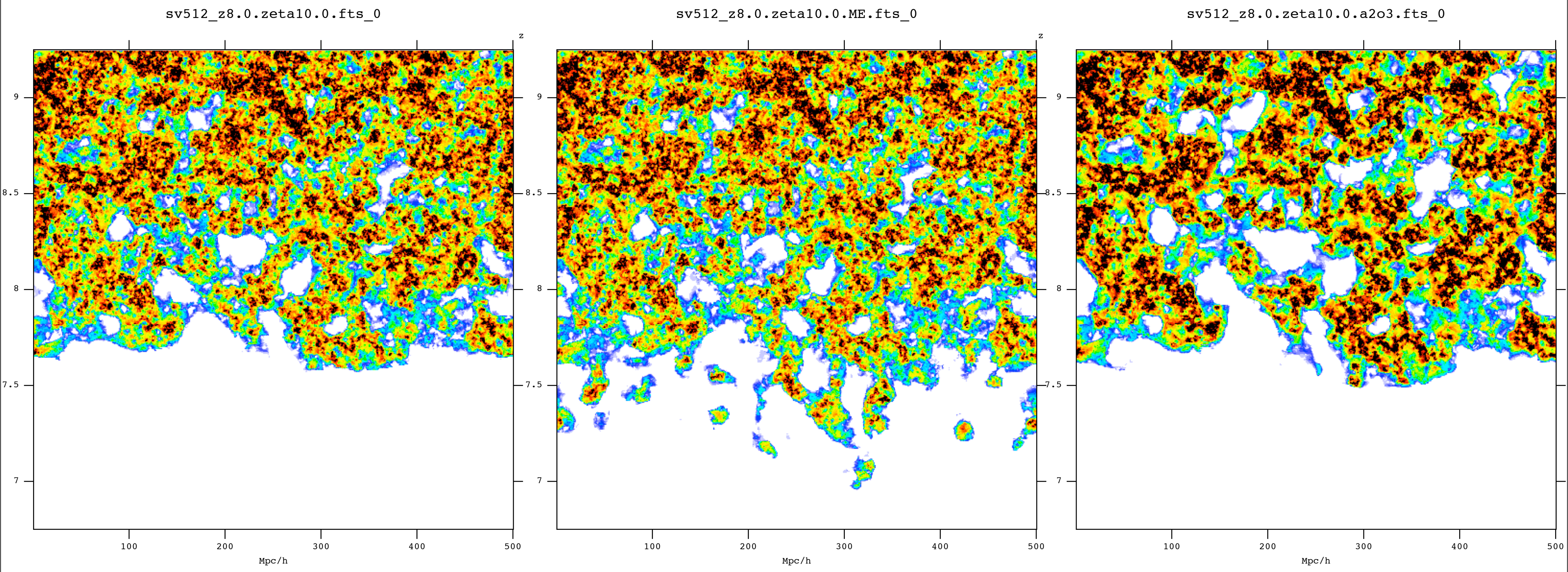

Ionization fraction

Reionization on the light cone:

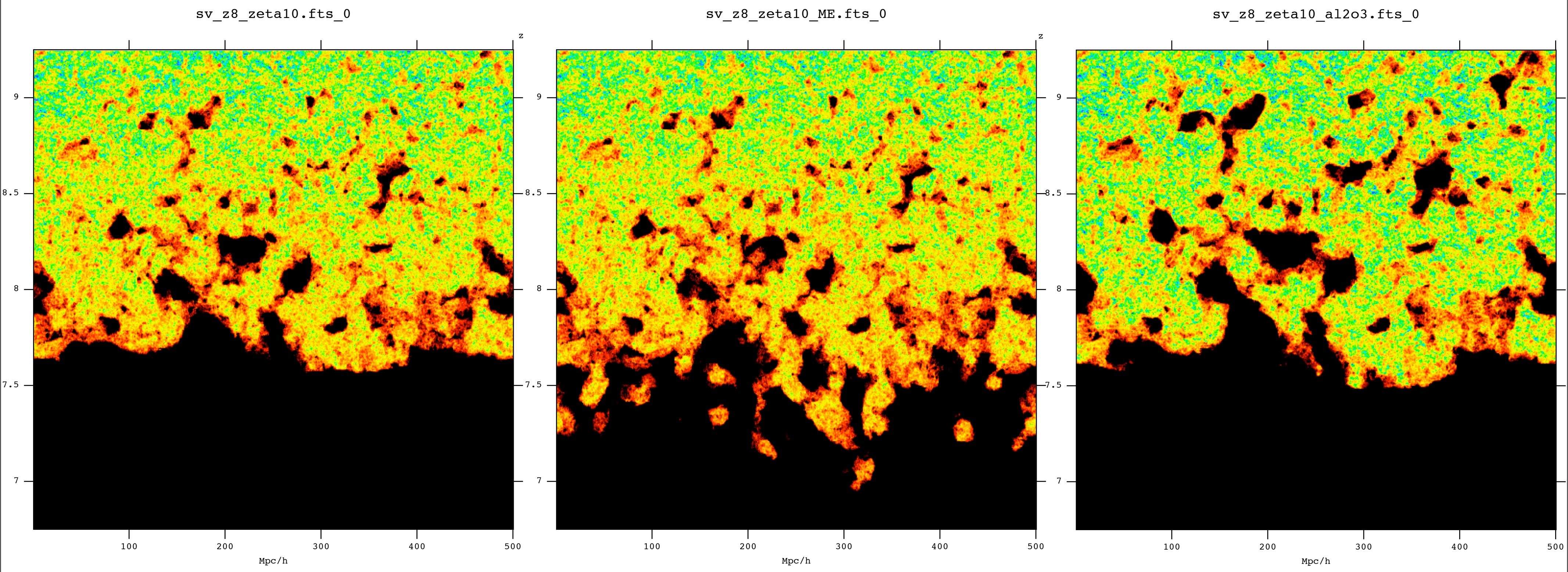

21 cm brightness fluctuation

Real space

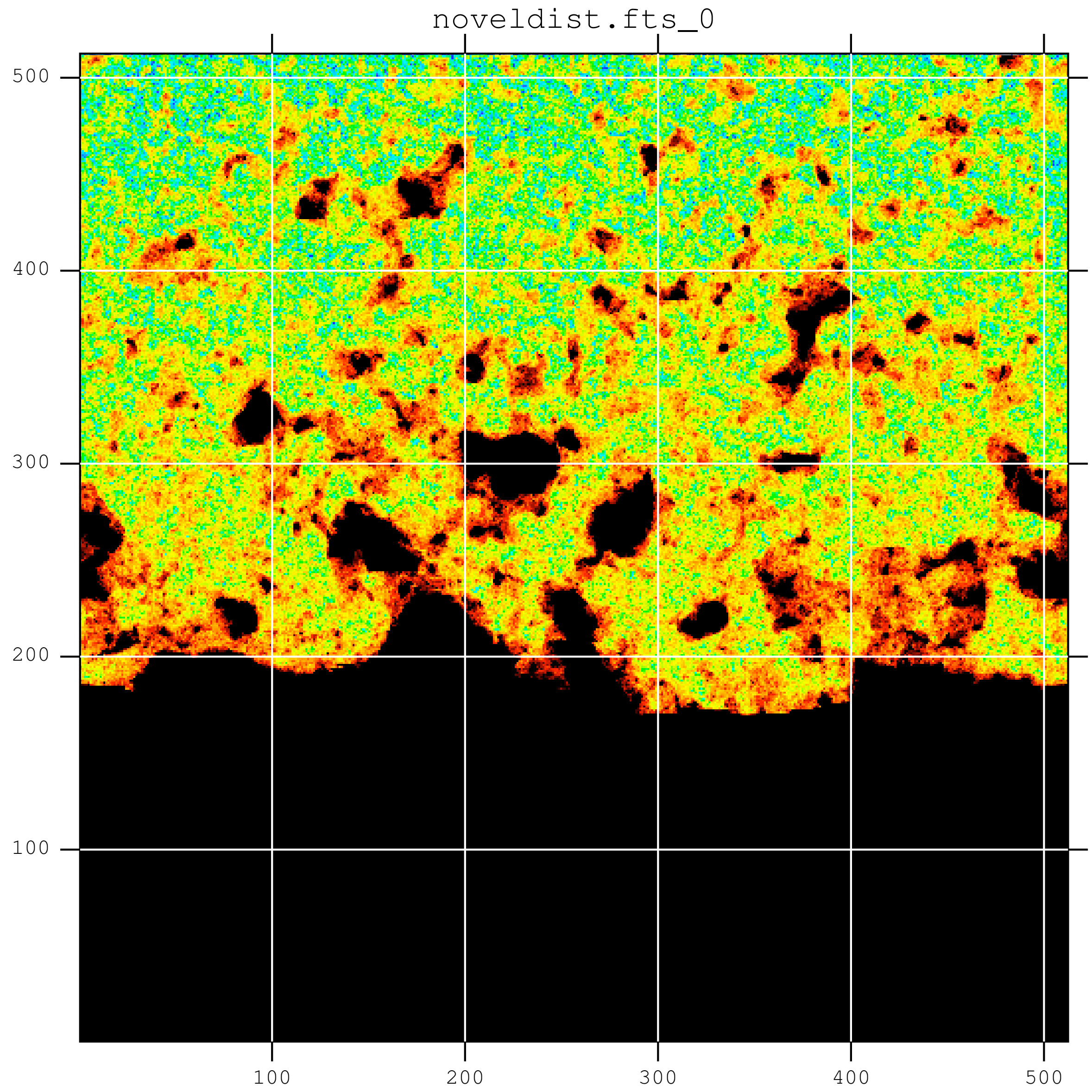

$$\vec{v}(\vec{k}z) = i\, f\, a\, H(a)\, \delta(\vec{k}, a)\, \vec{k}/k^2$$

Redshift space

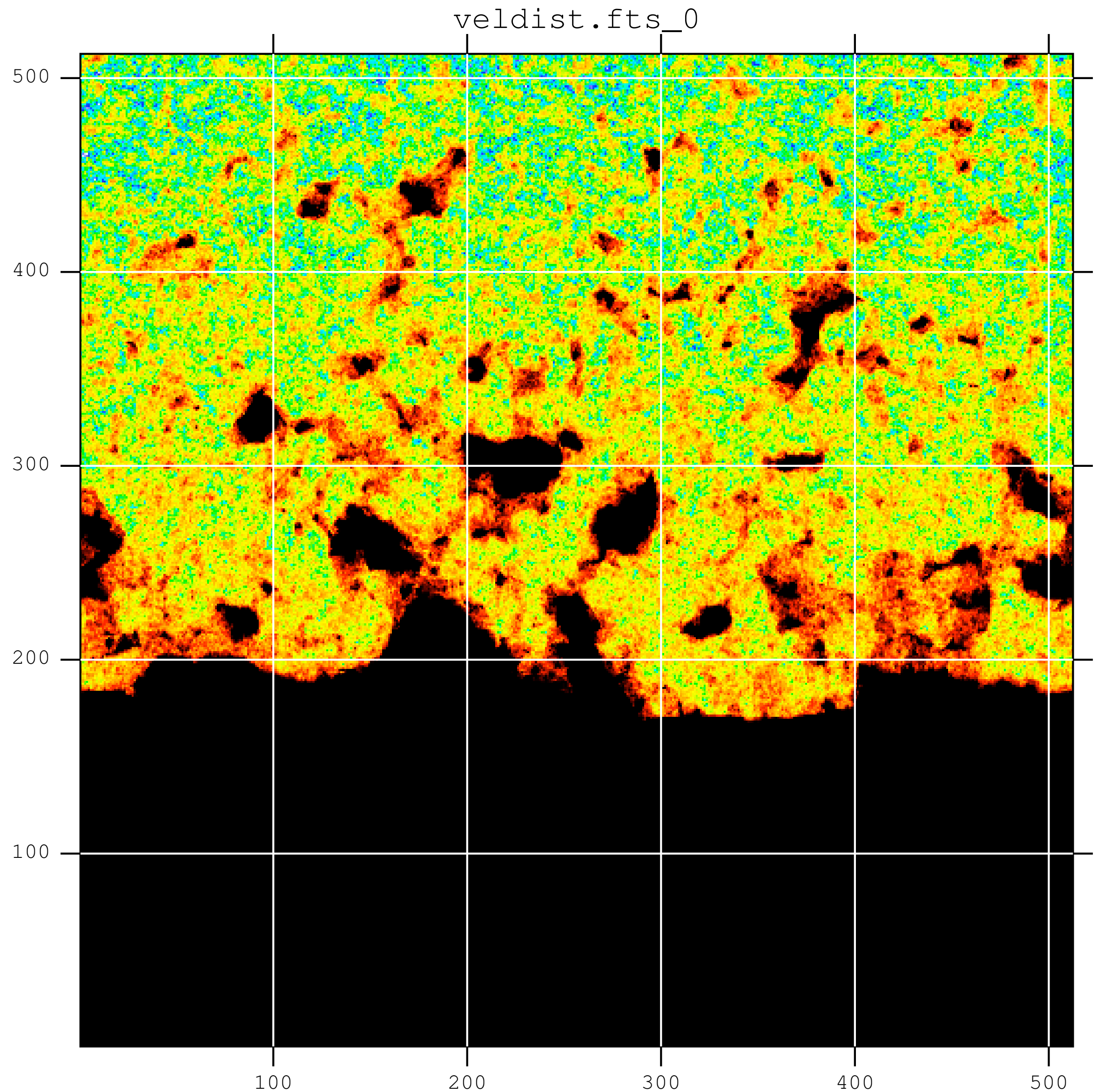

$$\vec{v}(\vec{k}\,z) = i\, f\, a\, H(a)\, \delta(\vec{k}, a)\, \vec{k}/k^2$$

Further evidence that the analytic model serves most practical purposes...

Dependence on sources (Zahn&Lidz et al. 2006):

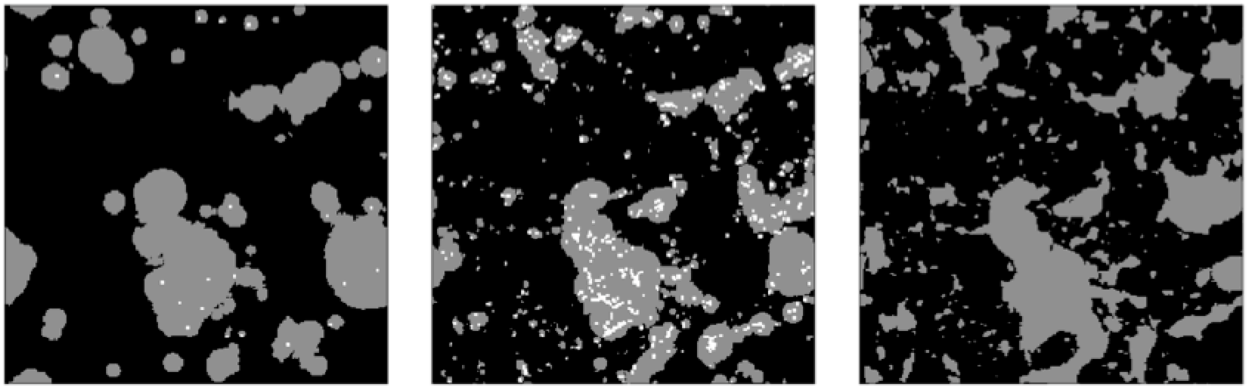

FIG. 8.— Dependence of reionization morphology on source density. In the *left panel* we show the ionization field from our halo-smoothing procedure using only sources (white points) with mass larger than $M \geq 4 \times 10^{10} M_\odot$ (note that some sources contributing to the ionized regions lie in front or behind the thin slice shown). With this choice, the number density of sources roughly matches that of $M \geq 2 \times 10^9 M_\odot$ sources at $z \sim 14$ (as in Iliev et al. 2005). The *center panel* shows the result with our usual source prescription, indicating a significantly more complex morphology. Finally the *right panel* shows, for comparison, the analytic model with $M_{\rm min} = 10^8 M_\odot$. Each panel is at $z = 7.26$, and in each case the source efficiencies are adjusted to match $x_{\rm i,v} = 0.35$.

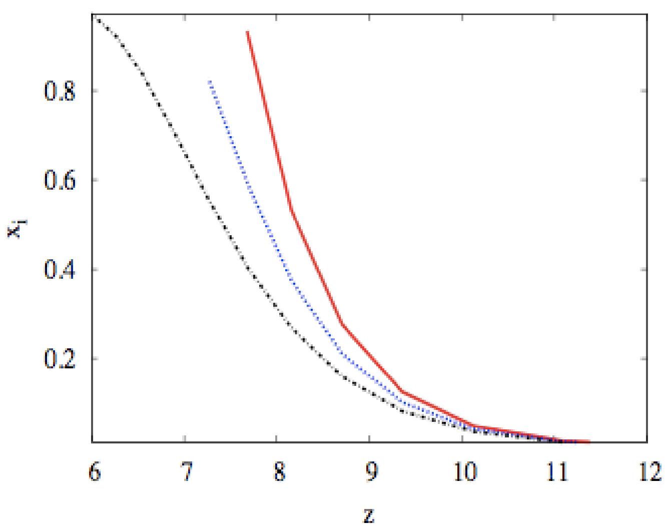

FIG. 9.— The volume-averaged ionization fraction for simulation M1 which has no minihalos (solid), M2 (dotted), and M3 (dash-dotted). In M3 the minihalos absorb more photons than in M2. All simulations have the same source prescription. The presence of minihalos extends the duration of reionization.

\`Collective' versus \`Poisson' reionization

Constraints on feedback and reionization will come from evolution of x

Feedback (McQuinn et al 2006):

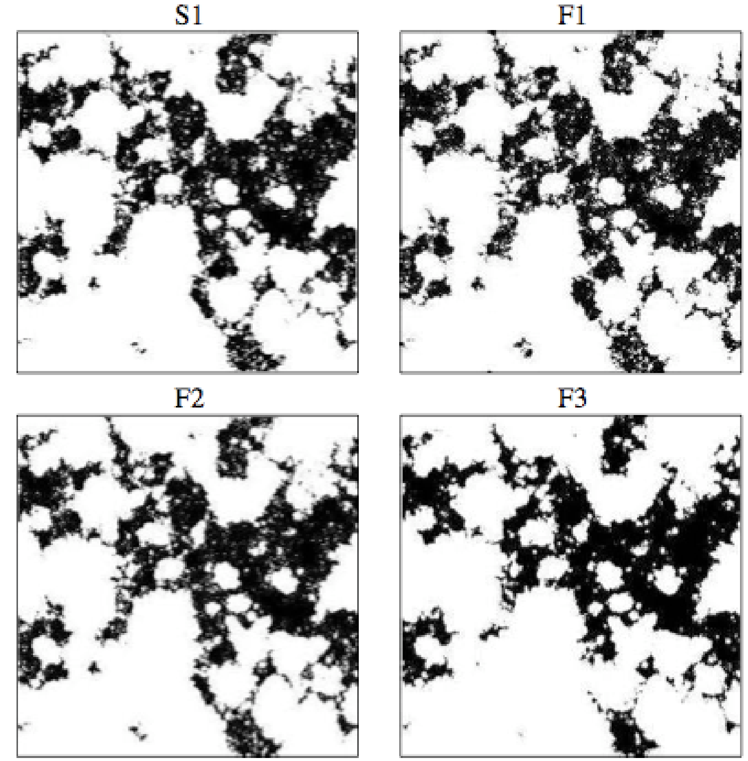

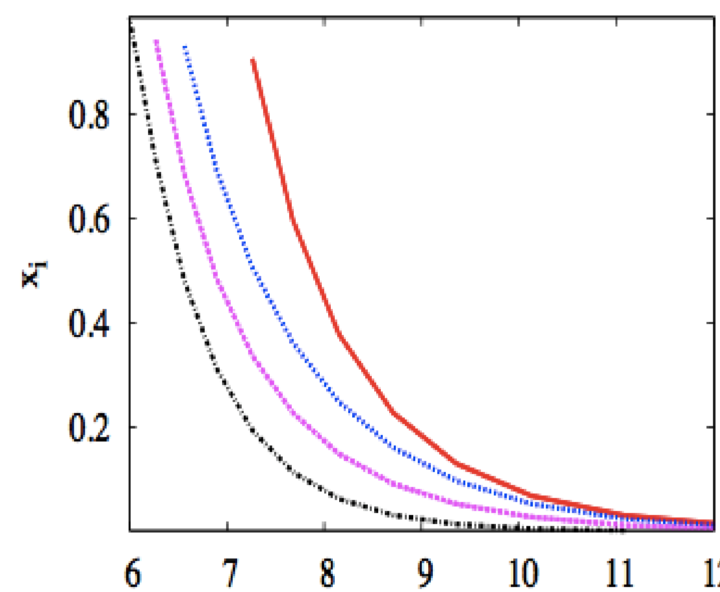

Comparison to only other LS RT simulation

•Iliev et al. (2005) `cookie-cutter' i.e. more bubbly morphology
•same particle resolution as we, similar ray tracing scheme
•one difference is that here reionization is happening at z=19-13, dominated by then very rare halos if not resolved down to the cooling mass

8 *I. T. Iliev, et al.*

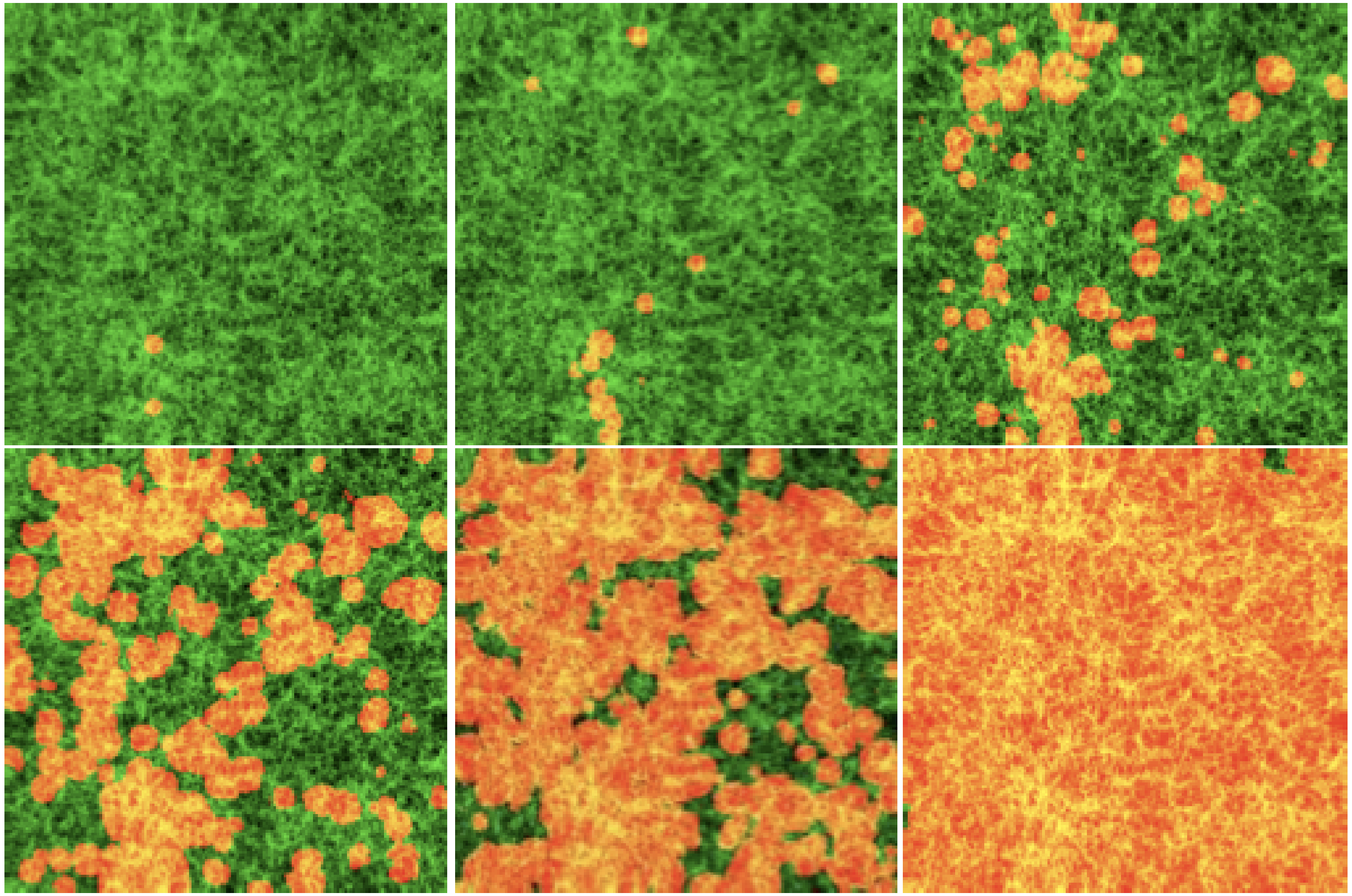

Figure 8. Slices through the simulation volume at redshifts $z = 18.5$, 16.1, 14.5, 13.6, 12.6 and 11.3. Shown are the density field (green in neutral regions, yellow in ionized regions) and the H II regions (red). See www.cita.utoronto.ca/$\sim$iliev/research.html for animations of this and other cuts through our simulation volume. For reference the simulation box angular size on the sky at this redshift range is from $\sim 45'$ (at $z = 18.5$) to $\sim 49'$ (at $z = 11.3$).

Benefits of the hybrid scheme

- within the hybrid scheme, we are able to capture non-spherical bubble structure
- we can quickly explore parameter spaces and gauge the importance of various physical effects (that are unknown) on the HII morphology. RT simulations still use many assumptions.
- side-by-side comparison with RT simulations can guide physical intuition.
- if we wanted to capture all halos/sources potentially responsible for reionization in a radiative transfer simulation, we would have to run a prohibitively large simulation:

$$\rho_{\rm crit} \simeq 10^{-29}\,\frac{g}{cm^3} \simeq 1.4\times10^{17}\,\frac{M_\odot}{(100\,{\rm Mpc})^3}$$

=> to resolve the typical cooling mass into 32 particles, would need $\frac{1.4\times10^{17}}{3\times10^{6}} = 4.6\times10^{10} \simeq 3500^3$ particles!

Instead, save electricity and use the analytic model :-)

Evolution of HII, 100 Mpc/h z=8, zeta=10, 1 sec.=10 Million years:

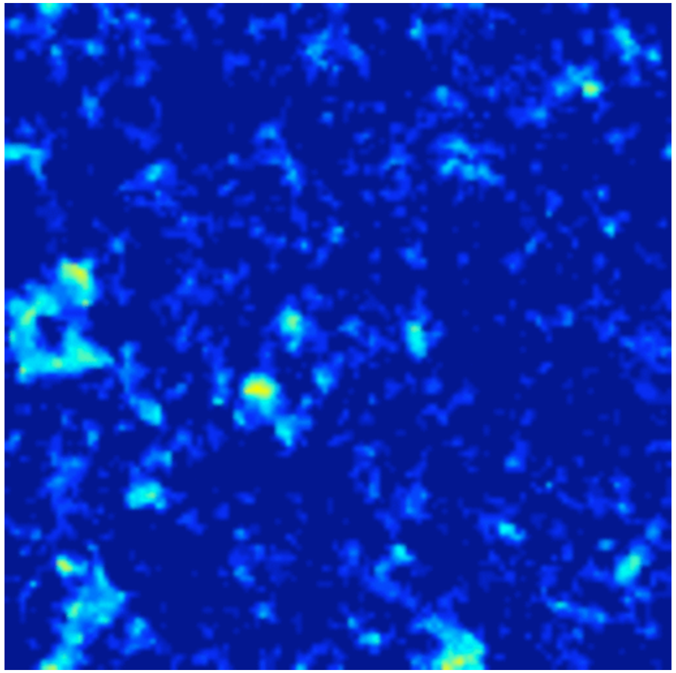

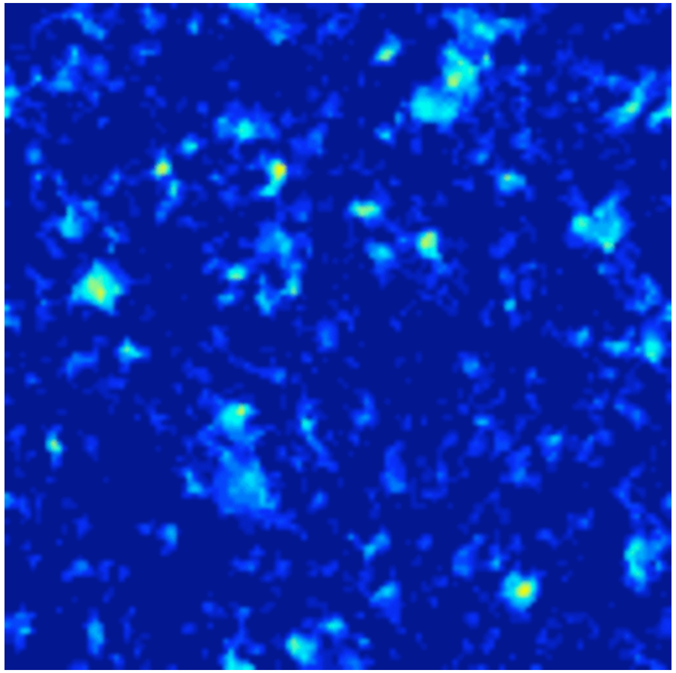

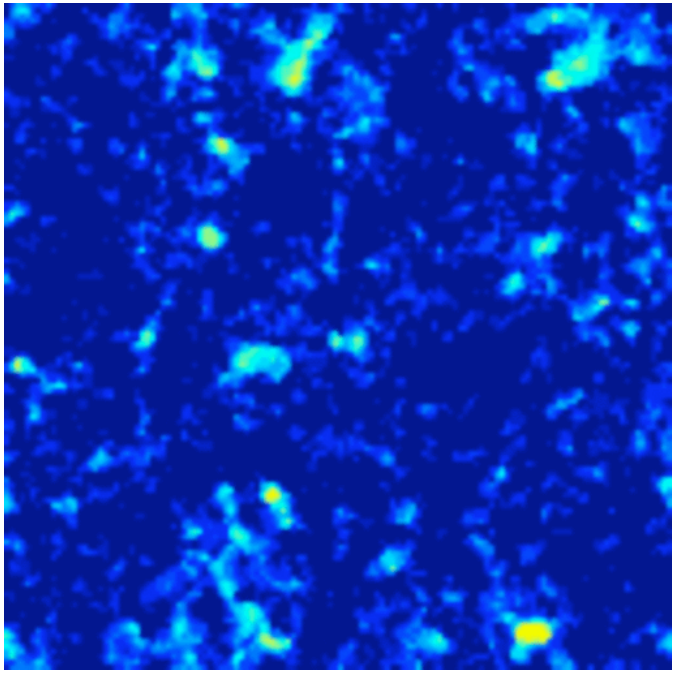

Flying from z=16-11at 2e15c

500 Mpc/h
~4 degrees

Flying from z=16-11at 2e15c

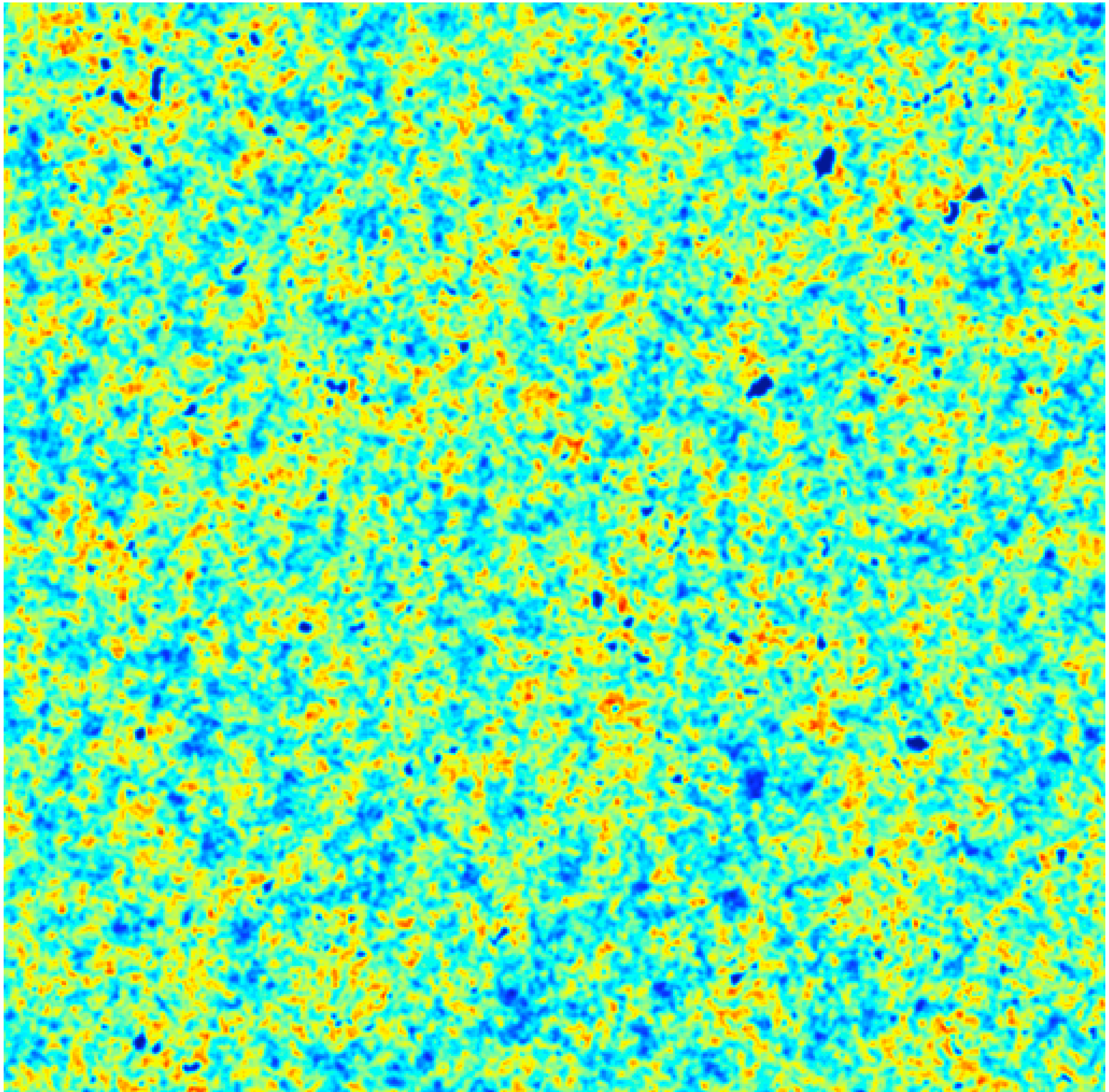

500 Mpc/h
~4 degrees

Questions:

- when we calculate the 21 cm power spectrum, used N-body delta. Naive thought that Gaussian random fields represent density well enough at z>6.
- why is the resulting small scale 21 cm power much larger than when using GRF's for density?

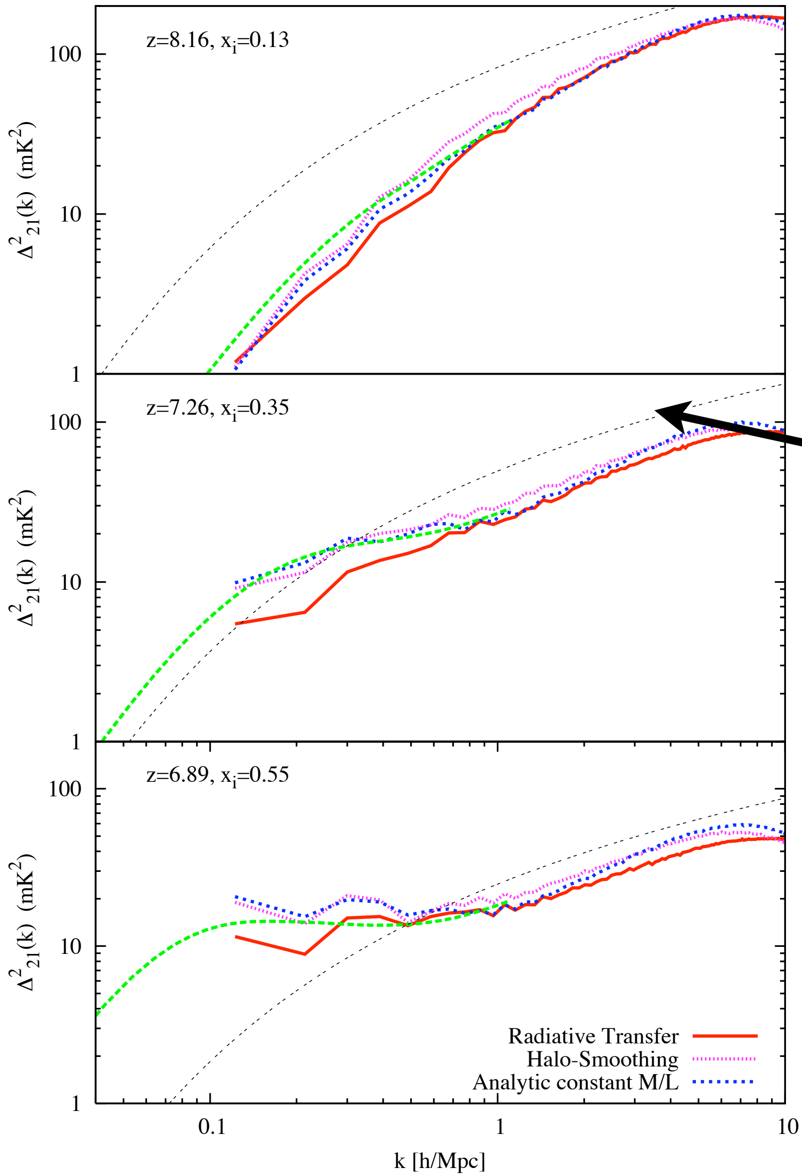

$\langle(1+\mu^2)^2\rangle$

$$1.87\,\overline{x}_H^2\,\overline{T}_b^2\,P_{\delta\delta}$$

same `Kaiser factor' as in galaxy surveys

The 21 cm power spectrum in pieces

$$\delta T(\nu) \approx 26\, x_H (1+\delta_\rho) \left(\frac{T_S - T_{\rm CMB}}{T_S}\right) \left(\frac{\Omega_b h^2}{0.022}\right) \left[\left(\frac{0.15}{\Omega_m h^2}\right) \left(\frac{1+z}{10}\right)\right]^{1/2} \mathrm{mK}$$

$$\delta T(\nu) \approx T_b\, \overline{x}_H (1+\delta_x)(1+\delta_\rho)$$

$$\Delta^2_{21}(k) = \langle T_b\rangle^2 \langle x_H\rangle^2 [\underbrace{\Delta^2_{\delta_{\rm x},\delta_{\rm x}}(k) + 2\Delta^2_{\delta_{\rm x},\delta_\rho}(k) + \Delta^2_{\delta_\rho,\delta_\rho}(k)}_{\text{low order terms}} + \underbrace{2\Delta^2_{\delta_{\rm x}\delta_\rho,\delta_{\rm x}}(k) + 2\Delta^2_{\delta_{\rm x}\delta_\rho,\delta_\rho}(k) + \Delta^2_{\delta_{\rm x}\delta_\rho,\delta_{\rm x}\delta_\rho}(k)}_{\text{3 and 4 point function terms}}]$$

Lidz&Zahn et al(2006b)

The (large) higher order contributions to the 21 cm power spectrum

- In gravitational clustering paradigm, small scale structure formation is faster in large scale overdensities, could these effects matter at high z?
- to get a feel, expand density to 2nd order EPT, valid on small scales, where ionization fraction contributions small
- for the two `three-point' terms we find:

$$P_{\delta_x\delta_\rho,\delta_\rho}(k_1) \sim \frac{45}{21} P_{\delta_\rho,\delta_\rho}(k_1) \int d\ln k_3 \Delta^2_{\delta_x,\delta_\rho}(k_3)$$

`density coupling term'

$$P_{\delta_x\delta_\rho,\delta_x}(k_1) \sim \frac{34}{21} P_{\delta_\rho,\delta_x}(k_1) \int d\ln k_3 \Delta^2_{\delta_x,\delta_\rho}(k_3)$$

`bubble coupling term'

- first term: integral gives ~-0.25, so effects roughly -2 times the density power spectrum.
- this trend will be reversed in models where reionization is `outside-in'
- second term is more important on large scales

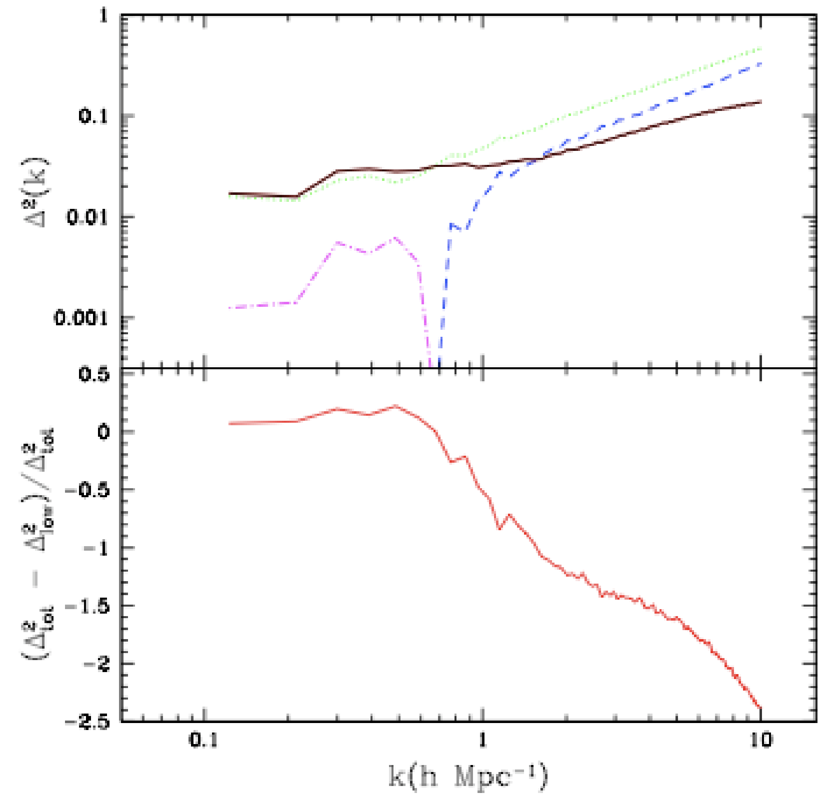

FIG. 1.— Importance of higher-order terms for 21 cm power spectrum calculations. *Top panel:* The black solid line shows the simulated 21 cm power spectrum in real (as opposed to redshift) space at $z = 6.89$, at which point the volume-weighted ionization fraction is $x_{i,v} = 0.48$. The green dotted line shows the contribution to the 21 cm power spectrum from the low-order terms. The magenta dot-dashed line shows the sum of the higher order terms for wave-numbers in which the sum is positive, while the blue dashed line shows the absolute value of the sum where it is negative. *Bottom panel:* The fractional contribution of the higher order terms as a function of scale. On small scales, our results differ from the low-order expectation at the $\sim 100 - 250\%$ level.

Mode-coupling can not be neglected in modeling!

dependence on box-size

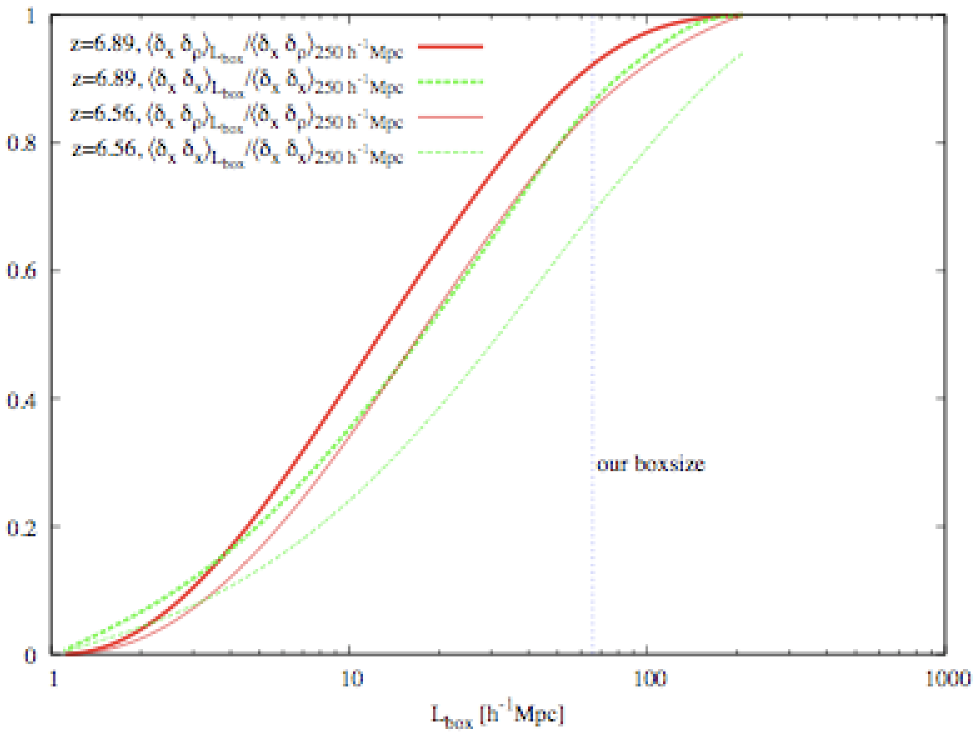

sensitivity to source properties

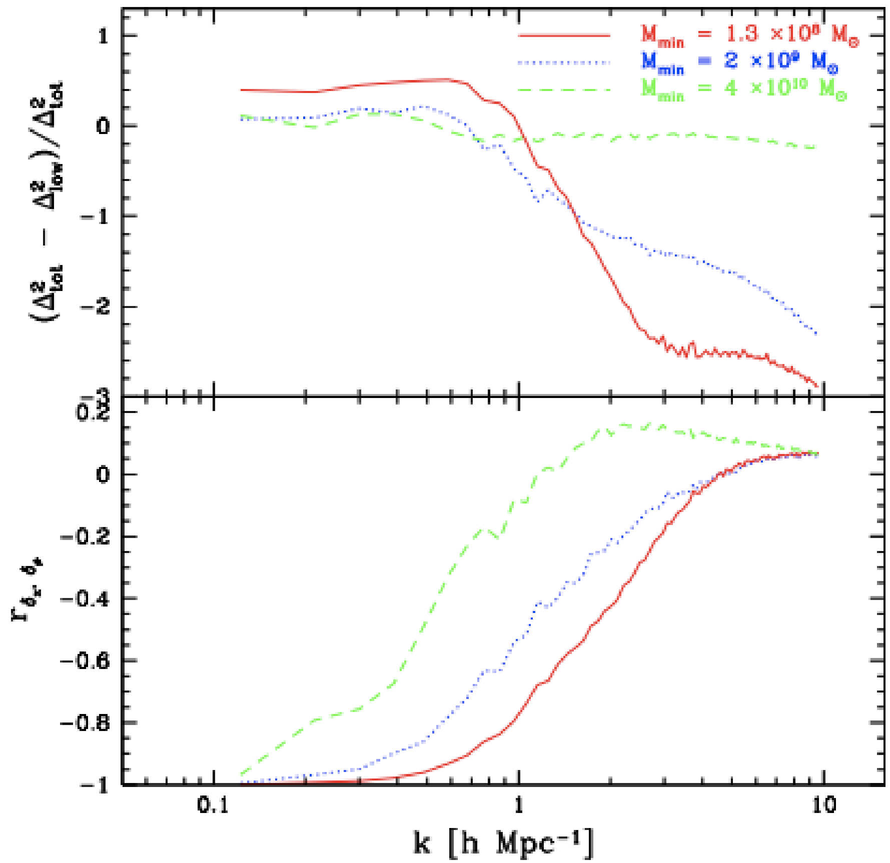

So what will happen to our fast `hybrid' scheme (originally based on Gaussian random fields)?.......

...it turns out that for the redshifts of interest, second order Lagrangian perturbation theory (2LPT) gives us all we need.

$$\boldsymbol{x} = \boldsymbol{q} - D_1 \nabla_q \phi^{(1)}(\boldsymbol{q}) + D_2 \nabla_q \phi^{(2)}(\boldsymbol{q})$$

$$\nabla^2 \phi^{(1)}(\boldsymbol{q}) = \delta^{(1)}(\boldsymbol{q}),$$

$$\nabla^2 \phi^{(2)}(\boldsymbol{q}) = \sum_{i>j} \{ \phi_{ii}^{(1)}(\boldsymbol{q}) \phi_{jj}^{(1)}(\boldsymbol{q}) - [\phi_{ij}^{(1)}]^2 \}$$

Buchert et al 1994, Scoccimarro 1998

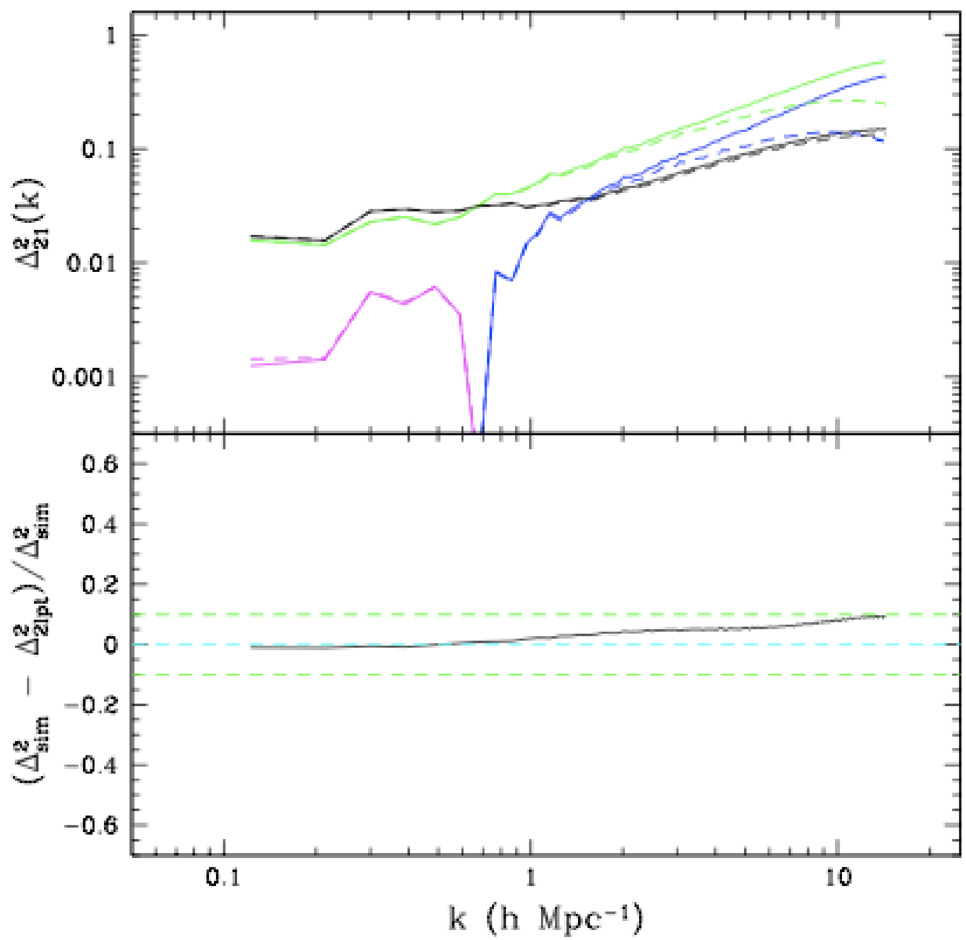

better than 10% agreement on scales of interest

redshift space evolution (in redshift space) of the higher order contributions

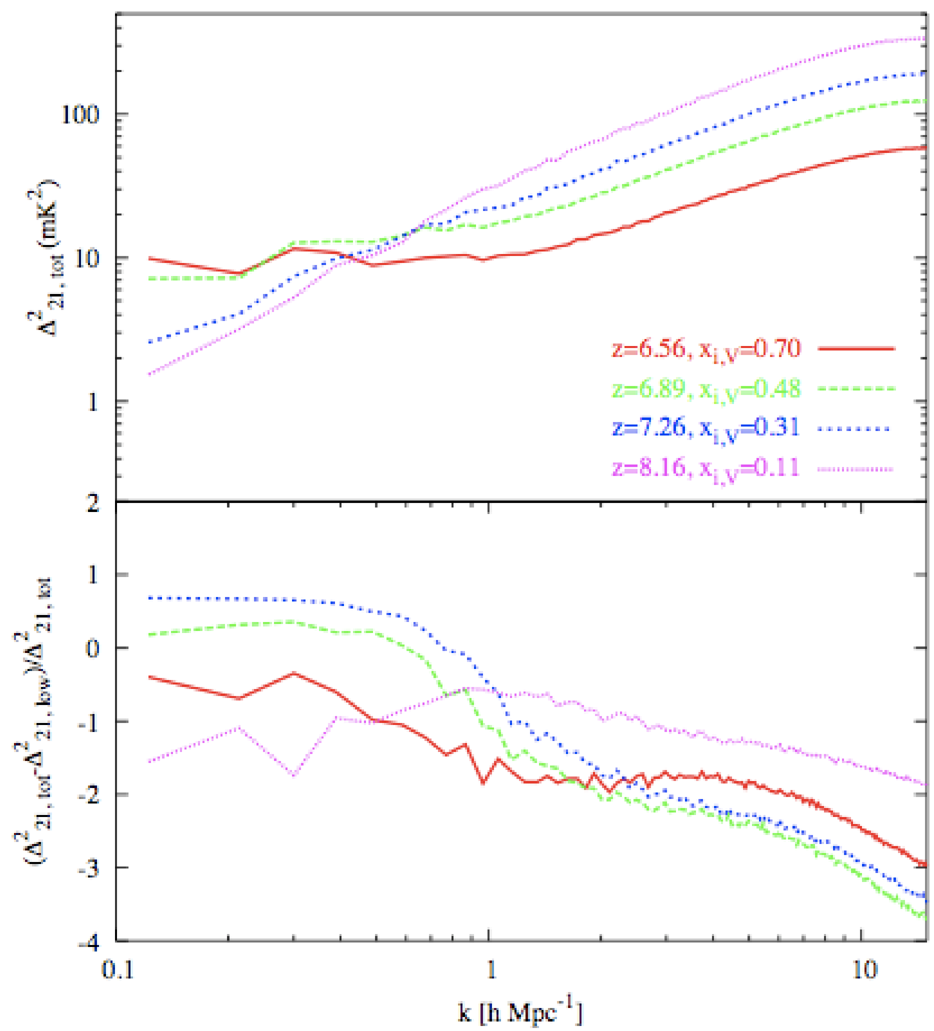

So how much will 1st and 2nd generation experiments be able to tell us about bubble morphology and evolution?

power spectrum sensitivity in the spherically averaged case:

$$\delta P_{\Delta T}(k) = \left[\sum_{\theta} \left(\frac{1}{\delta P_{\Delta T}(k,\theta)} \right)^2 \right]^{-1/2}$$

$$\approx \left[k^3 \int_{\arccos[\min(\frac{yk}{2\pi},1)]}^{\arcsin[\min(\frac{k_*}{k},1)]} d\theta \, \sin(\theta) \, \frac{1}{\left(D\, P_{21\mathrm{cm}}(k) + \frac{E}{n(k \sin(\theta))} \right)^2} \right]^{-1/2}$$

$$D = \sqrt{\frac{(2\pi)^2 \, A_e}{\lambda^2 \, x^2 \, y \, \epsilon}} \qquad E = \frac{2\pi \sqrt{x^2 y} \, \lambda^3 \, T_{\mathrm{sys}}^2}{\sqrt{\epsilon} \, A_e^{3/2} \, (B \, t_0)},$$

(Modulo connected 4-point function terms that increase variance and correlate different k...)

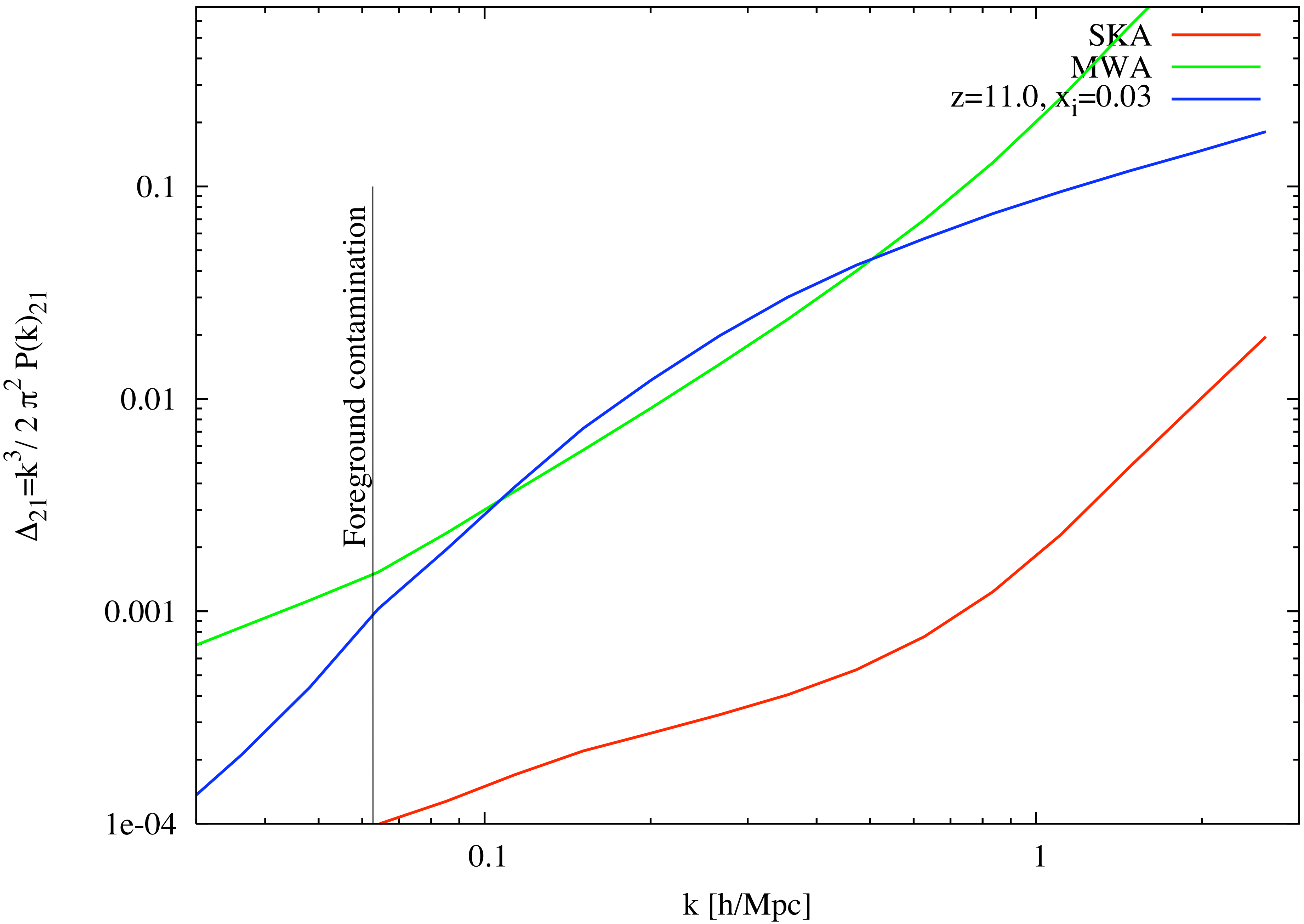
SKA
MWA
z=11.0, x_i=0.03
Foreground contamination
0.1
0.01
0.001
1e-04
0.1
1
k [h/Mpc]
Δ_21=k^3/ 2 π^2 P(k)_21

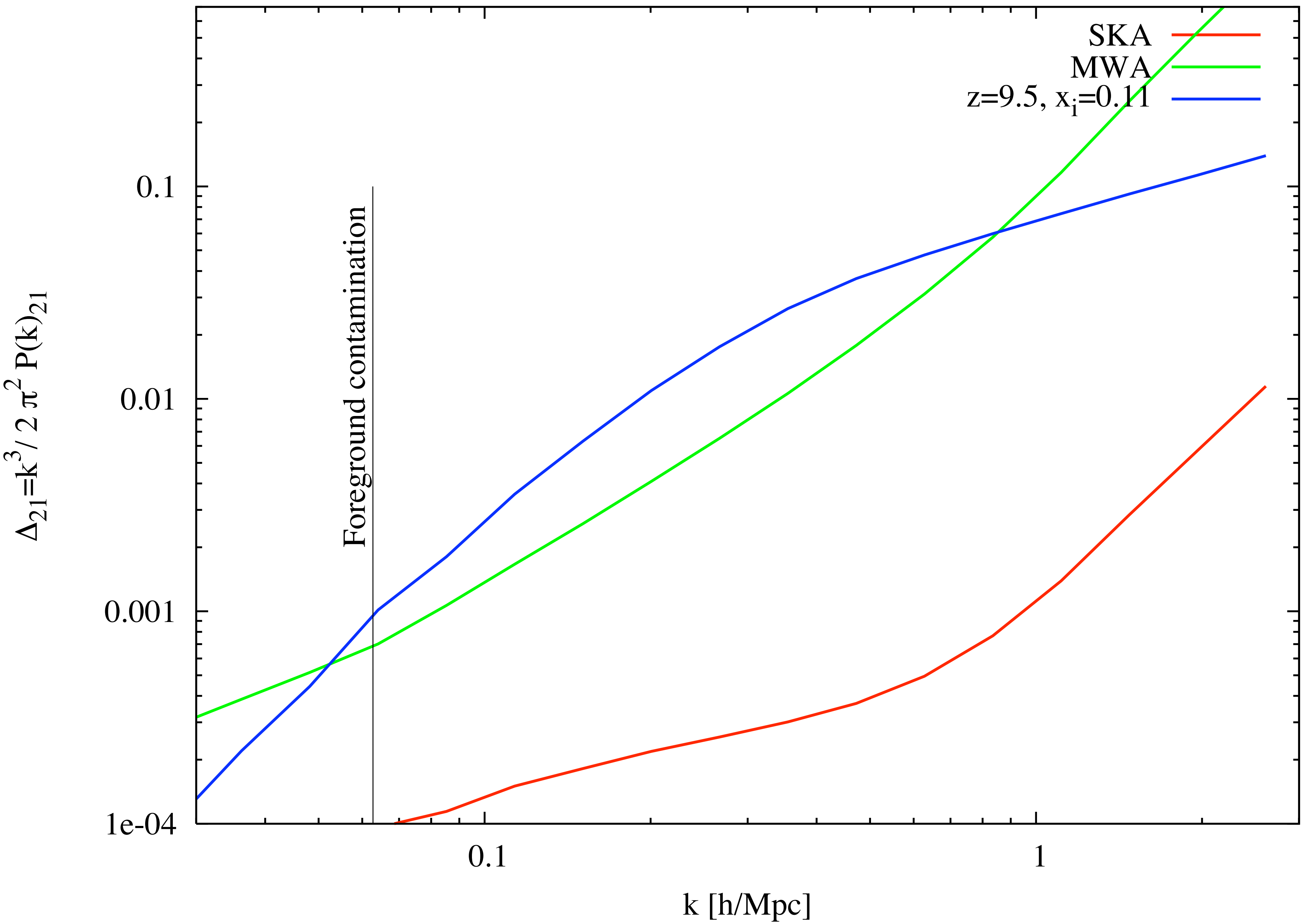

SKA
MWA
z=9.5, x_i=0.11
Foreground contamination
0.1
0.01
0.001
1e-04
0.1
1
k [h/Mpc]
Δ_21=k^3/ 2 π^2 P(k)_21

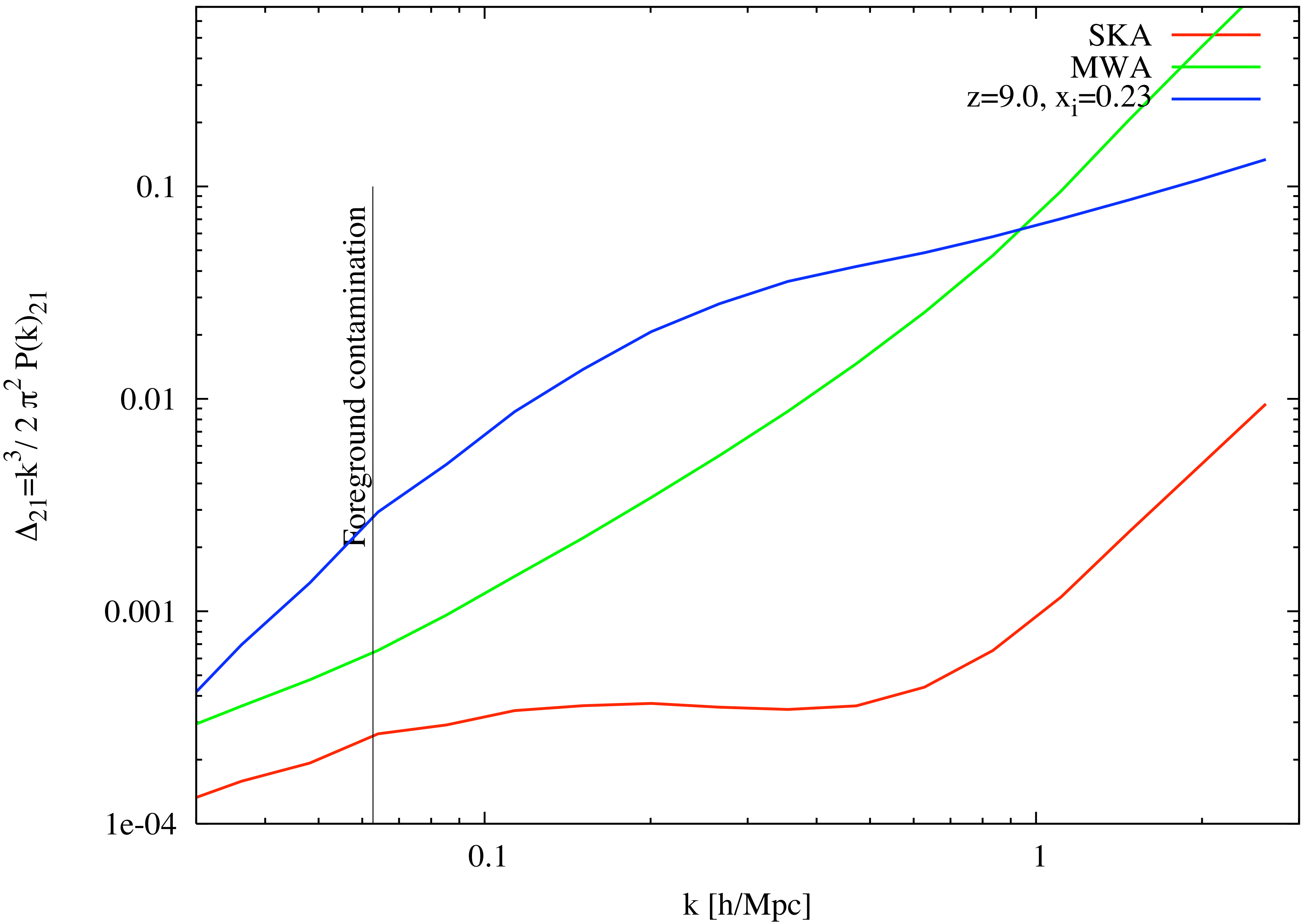
SKA
MWA
z=9.0, x_i=0.23
Foreground contamination
$\Delta_{21}=k^3/2\pi^2 P(k)_{21}$
k [h/Mpc]
0.1
0.01
0.001
1e-04
0.1
1

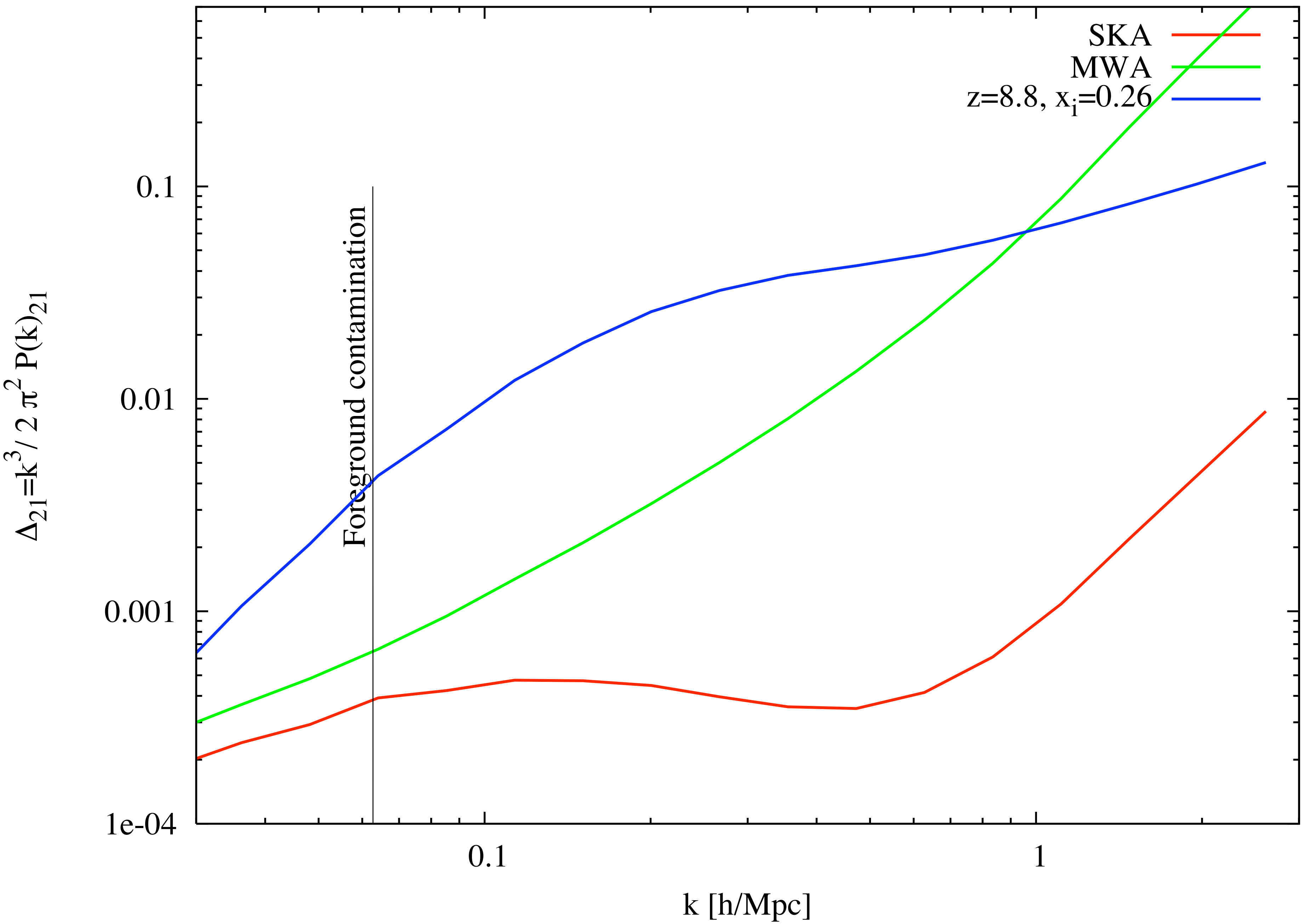

SKA
MWA
z=8.8, x_i=0.26
Foreground contamination
$\Delta_{21}=k^3/2\pi^2 P(k)_{21}$
k [h/Mpc]
1e-04
0.001
0.01
0.1
0.1
1

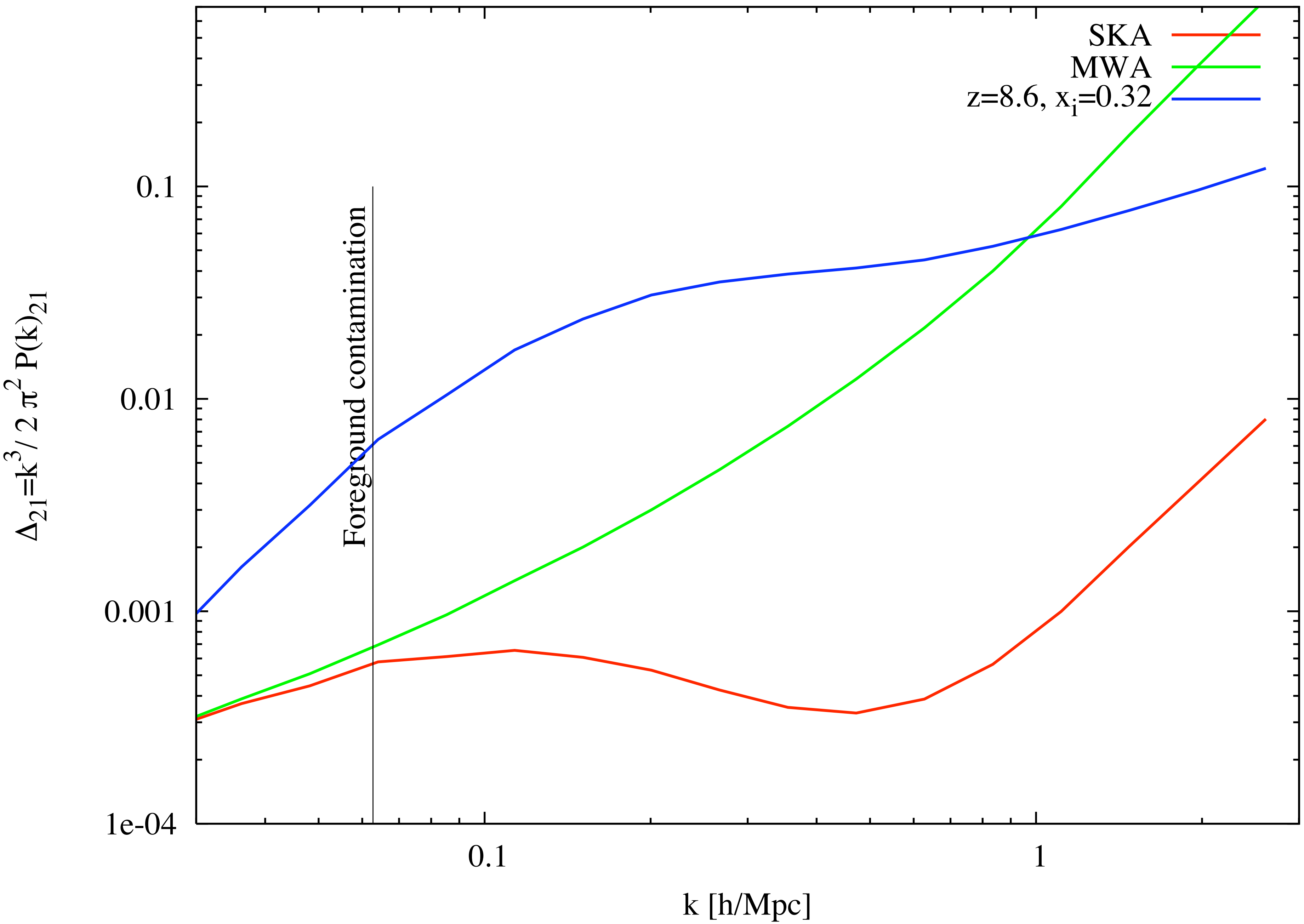

SKA
MWA
z=8.6, x_i=0.32
Foreground contamination
$\Delta_{21}=k^3/2\pi^2 P(k)_{21}$
k [h/Mpc]
0.1
0.01
0.001
1e-04
0.1
1

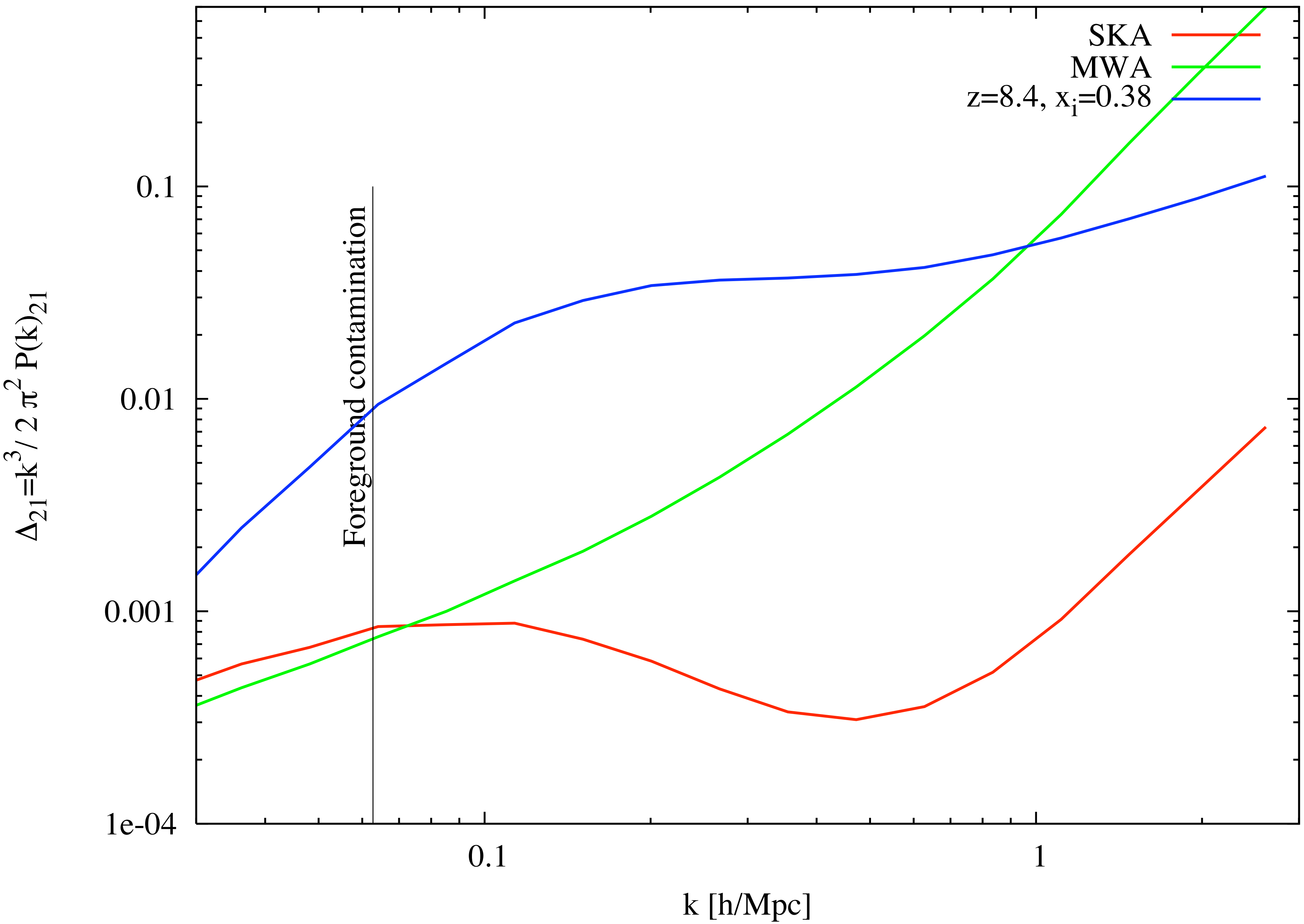

SKA
MWA
z=8.4, x_i=0.38
Foreground contamination
$\Delta_{21}=k^3/2\pi^2 P(k)_{21}$
k [h/Mpc]
0.1
0.01
0.001
1e-04
0.1
1

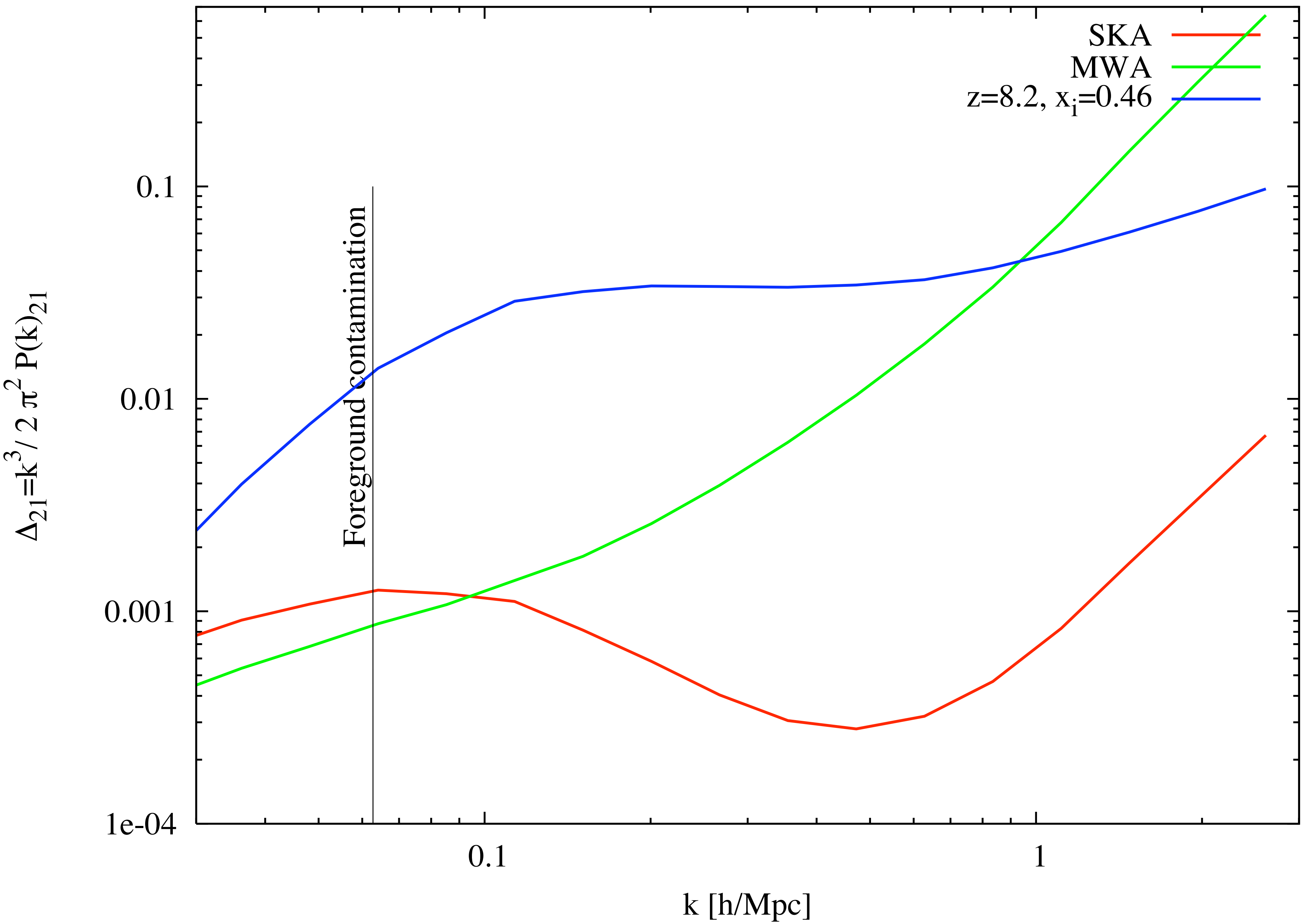

SKA
MWA
z=8.2, x_i=0.46
Foreground contamination
$\Delta_{21}=k^3/2\pi^2 P(k)_{21}$
k [h/Mpc]
0.1
0.01
0.001
1e-04
0.1
1

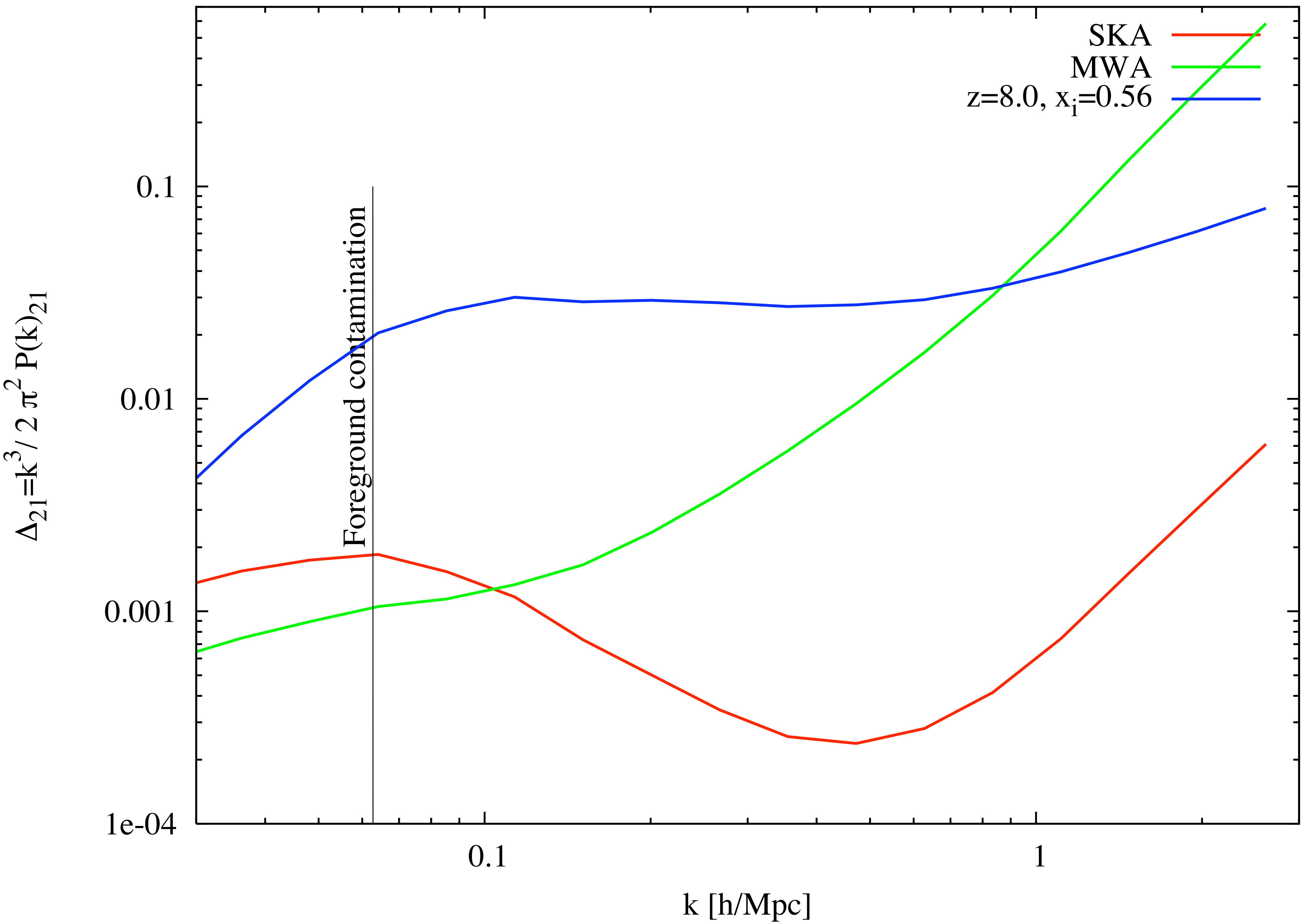

SKA
MWA
z=8.0, x_i=0.56
Foreground contamination
$\Delta_{21}=k^3/2\pi^2 P(k)_{21}$
k [h/Mpc]
0.1
0.01
0.001
1e-04
0.1
1

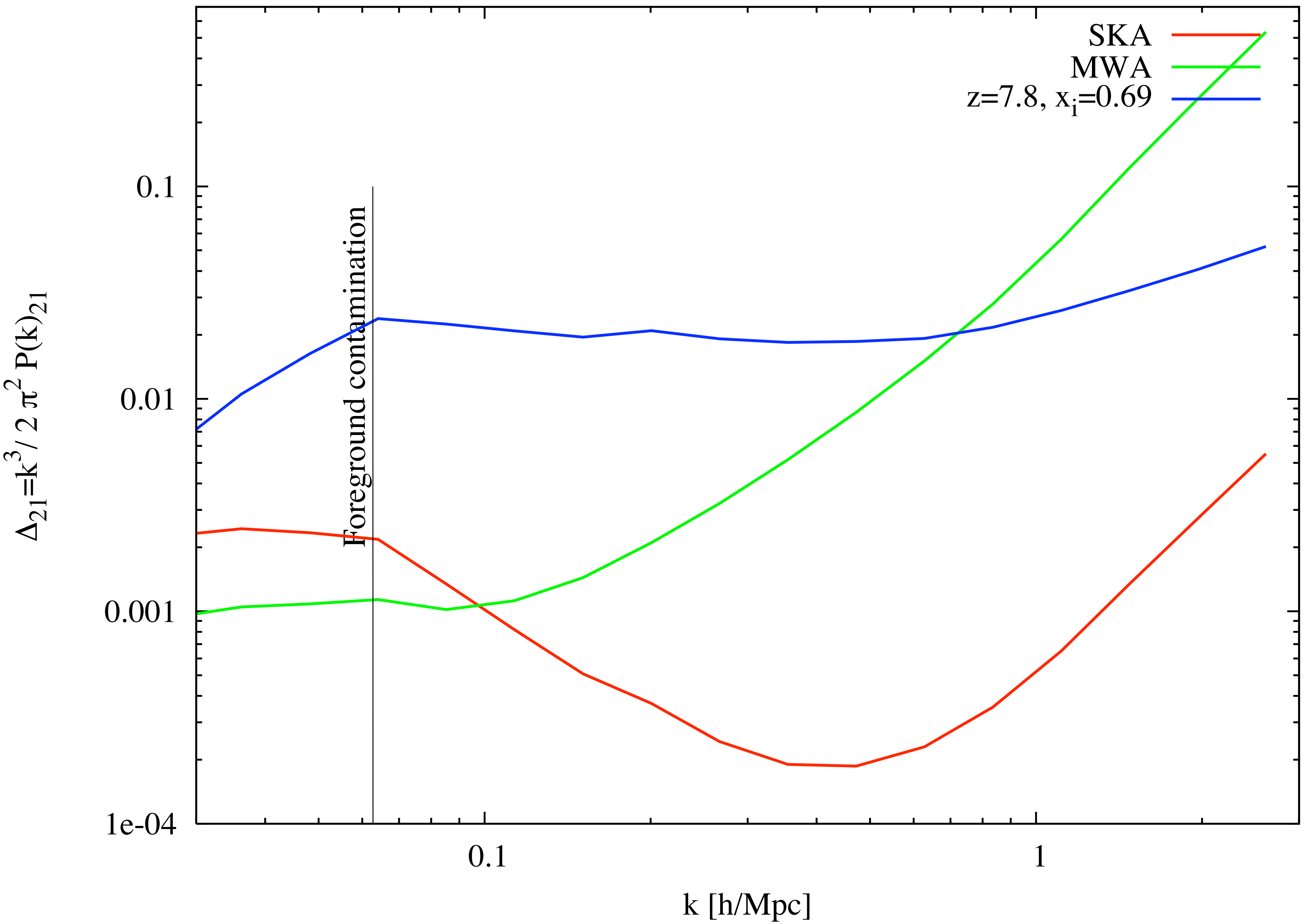

SKA
MWA
z=7.8, x_i=0.69
Foreground contamination
0.1
0.01
0.001
1e-04
0.1
1
k [h/Mpc]
$\Delta_{21}=k^3/2\pi^2 P(k)_{21}$

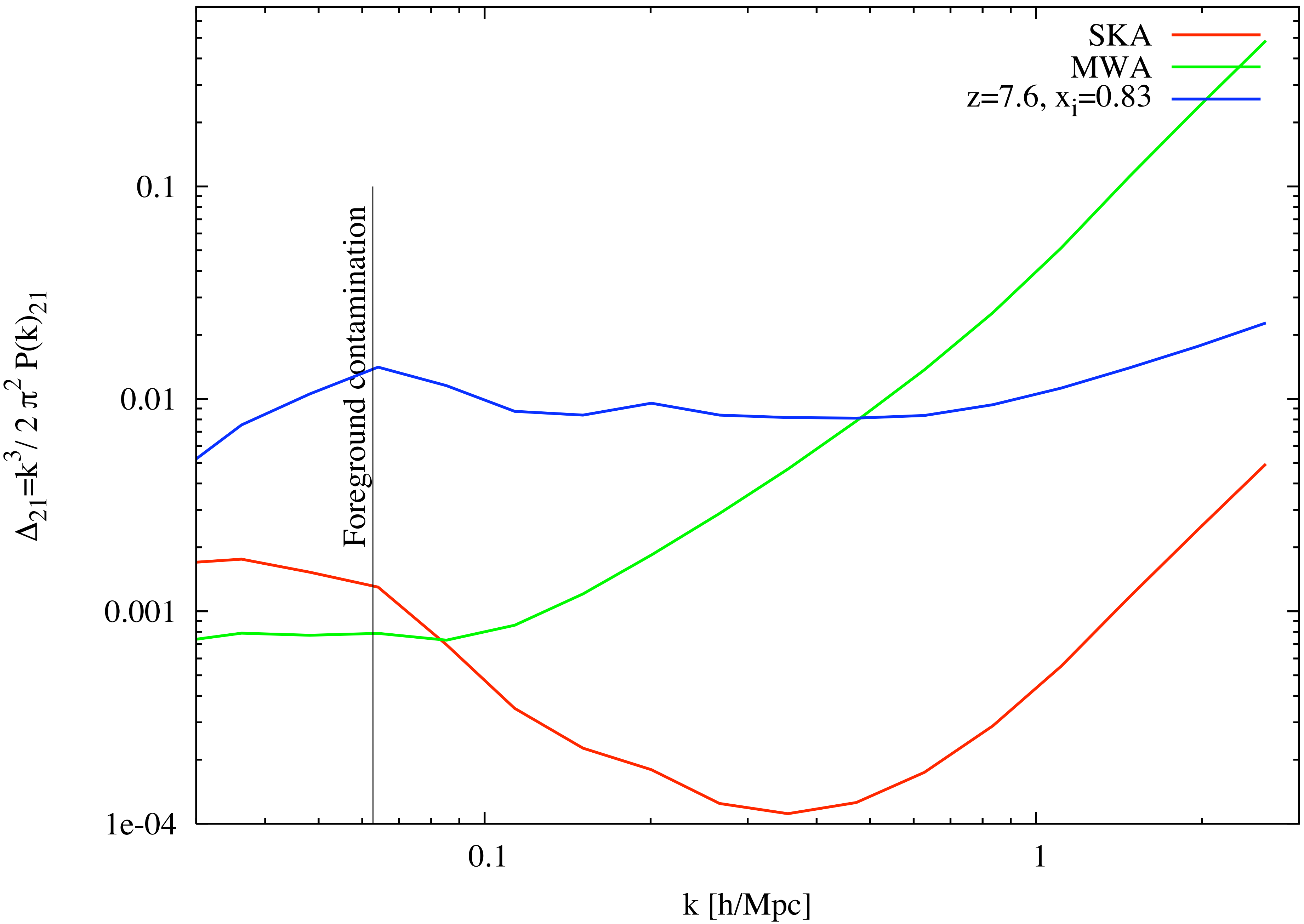
SKA
MWA
z=7.6, x_i=0.83
Foreground contamination
0.1
0.01
0.001
1e-04
0.1
1
k [h/Mpc]
$\Delta_{21}=k^3/\,2\,\pi^2\,P(k)_{21}$

Reionization parameter space exploration

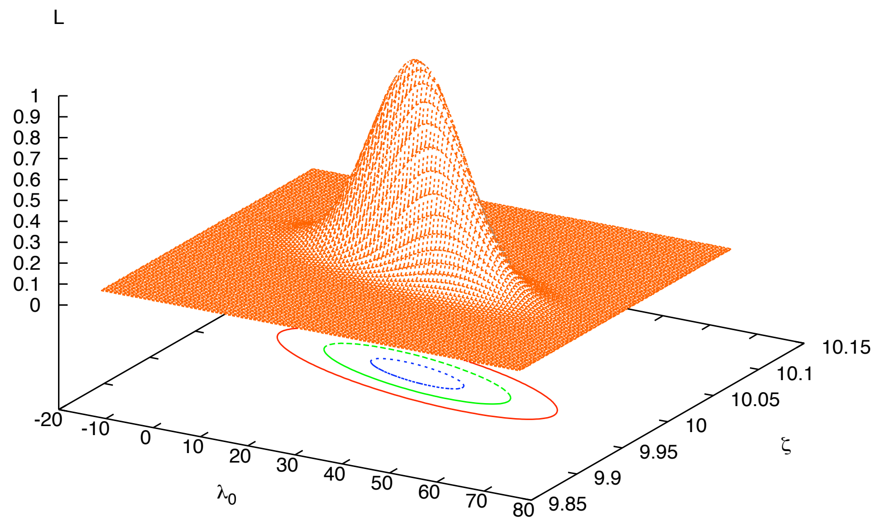

$\Delta x_H = 0.04$ (0.15) for SKA (MWA)

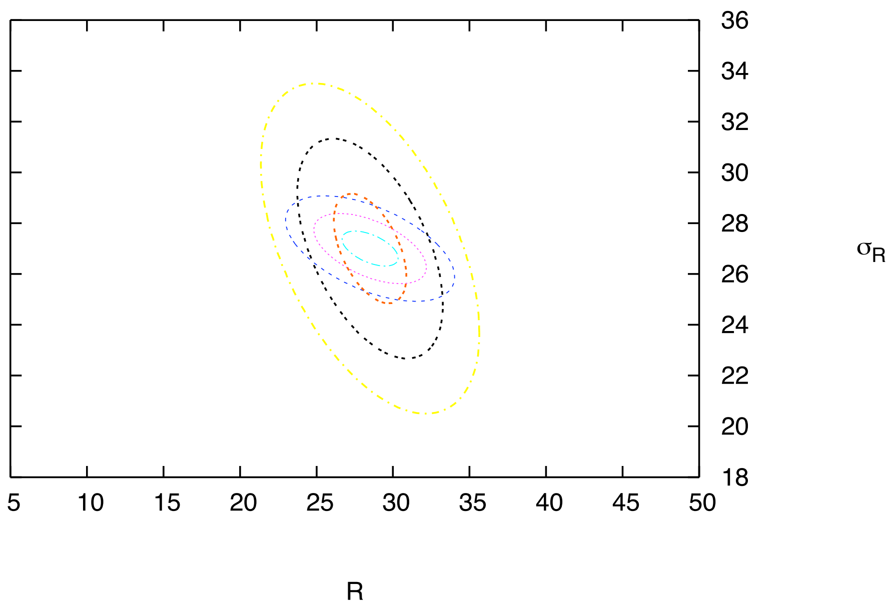

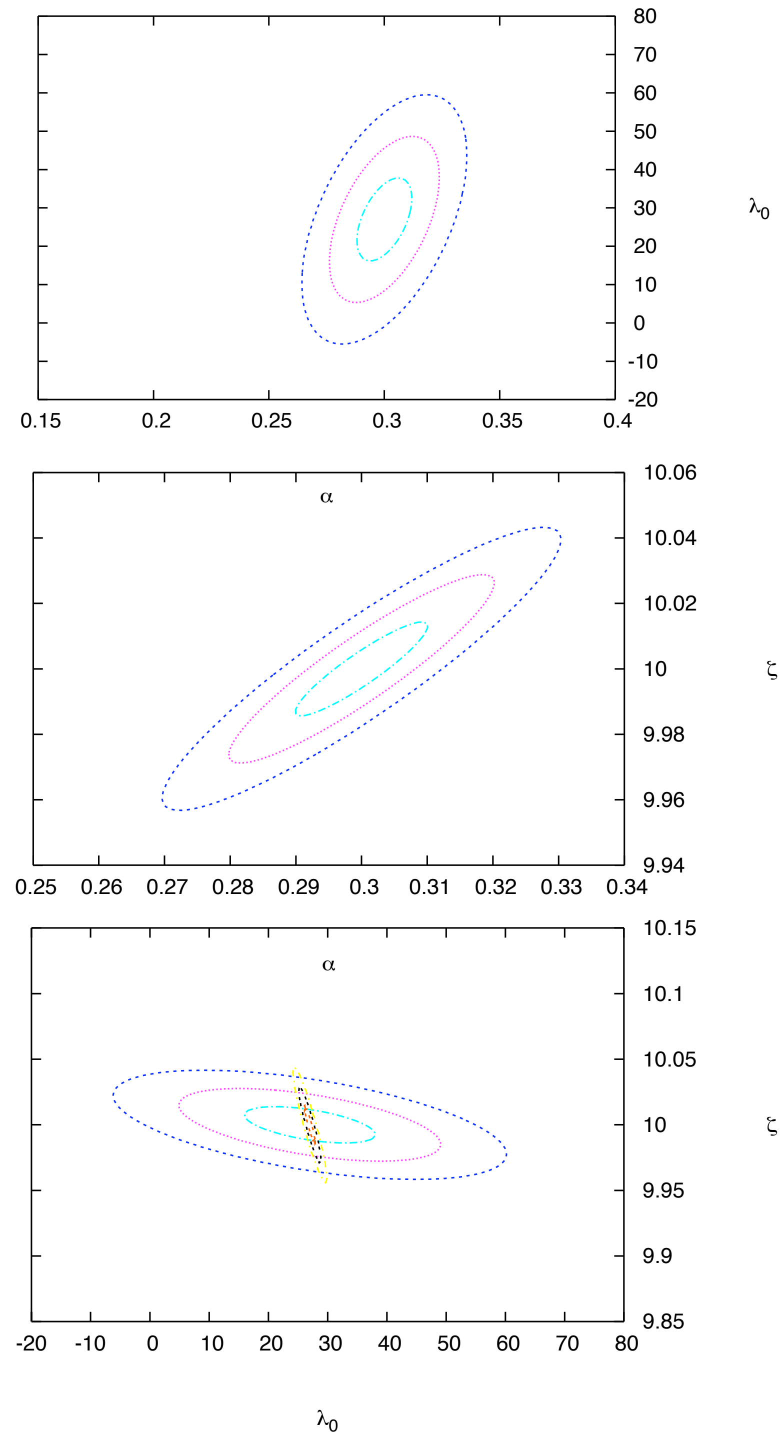

still need to do non-Gaussian error analysis and multi-redshift constraint on recombinations and feedback (Zahn et al. in prep.)

patchy kinetic Sunyaev-Zel'dovich effect

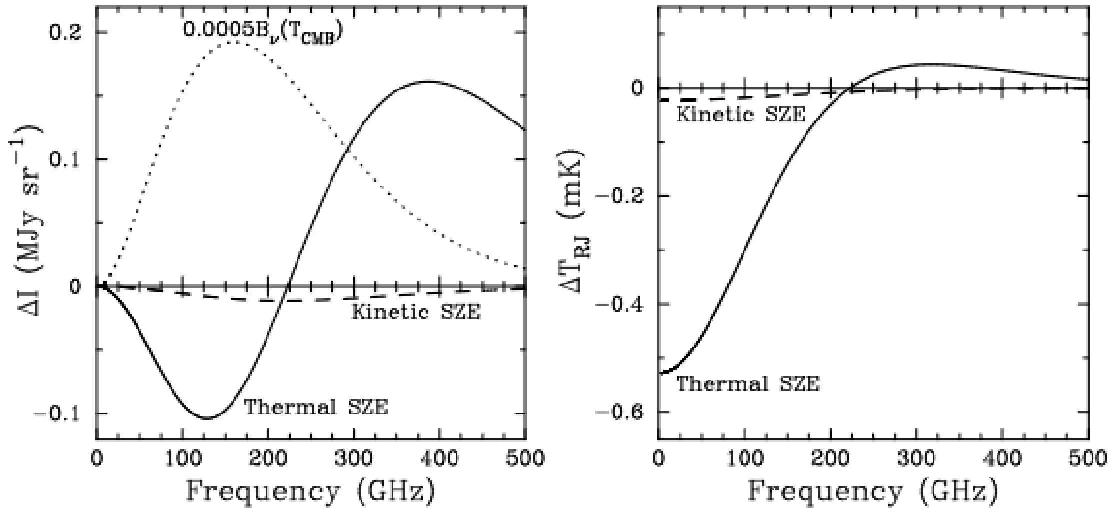

(from Carlstrom et al 2003)

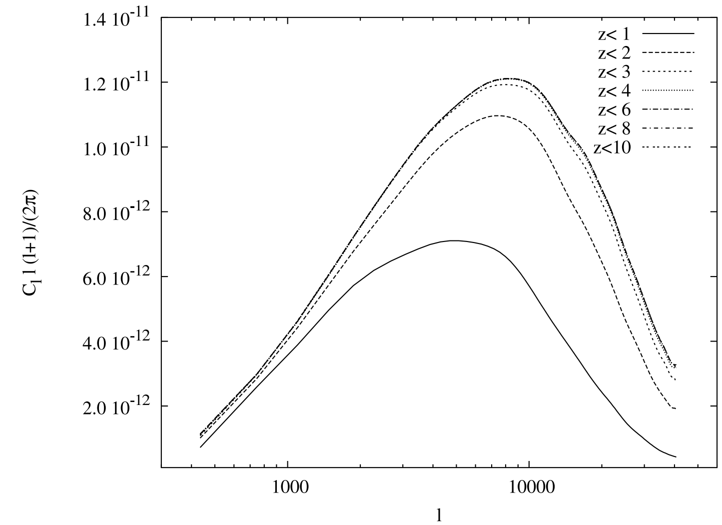

(Zahn et al 2005)

thermal Sunyaev-Zel'dovich effect:

$$\frac{\Delta T_{SZE}}{T_{CMB}} = f(x)\ y = f(x) \int n_e \frac{k_B T_e}{m_e c^2} \sigma_T \, d\ell,$$

$$f(x) = \left(x \frac{e^x + 1}{e^x - 1} - 4 \right) (1 + \delta_{SZE}(x, T_e))$$

kinetic Sunyaev-Zel'dovich effect:

$$\frac{\Delta T_{\rm k}}{T} = -\frac{v_{\rm r}}{c}\, \tau = -\int \frac{v_{\rm r}}{c}\, \sigma_{\rm T}\, n_{\rm e}\, dl$$

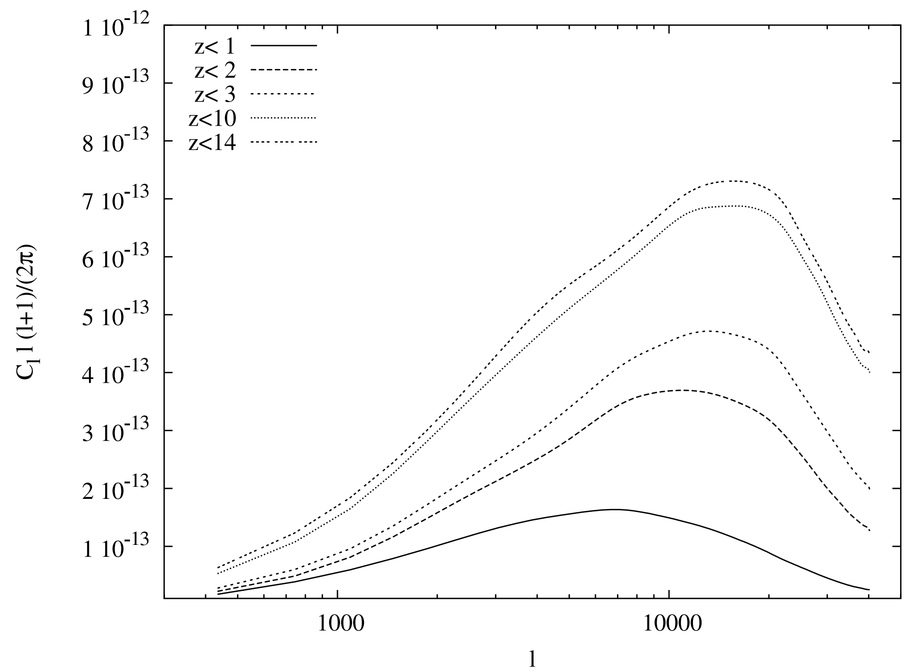

Large additional fluctuation from reionization:

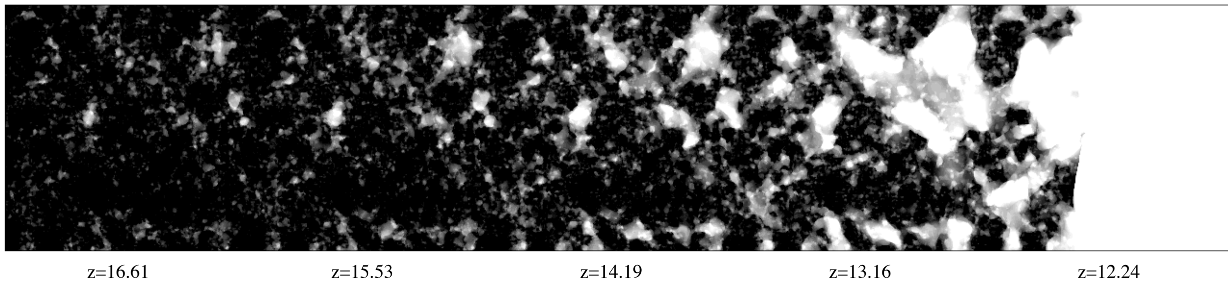

high z contribution to kSZ substantial:

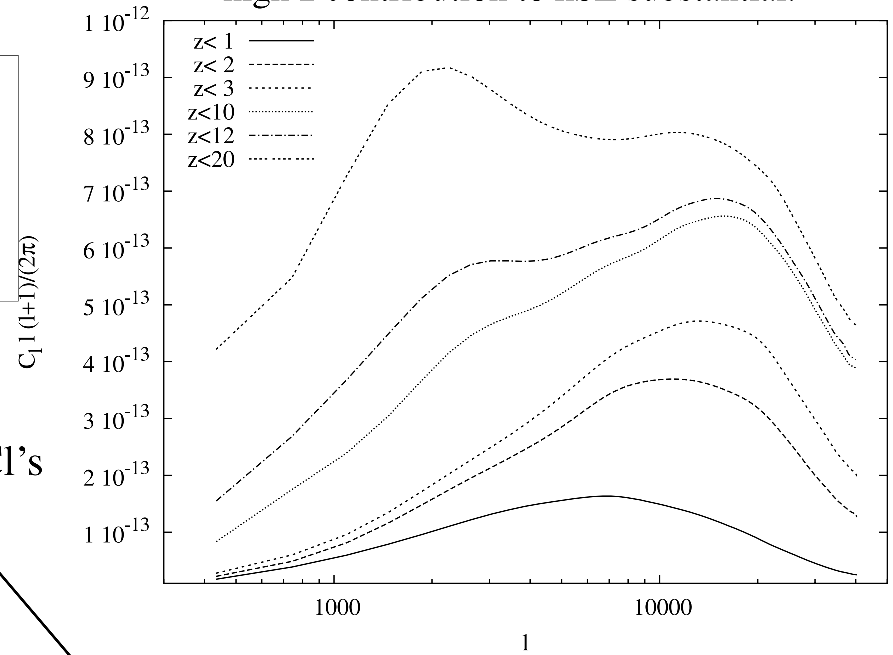

If OV modeled well enough, measurement of EoR will be easy from Cl's

peak of patchy signal swamped by primordial CMB:

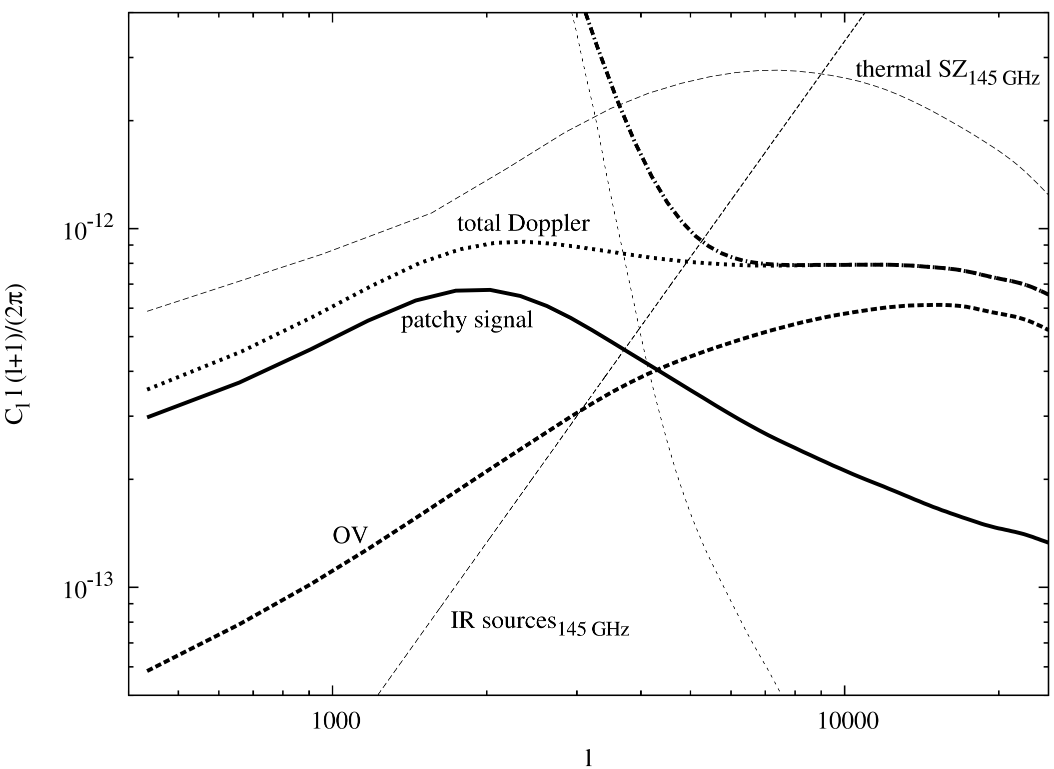

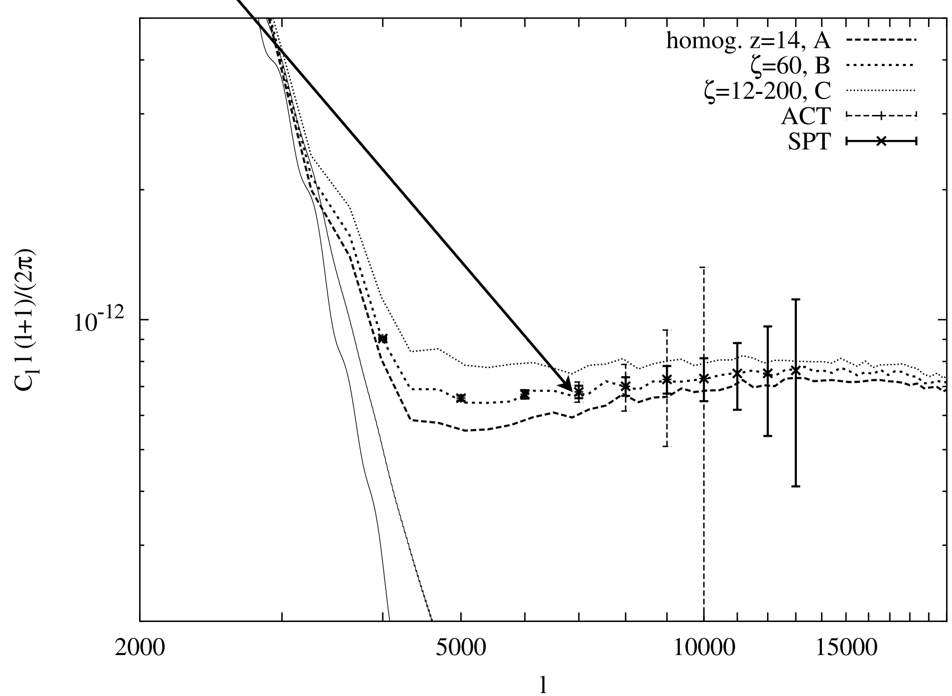

Beyond the power spectrum...?

z=0-3

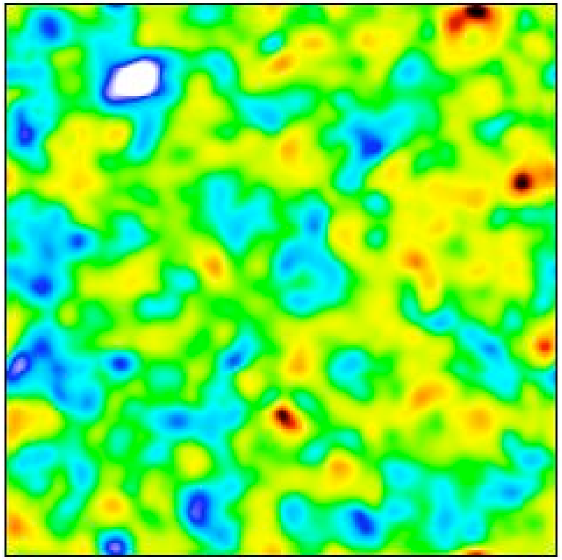

z=3-10

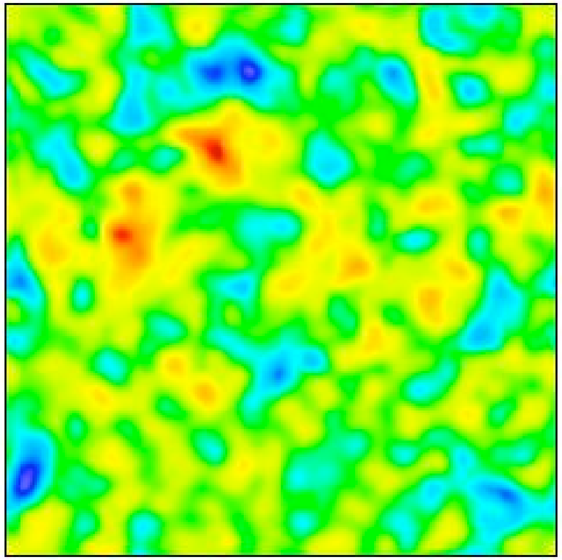

z=10-18

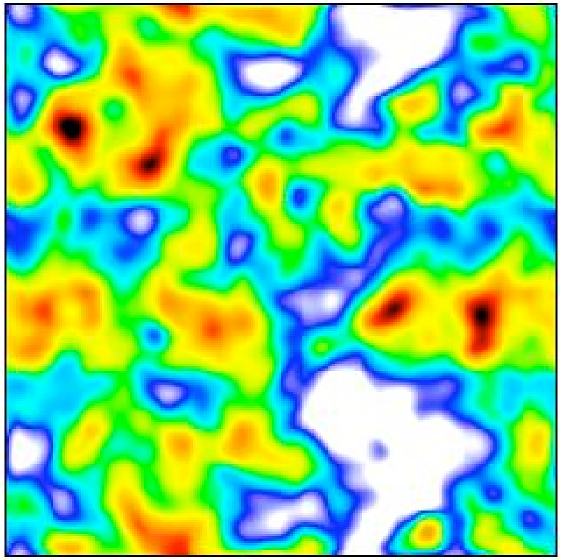

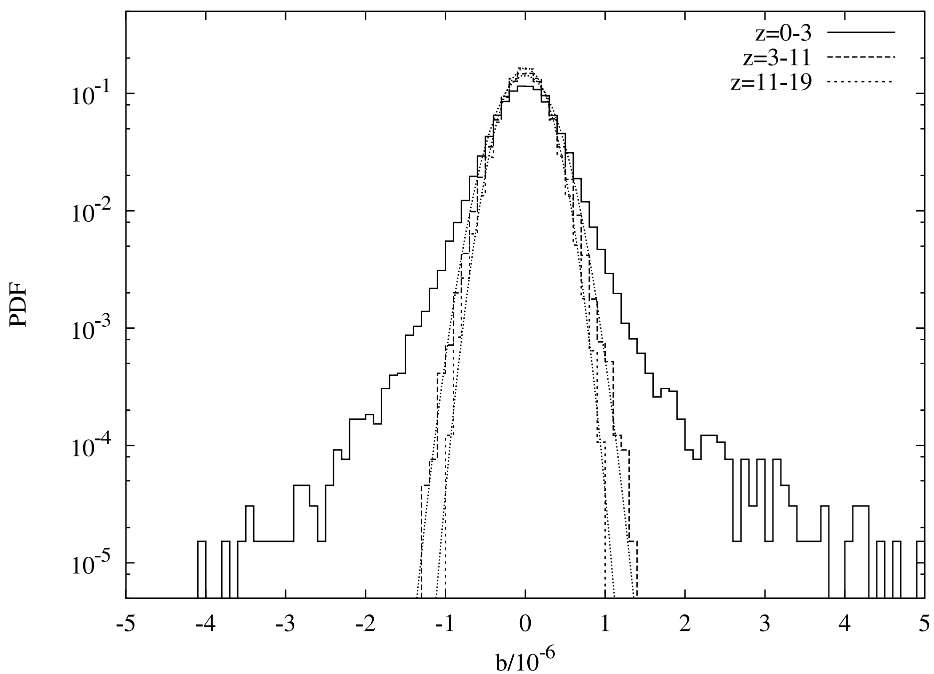

$$\Theta_4 \equiv \frac{\langle(\Delta T/T)^4\rangle}{\sigma_T^4} - 3$$

Kurtosis turns out to be 100-1000 times larger for non-linear OV then for patchiness, depending on filtering scale => may be difficult to find a higher order configuration that picks out the patchy signal

Riquelme&Spergel (2006): try to disentangle lensing from (patchy) kinetic SZ with four-point statistic, to get better handle on reionization

$$\langle \theta^3(\mathbf{x})\theta(\mathbf{y})\rangle_c \equiv \langle \theta^3(x)\theta(y)\rangle - 3\langle \theta(x)^2\rangle\langle \theta(x)\theta(y)\rangle$$

Possible problems:

- only vanishes for lensing to first order expansion in the deflection field
- can't wiener filter out large scale CMB because lensing statistics changes
- kSZ dominates over lensing on most scales, not other way around.
- CMB will enter into the variance on all scales (real space statistic), estimate by describing as product of two Gaussians (lower limit on error)

$$\langle [\theta^3(x) - 3\sigma^2\theta(x)]\theta(y)\rangle \equiv \langle \theta^*\theta\rangle$$

$$\Delta C_l = \sqrt{\frac{1}{(f_{sky}(2l+1)}}\sqrt{C_l^{\theta^*\theta\,2} + C_l^{\theta^*}C_l^{\theta}}$$

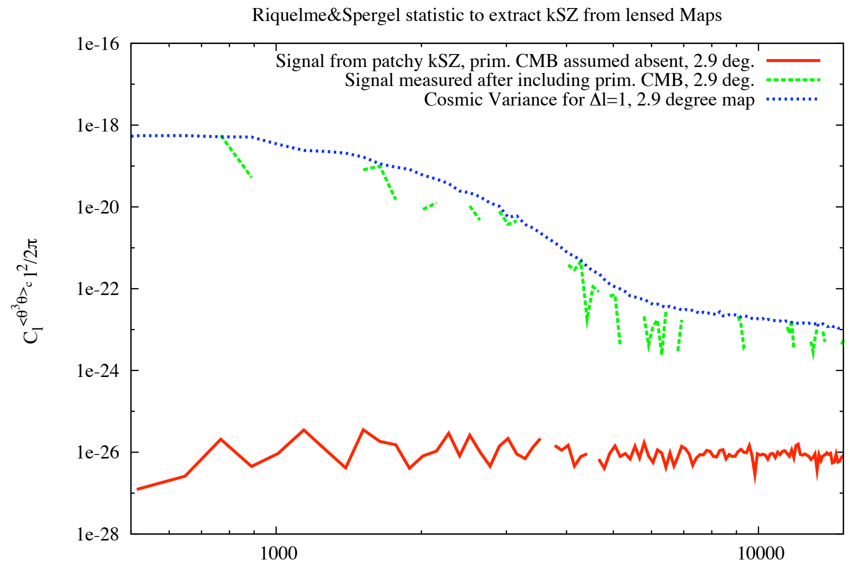

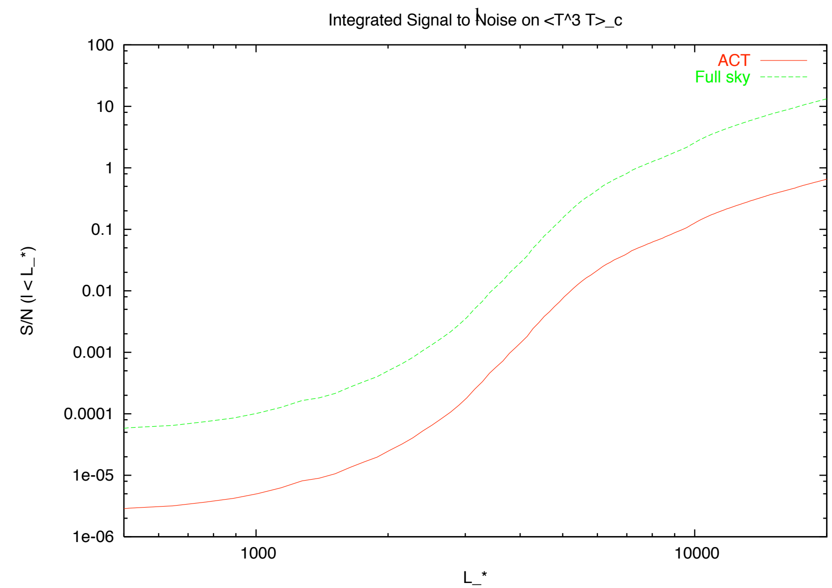

Too bad, does this mean that we're `stuck' with the power spectrum...?

Sensitivity of lensing to kSZ

$$\kappa_{\rm est}(\boldsymbol{\ell}) = b_\ell \kappa(\boldsymbol{\ell}) + n_\ell$$

multiplicative bias (shows up in the cross power)

additive bias (shows up in power)

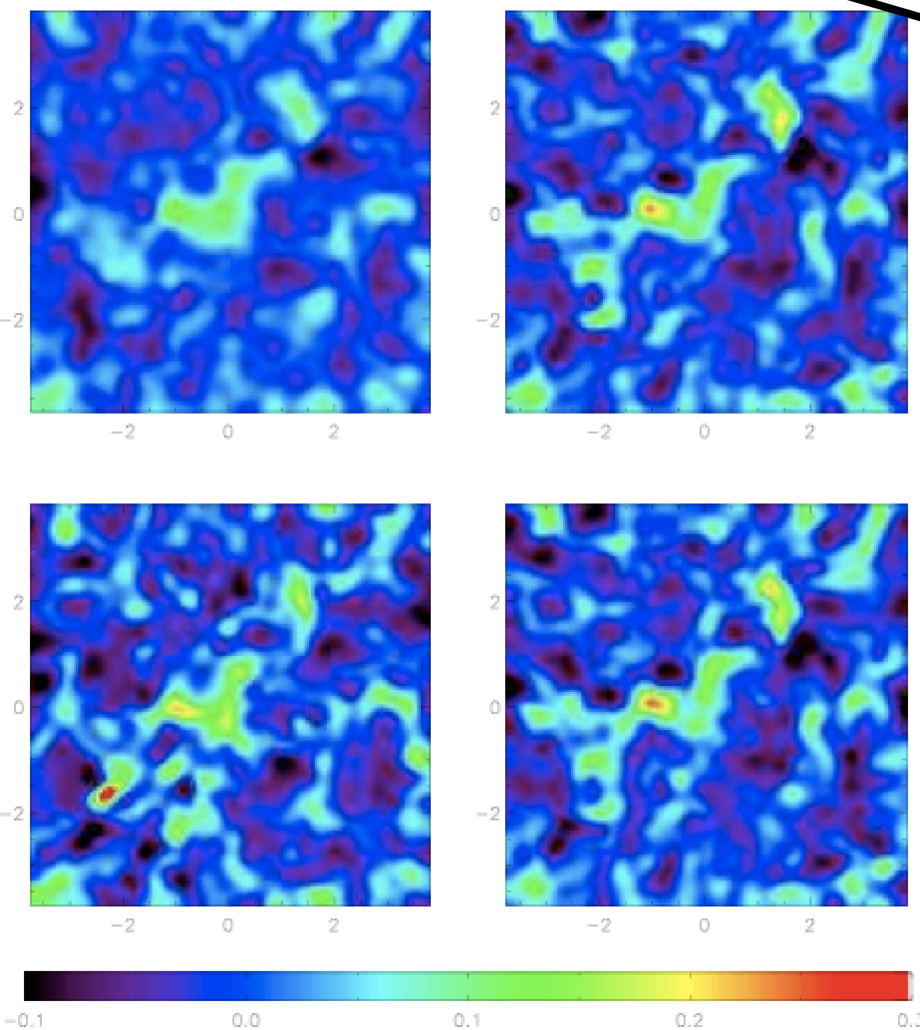

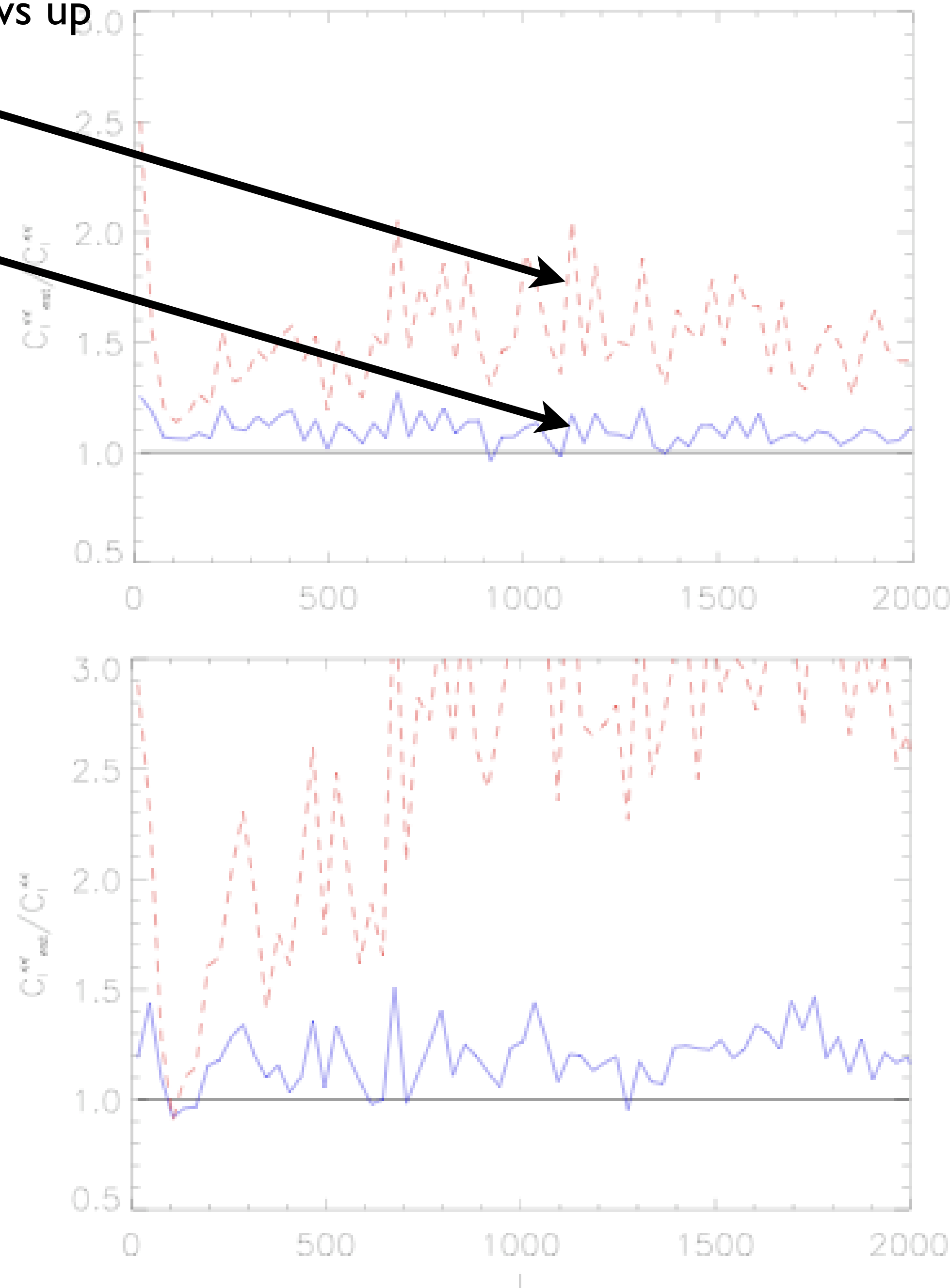

Amblard, Vale, White (2004)

Reconstruction of lensing field: CMB versus 21 cm

Unlensed

CMB

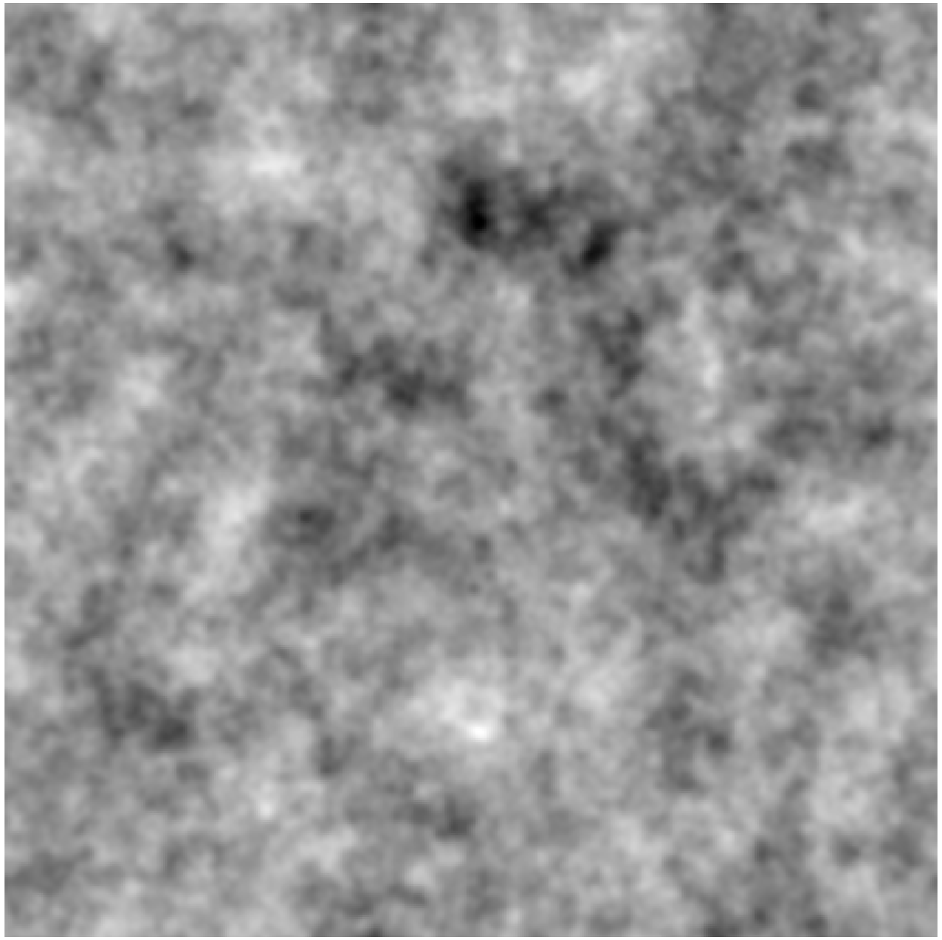

21 cm

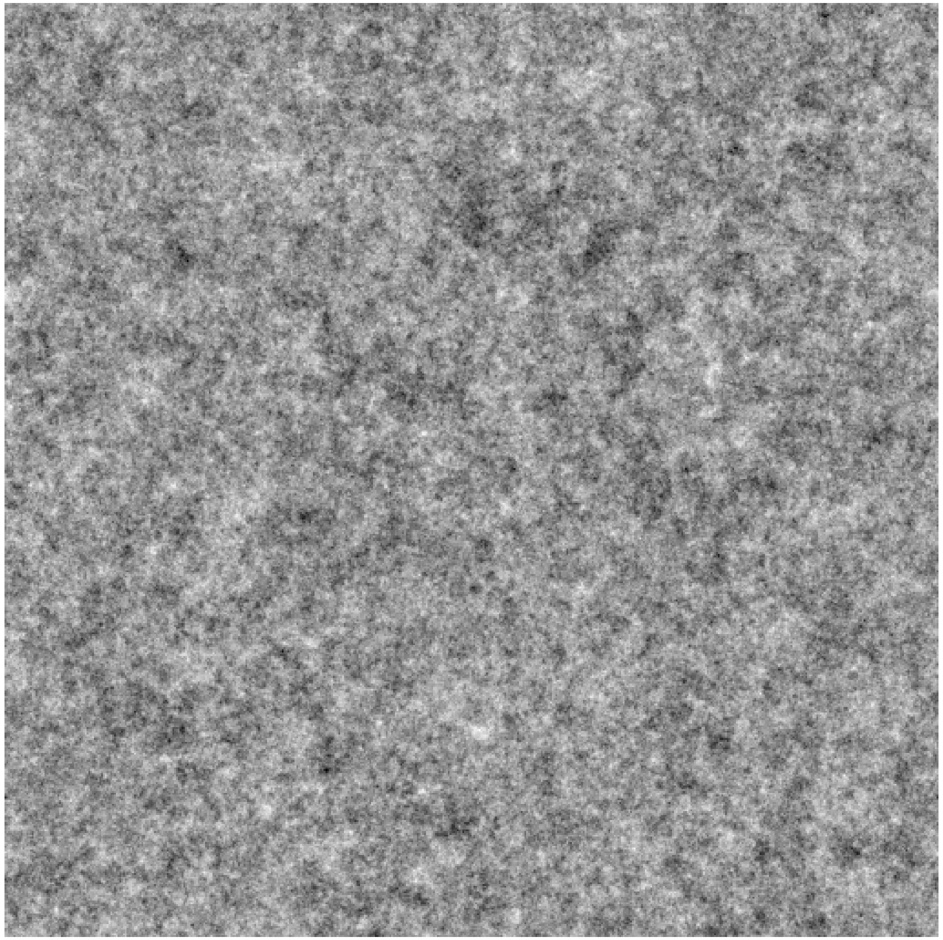

Reconstruction of lensing field: CMB versus 21 cm

Lensed

CMB

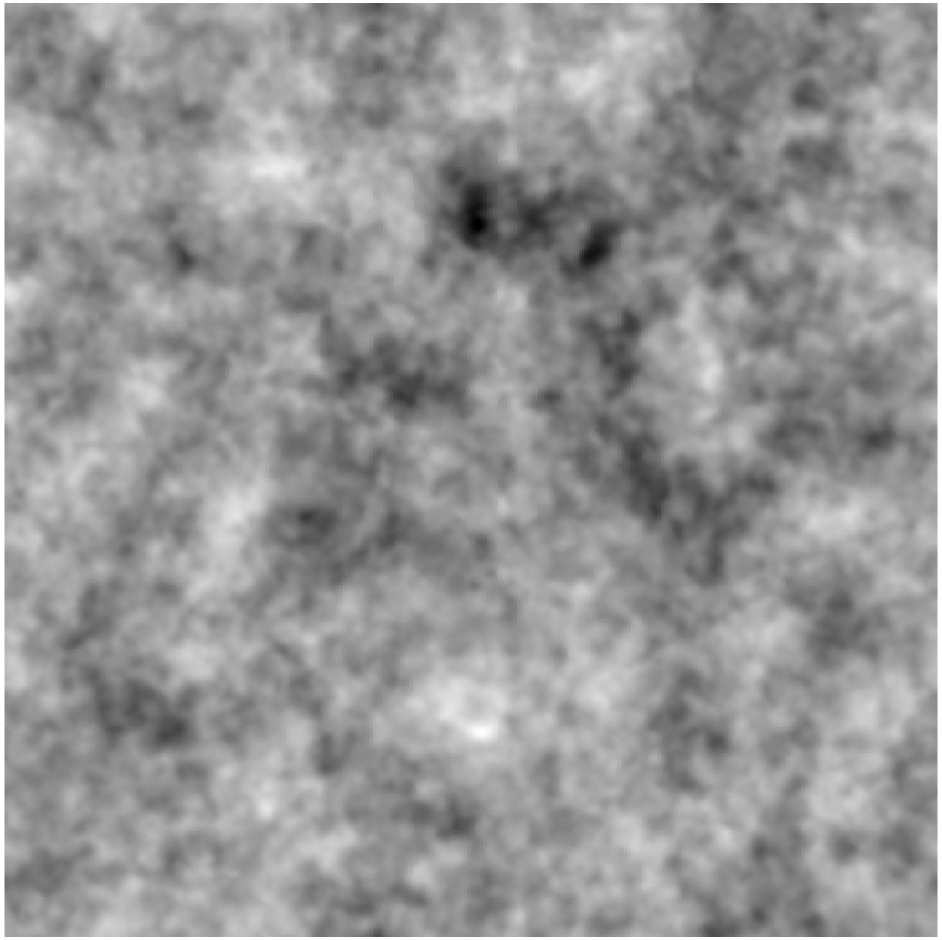

21 cm

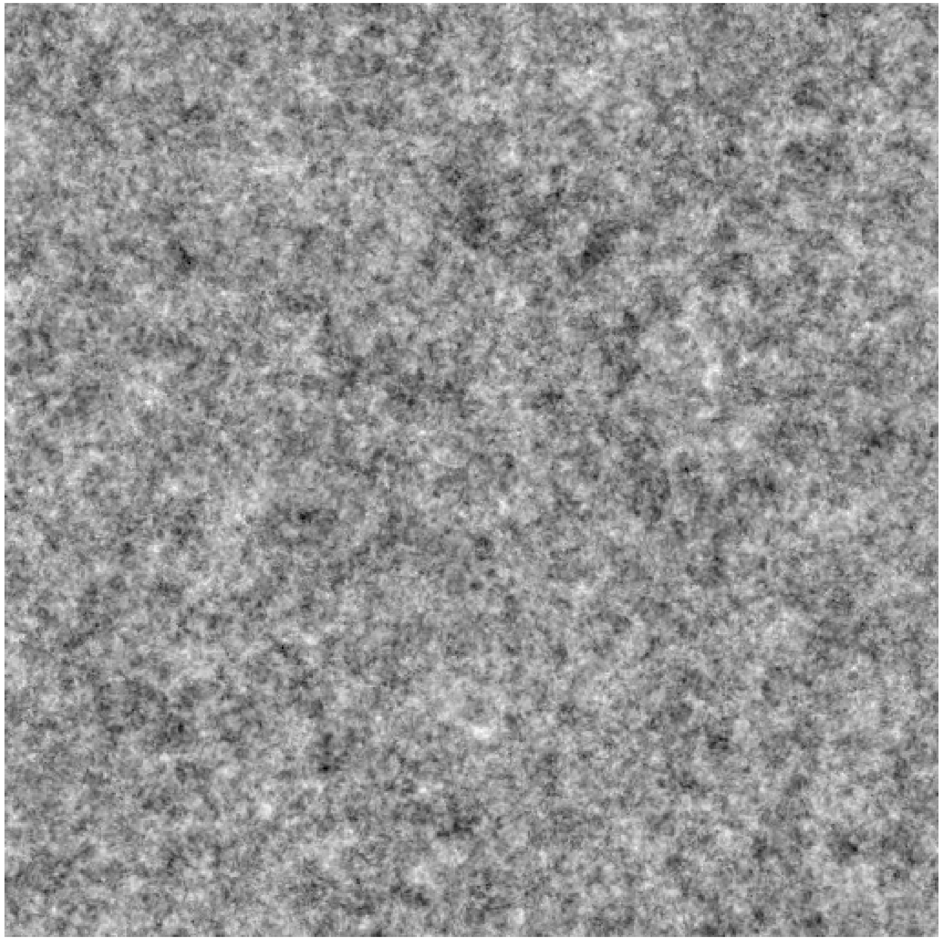

Reconstruction of lensing field: CMB versus 21 cm

Decrement

CMB

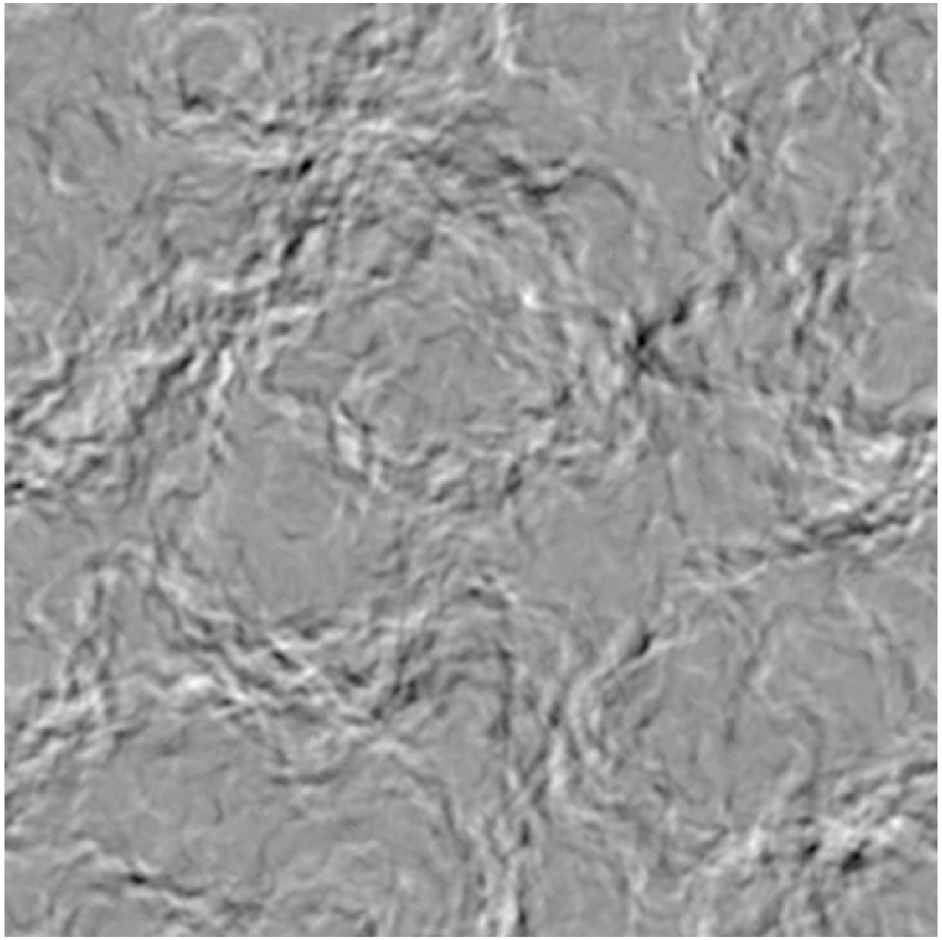

21 cm

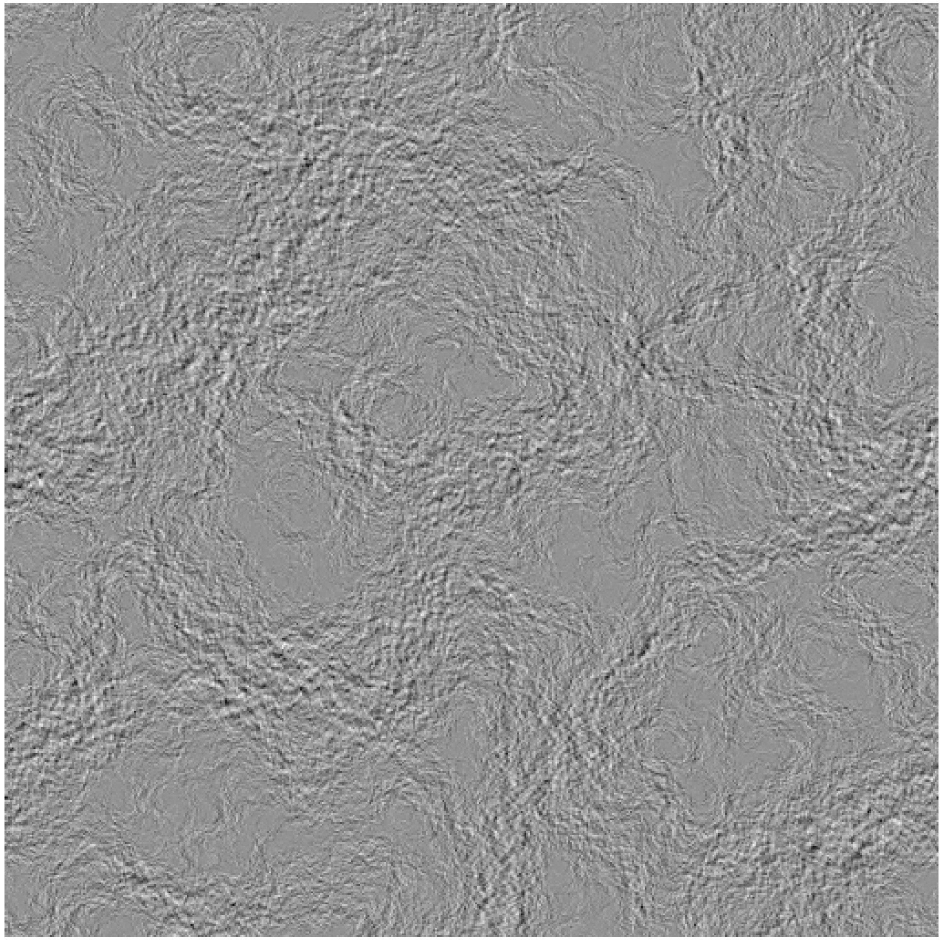

Quadratic estimation of lensing field

- as odd powers should vanish for lensed CMB, try quadratic combinations, i.e. of the form
- requiring that the estimator is unbiased and minimizing its variance leads to
- four point function is most important (Zaldarriaga 2000), a quadratic estimator contains all the information in it (Hu 2001).
- Q.E. turns out to be close to best possible estimator in case of CMB (Hirata&Seljak 2003)
- does the q.e. generalize to three dimensions?
- straightforward for a Gaussian r.f. source, just need to show that can combine estimators for several k modes along the lines of sight without making quadratic combinations of them (Zahn& Zaldarriaga 2005)

$$\hat{\psi}(\mathbf{L}) = N(\mathbf{L}) \int \frac{d^2 l}{2\pi} \tilde{\theta}(\mathbf{L}-\mathbf{l})\tilde{\theta}^*(\mathbf{l}) g(\mathbf{L},\mathbf{l}) .$$

$$g(\mathbf{L},\mathbf{l}) = \frac{(\mathbf{L}-\mathbf{l})\cdot\mathbf{L}C^{\theta}_{|\mathbf{L}-\mathbf{l}|} + \mathbf{l}\cdot\mathbf{L}C^{\theta}_{l}}{2\tilde{C}^{tot}_{l}\tilde{C}^{tot}_{|\mathbf{L}-\mathbf{l}|}}$$

where we used the first order expansion in the deflection field

$$\tilde{\Theta}(\mathbf{l}) \approx \Theta(\mathbf{l}) - \int \frac{\mathrm{d}^2\mathbf{l}'}{2\pi} \mathbf{l}'\cdot(\mathbf{l}-\mathbf{l}')\psi(\mathbf{l}-\mathbf{l}')\Theta(\mathbf{l}')$$

the normalization is

$$N(\mathbf{L}) = \left[\int \frac{d^2\mathbf{l}}{(2\pi)^2} \frac{[(\mathbf{L}-\mathbf{l})\cdot\mathbf{L}C^{\theta}_{|\mathbf{L}-\mathbf{l}|} + \mathbf{l}\cdot\mathbf{L}C^{\theta}_{l}]^2}{2\tilde{C}^{tot}_{l}\tilde{C}^{tot}_{|\mathbf{L}-\mathbf{l}|}} \right]^{-1}$$

For reconstruction, define:

$$\mathbf{F}_1(\mathbf{l}) = \frac{-i\mathbf{l}C^{\theta}_{l}\tilde{\theta}(\mathbf{l})}{\tilde{C}^{tot}_{l}} \quad F_2(\mathbf{L}-\mathbf{l}) = \frac{\tilde{\theta}(\mathbf{L}-\mathbf{l})}{\tilde{C}^{tot}_{|\mathbf{L}-\mathbf{l}|}}$$

$$\hat{\psi}(\mathbf{L}) = iN(\mathbf{L})\mathbf{L}\cdot\int \frac{d^2x}{2\pi} e^{-i\mathbf{L}\cdot\mathbf{x}} F_1(\mathbf{x})F_2(\mathbf{x})$$

Comparison between CMB and 21 cm lensing reconstruction

- CMB field has more structure overall, good. 21 cm rather scale invariant
- CMB decays on small scales because of Silk damping, not so good
- only theoretical limit for 21 cm is the Jeans scale
- for one slice and resolution to l~3000, the CMB is much better
- however for 21 cm we have a large redshift volume to probe
- slices would be correlated, but Fourier modes not if GRF

$$C_{l,j} \equiv (1+\mu_k^2)^2 \frac{P(\sqrt{(l/\mathcal{D})^2+(j\,2\pi/\mathcal{L})^2})}{\mathcal{D}^2\mathcal{L}}$$

for a 5 MHz, dz=0.26 volume
the first few k|| can be used

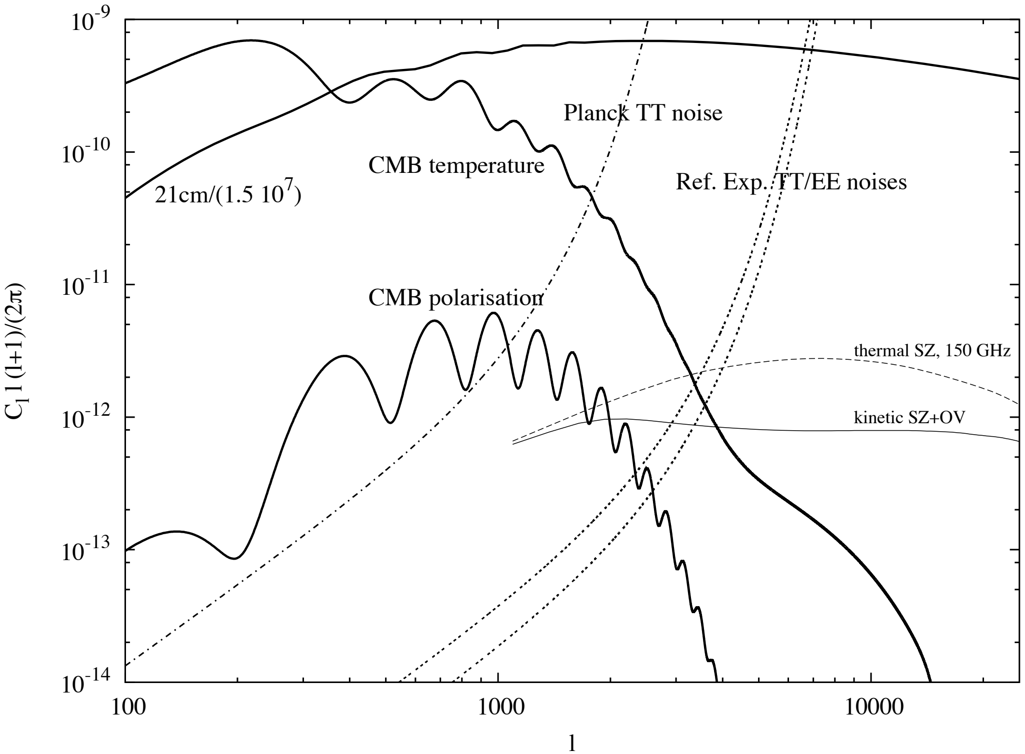

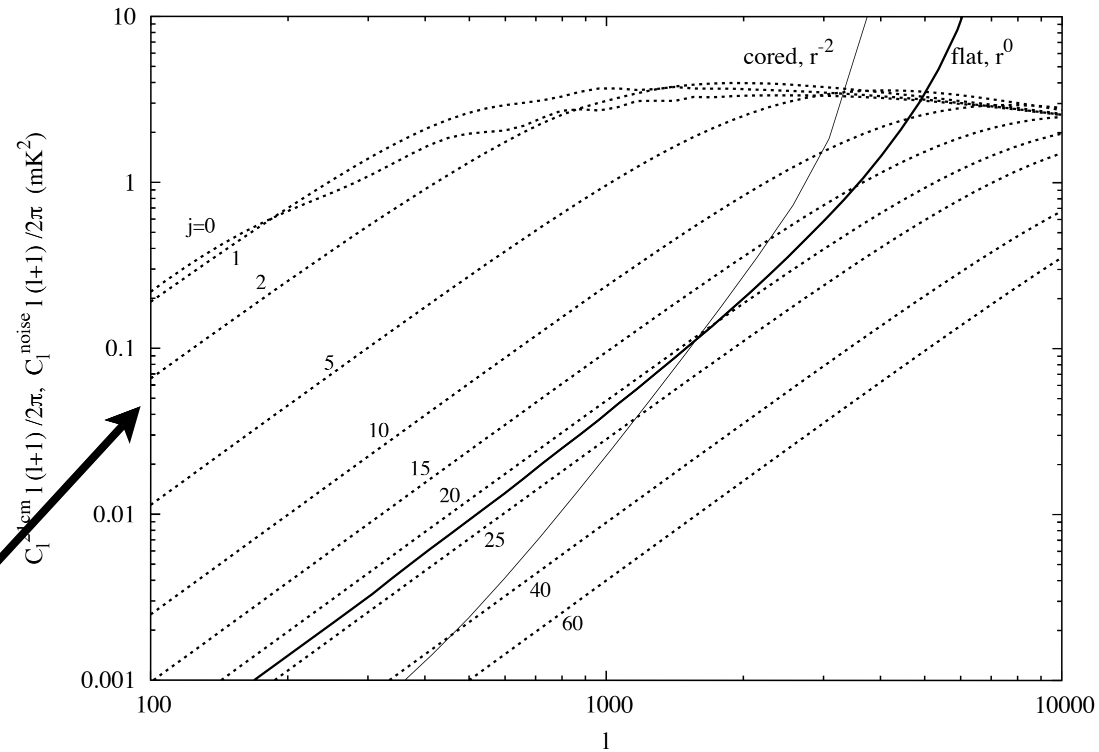

Reconstructed Field with Planck

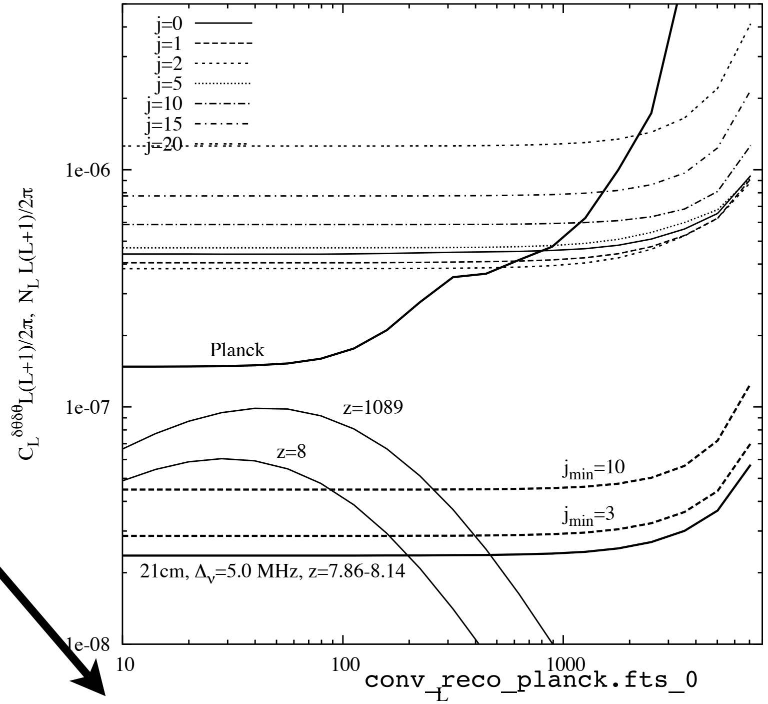

reconstruction noise for Planck and 21 cm narrow band

Input field

`conv_in.fts_0`

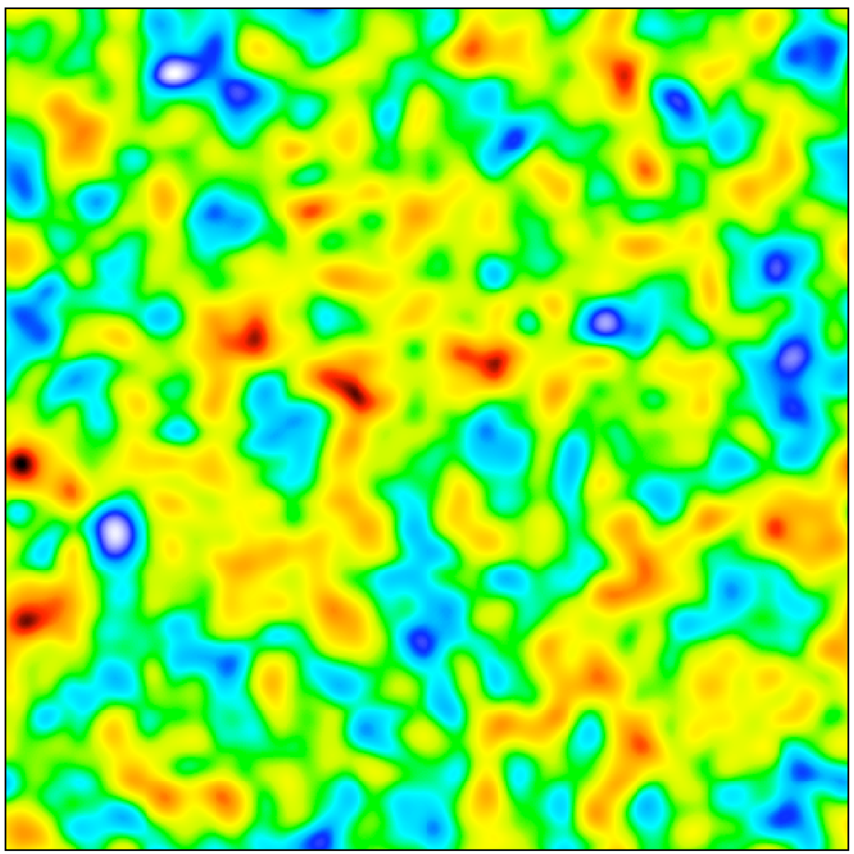

`conv_reco_planck.fts_0`

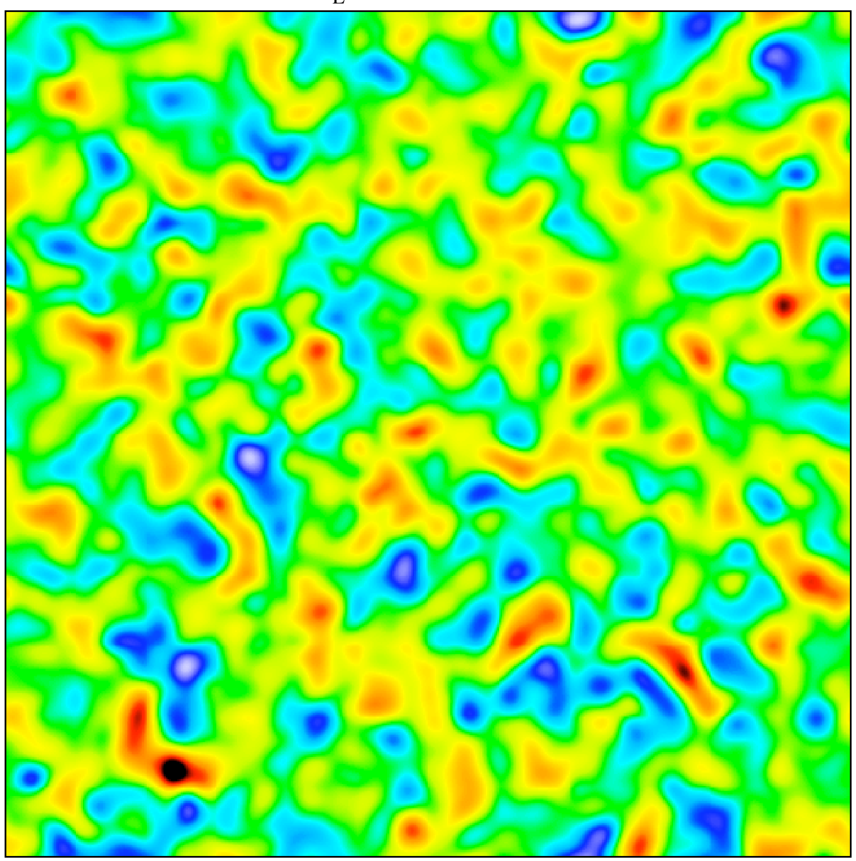

Reconstructed Field with 21 cm (5MHz, dz=0.26)

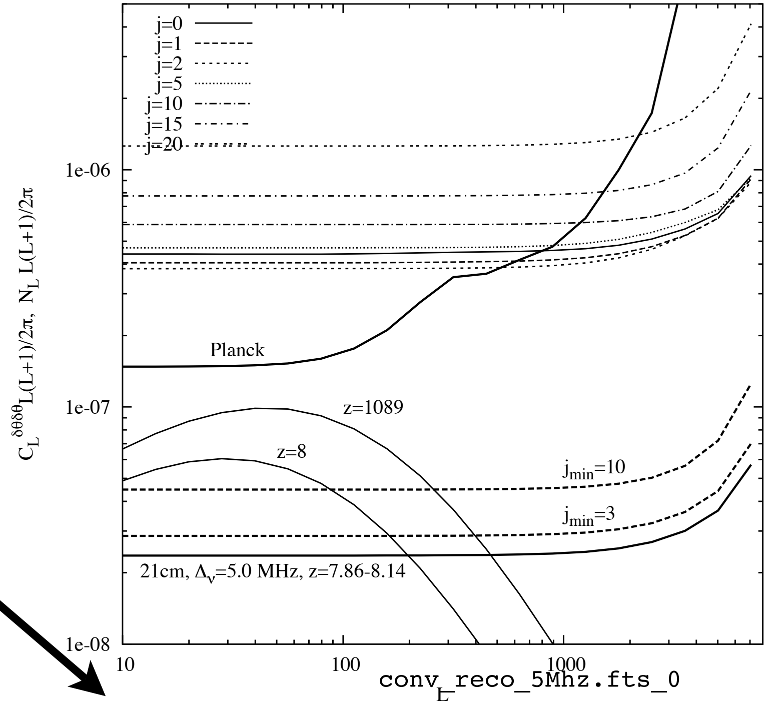

reconstruction noise for Planck and 21 cm narrow band

Input field

`conv_in.fts_0`

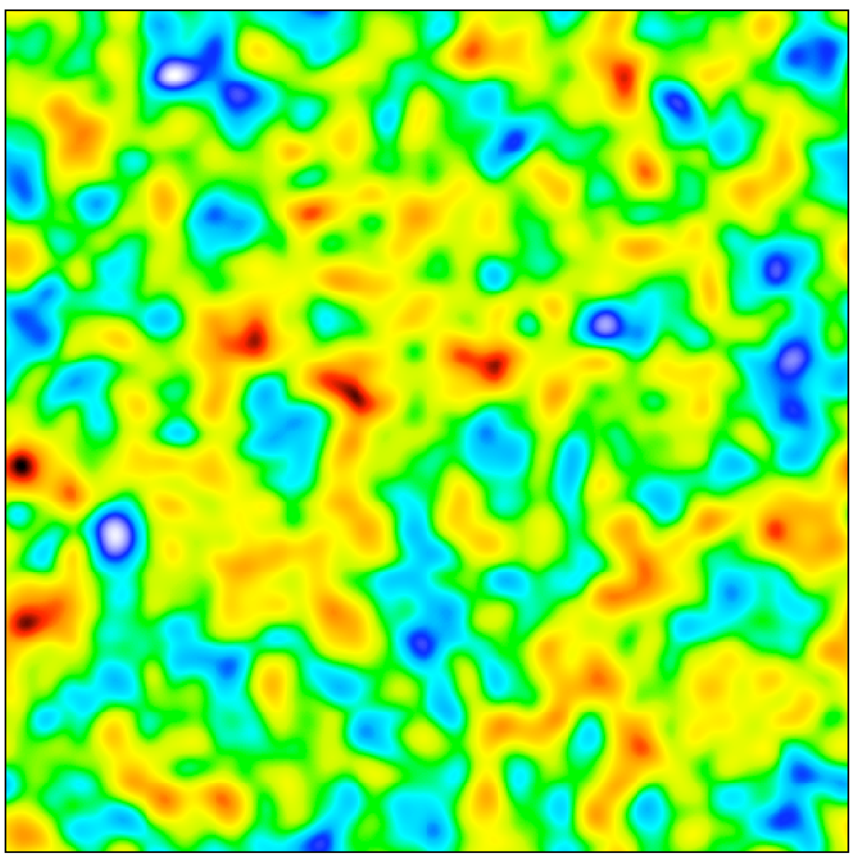

`conv_reco_5Mhz.fts_0`

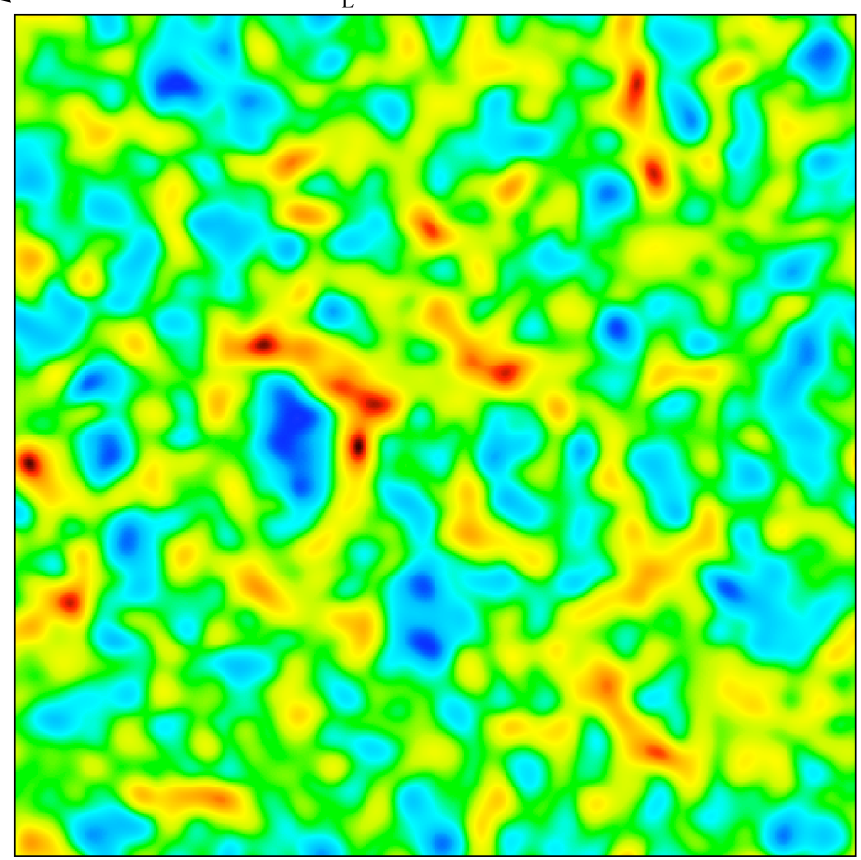

Applications of 21 cm lensing

- using information from number of redshifts would make 21 cm lensing better than CMB incl. polarization quadratic estimator (could use instead iterative maximum likelihood scheme (Hirata&Seljak 2003))

- Sigurdson&Cooray (2005): delense the CMB to get at gravity waves, problem is different lensing kernel, so need to go to z=30 =>to do so would need >100 km^2 of collecting area...

- what about cluster lensing reconstruction (for CMB e.g. Zaldarriaga&Seljak 1999, Dodelson 2003 Vale et al 2003, Lewis&King 2005)? Potential should be great because 21 cm has comparatively more small scale structure and no kSZ contamination.

- may have to wait for SKA though, (or earlier: Ue-Li's cylindrical HSHS receivers?)

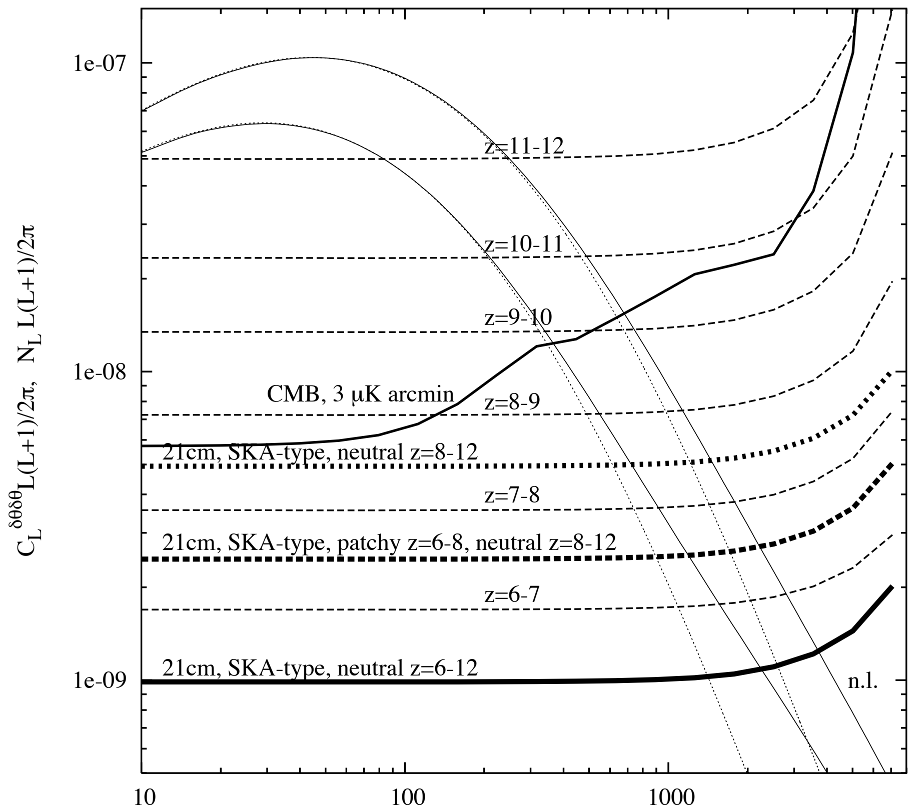

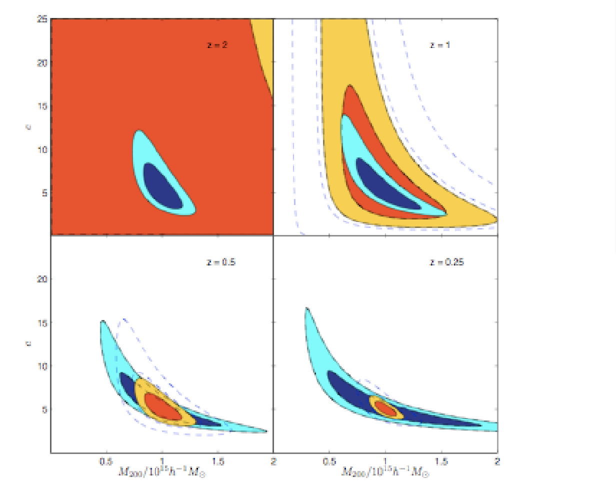

FIG. 5: Mean log likelihood constraints for a $M_{200} = 10^{15} h^{-1} M_\odot$ cluster with concentration parameter $c = 5$. Dark solid is CMB lensing for 1μK noise per 0.5arcmin pixel marginalized over the moving lens signal, red solid is for space-based galaxy lensing with 100 galaxies arcmin^{-2}, dashed lines are for current ground-based galaxy lensing with 30 galaxies arcmin^{-2}. All galaxies have known redshifts, $\sigma_e = 0.3$, and their distribution has $\langle z \rangle = 1$. Contours show where the exponential of the mean log likelihood drops to 0.32 and 0.05 of the maximum.

21 cm and galaxies in cross correlation (with Steve and Adam)

$$\Delta^2_{21,gal}(k) \propto \Delta^2_{\delta x,gal}(k) + \Delta^2_{\delta\rho,gal}(k) + \Delta^2_{\delta x*\delta\rho,gal}(k).$$

- (with Furlanetto and Lidz in prep.)
- Galaxies make the bubbles
- 21 cm stems from the surrounding medium
- => the cross power spectrum should be negative
- on small scales, the cross term between overdensity and galaxies wins over the `3-point'-term
- cross correlation of these (and other) observable will prove useful for first generation experiments that are sensitive to different contaminants.

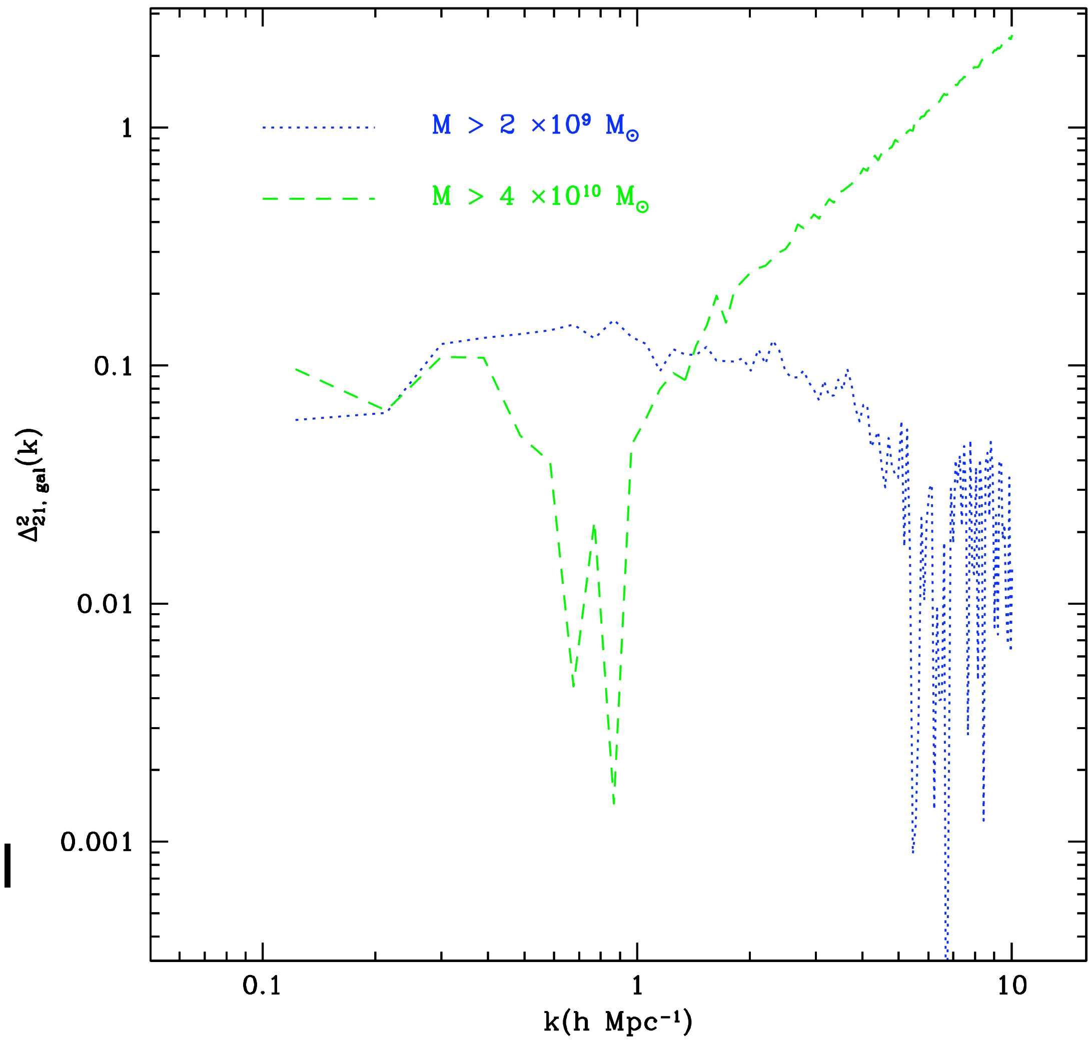

Summary

•Because modeling reionization on large scales and resolving the smallest sources is hard, instructive to develop analytic models for the HII morphology

- -these schemes give us analytic control in dealing with the simulations and agree with them quite well.
- -models now begin to converge and we may have to wait for the first data to make further real progress, also explorer missions such as PAPER to tell us more about what to expect from the foregrounds.
- -with further improvements (see e.g. Cohn&Chang 2006, Kramer et al. 2006) we will be able to explore complex likelihood surfaces in multi-dimensional reionization parameter spaces, similar to MCMC with the CMB data.

•Patchy kinetic SZ effect. Precise modeling of secondary anisotropies will be crucial, not only for constraining reionization. Perhaps can use higher order statistics.

•21 cm lensing reconstruction (generalization of CMB quadratic estimator). More work possible reconstruction of individual objects.

•Should correlate all probes available to us, such as high-galaxy surveys to understand systematics better.